Seismic Retrofit of Deficient Reinforced Concrete Shear Walls using Fibre-reinforced Polymer Sheets: Experimental Study and Anchor Design

A thesis submitted to
the Faculty of Graduate and Postdoctoral Affairs
in Partial Fulfillment of the requirements for the degree

Master of Applied Science

by

Joshua E. Woods

Department of Civil and Environmental Engineering
Carleton University

Ottawa-Carleton Institute of Civil and Environmental Engineering

September

ABSTRACT

Modern design standards allow engineers to design shear wall structures to resist lateral loads induced by major earthquakes by ensuring the structures have adequate strength, ductility and energy dissipation capacity to prevent loss of life. However, despite the advances in earthquake resistant design, there is still a large existing stock of shear wall structures designed according to older less stringent design standards (ACI 318-68; CSA A23.3-77) which are potentially at risk of suffering severe damage under moderate to large earthquakes. The common deficiencies in old shear wall structures include insufficient in-plane stiffness, shear strength and ductility. There are many existing techniques to retrofit and strengthen deficient structures to enhance their safety and improve their seismic performance. An attractive alternative to conventional retrofitting techniques is the use of externally-bonded fiber-reinforced polymer (FRP) sheets. Previous studies have demonstrated the feasibility of using externally bonded FRP sheets as a retrofitting strategy for enhancing the flexural strength of reinforced concrete shear walls. In this study, the effectiveness of applying FRP sheets to enhance the seismic performance of deficient reinforced concrete shear walls is evaluated. These walls exhibit brittle shear behaviour due to insufficient shear reinforcement and poor confinement of the boundary elements in their design, leading to poor seismic performance. The shear wall specimens are either strengthened or repaired using FRP sheets and then cyclically tested to failure. A crucial component of this FRP retrofitting system is an innovative tube anchor system. The performance objective of this anchoring system is to ensure that the load carried by the vertical FRP sheet(s) is efficiently transferred to adjacent supporting

structural elements and premature failure of the FRP sheet due to FRP-concrete debonding is prevented. Finite-element studies conducted to investigate the performance characteristics of the tube anchor system and to develop an optimized design procedure are presented in this thesis. Experimental results obtained from testing FRP-strengthened deficient reinforced concrete shear walls with the new tube anchor system are compared and correlated with the analytical predictions by the finite element models. Experimental results confirm the ability of the FRP retrofitting system to increase in-plane stiffness, flexural strength, ductility and energy dissipation capacity in shear deficient wall specimens. The system is also capable of recovering the initial stiffness in severely damaged shear wall specimens.

ACKNOWLEDGEMENTS

The author would first like to thank Professor David T. Lau, for his support and guidance over the past two years. Without him, the work would not have been possible. The author would also like to acknowledge Professor Carlos A. Cruz-Noguez for his contributions in the early stages of this project, as well as his unwavering support, guidance, and friendship during his time at Carleton University.

The author would also like to thank the contributions from the staff in the structures lab at Carleton University, including Stanley Conley, Pierre Trudel, Jason Arnott, Kenneth Akiwu and Donovan Tremblay. Without the countless hours of work from the lab staff this project would not have been possible.

Finally, the author would like to thank the support from his family and friends during this work. Specifically, his girlfriend Marie for her constant support, his parents Paul and Kelly, brother Sheldon, and fellow graduate students Pedram Mortazavi, Colin Gilbert, Ahmed Hassan, Ryan Gholich, Eytan Fiszman, and Jon Grimes.

TABLE OF CONTENTS

LIST OF FIGURES

LIST OF TABLES

LIST OF SYMBOLS

f'_c - concrete compressive strength
f_y - steel yield strength
h_w - height of the shear wall
l_{df} - development length of FRP sheet
l_w - length of the shear wall
n_s - number of fibre-reinforced polymer sheets
p_c - pressure over the curved surface of the tube anchor
$p_{c,\max}$ - maximum pressure acting over the tube anchor system
$P_{c,\max}$ - maximum resultant load carried by the fibre-reinforced polymer sheet
r_o - outer radius of the tube anchor
t_w - thickness of the shear wall
t_s - thickness of the fibre-reinforced polymer sheet
$\tau_{\max}$ - maximum shear stress acting over the flange of the steel angle anchor system
Δ_u - displacement at the ultimate load level
Δ_y - yield displacement of the wall specimen
$\varepsilon_{fracture}$ - fracture strain
ε_{sh} - strain hardening strain
ε_u - ultimate strain
μ_Δ - displacement ductility
σ_u - ultimate tensile stress of the fibre-reinforce polymer

CHAPTER 1: INTRODUCTION

Reinforced concrete (RC) shear walls are lateral load resisting structural systems widely used in seismically active regions around the world. The construction of cast-in-situ reinforced concrete shear walls began in the 1950s and 1960s in urban regions of high seismicity for medium-to high-rise buildings (Fintel, 1995). Research over the past 50 years has resulted in advances in understanding the seismic behaviour and significant improvements in the performance of shear wall structures. These advances are reflected in the current design standards for reinforced concrete structures (ACI 318-08; CSA A23.3-04). The conventional performance objective in the current design standards for earthquake resistant design of structures is life safety, in preventing loss of life and injury of the occupants during a major or design earthquake. However, the recent development of performance-based seismic design has led to the adoption of separate performance objectives for different hazard levels of earthquake events. For small to medium earthquakes expected to occur once or multiple times during the service life of a structure, the performance objectives of limiting damage and reducing economic loss are also considered in addition to the life safety performance objective in current design practice. However, despite these advances in earthquake resistant design, there is a large inventory of existing shear wall structures constructed and designed using older less stringent design guidelines (ACI 318-68; CSA A23.3-77). From past earthquake experiences, these older shear wall structures are susceptible to severe damage under moderate

to large earthquakes due to their inadequate design. The common structural deficiencies associated with old shear wall structures include insufficient in-plane stiffness, flexural strength, shear strength and/or ductility (Lombard et. al. 2000). To address these deficiencies, there are many existing techniques available to improve the performance of old shear wall structures to ensure their safety under lateral loads induced by major earthquakes. Commonly used retrofitting techniques include the application of shotcrete, filling of openings with masonry infills, or the addition of new shear walls or steel bracing elements (FEMA, 1997). Although these retrofitting strategies are effective in increasing the resistance of the structure, many of these techniques add significant weight to a structure, which can change its dynamic characteristics and result in redistribution of the load demands during an earthquake not anticipated in the original design of the structure. Furthermore, the aforementioned retrofitting techniques are labour intensive and thus often result in significant disruption to the occupants and operation or function of the facilities. An attractive alternative to conventional retrofitting techniques is the use of externally-bonded fibre-reinforced polymer (FRP) sheets. The advantages of this system include its ease of application combined with its high strength-to-weight ratio. The application of FRP sheets in existing structures is also much less disruptive to the operation of the building and does not significantly alter the shape or architectural appearance of the structural members. Over the past two decades, there has been a significant amount of research pertaining to the use of advanced composite materials in structural applications, particularly in the retrofit and rehabilitation of RC structures (Teng et al., 2002). Studies have demonstrated that in addition to increasing the strength, ductility and energy dissipation capacity of RC structures, retrofitting using FRP can also be a very effective

tool to enhance the seismic performance of deficient RC structures and meet the multiple performance objectives associated with performance-based seismic design. A brief overview of several studies focused on the seismic retrofit of RC shear walls using externally bonded FRP sheets are described in the next section.

1.1 Literature Review

Most of the research conducted on the retrofit of RC shear walls using FRP is on the feasibility of using FRP as a structural material and/or addresses the enhancement of shear strength and energy dissipation capacity in shear wall specimens. An investigation by Antoniades et al. (2003) studies the use of externally bonded FRP jackets for the seismic retrofit of RC shear wall specimens designed according to modern design standards (Eurocode 8). The test specimens include four RC squat walls retrofitted using lap-welding of fractured reinforcement and the application of horizontal FRP sheets wrapped around the wall. The study concludes that the application of the FRP sheets improves the shear strength of the test specimens but cannot significantly improve the energy dissipation capacity in severely damaged walls. Alternatively, a study by Patterson and Mitchell (2003) tested four flexural shear walls designed according to older design standards. As a result, the wall specimens are detailed with several common structural deficiencies associated with older design standards including lap splices in the plastic hinge region and a lack of confinement in the boundary elements. The retrofitting scheme included the addition of headed reinforcement, horizontal carbon fibre wrap, and reinforced concrete collars at the base of the wall to improve the seismic performance of flexural RC core walls. Results of the study show that the use of

headed reinforcement and a horizontal FRP jacket is capable of improving the confinement and shear strength of the wall specimen. A similar investigation conducted by Ghobarah and Khalil (2005) studies the seismic retrofit of shear deficient RC shear walls using woven FRP sheets applied at a 45 degree angle. By inclining the FRP, the retrofitting scheme aims to increase the shear strength and ductility of the wall specimens. Results of the study demonstrate that by applying the carbon fibre wrap at a 45 degree angle, significant improvements to the shear strength and ductility of the wall specimens can be achieved. The study also found that adequate anchorage of the FRP sheets improves the overall efficiency of the retrofitting scheme. More recently, another study by Layassi and Mitchell (2012) tested four flexural RC shear walls designed with non-ductile details including lap splices of the longitudinal reinforcement in the plastic hinge region and inadequate confinement of the boundary elements. The walls are retrofitted using a fibre-reinforced self-consolidating concrete jacket and a horizontal FRP wrap. The study demonstrated that the retrofitting technique is capable of improving the ductility and prevents premature failure of the lap splice. The primary focus of each of these studies is on the use of FRP sheets wrapped around the wall to increase the confinement of the boundary elements and shear strength in RC walls. Although the use of carbon fibre jackets has been shown to improve the concrete confinement in the boundary elements, in many cases the sides of a RC shear wall are not exposed, and therefore it may be impractical to apply the FRP sheets around the wall. In addition, flexural strengthening of RC shear walls may be required in walls that need enhancement of lateral load resistance in addition to shear strengthening to meet current design standards, something which has not been addressed in previous studies.

In contrast to previous studies, two studies by Lombard (1999) and Hiotakis (2004) at Carleton University investigate the use of FRP to increase or recover the flexural strength of ductile reinforced concrete shear walls designed according to modern design standards (CSA A23.3-94). In both studies, the FRP sheets are not wrapped around the wall to ensure the practicality of the retrofitting scheme. An experimental program by Lombard (1999) focuses on the repair and strengthening of four flexural RC shear walls, retrofitted with externally bonded FRP sheets and a steel angle anchor system. While results of the study show good performance of the FRP retrofitting system in improving the seismic behaviour of the shear wall specimens, premature failure of the steel angle anchor system and significant out-of-plane deformations of the wall specimens contributed to a reduction in the efficiency of the retrofitting scheme, which is discussed in more detail in Chapter 3. Following the experimental study by Lombard (1999), a second experimental investigation by Hiotakis (2004) expands on previous research by Lombard (1999) and addresses previously noted issues including improvements to the FRP anchor system and better control of out-of-plane deformation of the wall specimens. The study by Hiotakis (2004) examines the seismic retrofit of five RC shear walls, once again designed according to modern design standards with the same dimensions as those tested by Lombard (1999). The walls are repaired or strengthened using vertical and horizontal externally bonded FRP sheets, which are once again not applied around the wall to ensure the practicality of the retrofitting system. Results of the study by Hiotakis (2004) demonstrate that the use of FRP sheets is an effective means for improving the seismic performance of RC shear walls. The newly implemented tube anchor system is also shown to

be a superior alternative when compared to the previously studied angle anchor system by Lombard (1999) and improves the overall efficiency of the retrofitting scheme. However, experimental observations on the performance of the tube anchor system by Hiotakis (2004) show that significant improvements can be made to the design of the tube anchor system to improve its efficiency. Although the shear walls tested by Lombard (1999) and Hiotakis (2004) are expected to behave in a flexural manner, the objective of the earlier studies (Lombard, 1999; Hiotaki, 2004) is to evaluate the effectiveness of the FRP retrofitting system in enhancing the flexural strength of the wall specimens without the complication of brittle shear behaviour, typical in old deficient shear walls.

1.2 Objectives and Scope

In this study, the effectiveness of externally bonded FRP sheets to enhance the seismic performance of shear walls designed according to older design standards (ACI 318-68; CSA A23.3-77) is investigated. Two shear wall specimens, expected to exhibit brittle shear behaviour due to insufficient shear reinforcement and poor concrete confinement in the boundary elements, are strengthened or repaired and then cyclically tested to failure. The wall specimens have the same dimensions as those studied by Lombard (1999) and Hiotakis (2004) to compare the performance of the FRP retrofitting system in old deficient shear walls to those designed according to modern design standards. The ability of the FRP retrofitting system to increase the flexural strength, shear capacity, ductility and energy dissipation capacity of the deficient wall specimens is evaluated. The goal of increasing the shear capacity of the wall is to allow flexural failure to govern the seismic response and performance of the wall,

resulting in a ductile structure with flexurally dominant behaviour. The FRP sheets are once again not wrapped around the wall to ensure the practicality of the retrofitting system. The innovative tube anchor system is once again used to transfer the tensile forces carried by the FRP to the supporting structural elements. Finite element studies are conducted to investigate the performance characteristics of the tube anchor system to develop an optimized design procedure to improve the efficiency of the tube anchor system. Experimental results on the performance and effectiveness of a new tube anchor system will be presented.

CHAPTER 2: EXPERIMENTAL PROGRAM

The ability of a comprehensive retrofitting scheme using externally bonded FRP sheets and an innovative anchor system to improve the seismic performance of shear walls designed according to older design standards is conducted at Carleton University. The test specimens discussed in this thesis include two reinforced concrete shear walls designed according to the ACI 318-68 building code, which is similar to the Canadian CSA A23.3-77 reinforced concrete design standard. The wall specimens are detailed with several structural deficiencies commonly found in old shear wall structures constructed during the 1960s and 1970s. These deficiencies include insufficient shear reinforcement, poor confinement of the boundary elements and low concrete strength resulting in a shear dominant wall specimen, expected to fail in a brittle manner. Each of the shear walls specimens is strengthened or repaired and then cyclically tested to failure.

2.1 SHEAR WALL SPECIMENS AND REINFORCING DETAILS

The wall specimens described in this thesis include two 2/3-scale RC shear walls which measure 1.8x1.5x0.1m resulting in an overall aspect ratio (h_w/l_w) of 1.2, as shown in Figure 2-1. The longitudinal and horizontal reinforcement ratios of the wall specimens are 3.0% and 0.25% respectively. The steel reinforcement details for a typical wall specimen is shown in Figure 2-1. The first wall specimen is a control wall (SLCW), which is cyclically tested up to failure and then repaired. The wall is then tested again to evaluate the effectiveness of the FRP

retrofitting system in repair applications (SLRW), including its ability to restore the initial stiffness of the wall and increase the shear and flexural strengths, ductility and energy dissipation capacity. This part of the investigation provides insight on using the FRP retrofitting system in repair applications for walls which have experienced seismic damage during an earthquake and must be repaired to restore the safety of the structure. The second wall specimen (SLSW) is strengthened with FRP sheets prior to testing with no previous damage. The performance of this wall specimen is compared with the control wall to evaluate the effectiveness of externally bonded FRP sheets as a retrofitting system in deficient shear wall structures. The FRP reinforcing details used for the repaired and strengthened wall specimens are identical. This allows the results from the strengthened and repaired walls to be compared and to evaluate the different performance of the FRP retrofitting system in the two different application scenarios. Each of the wall specimens are retrofitted with a combination of uni-directional vertical and horizontal FRP layers, as shown in Figure 2-1. Although the use of vertical FRP sheets to increase the flexural strength in shear deficient walls may be counterintuitive, it may be necessary in some cases to increase the flexural strength of the wall to meet current design code requirements, especially in retrofit scenarios (Cruz et al., 2014). Each of the wall specimens is flexurally strengthened using one vertical FRP layer which is anchored at the base of the wall. Three horizontal FRP sheets are placed on top of the vertical layer to increase the shear strength of the wall and ensure that a ductile flexural failure mode will occur prior to brittle failure modes associated with shear. By ensuring that the flexural strength of the wall is higher than its shear capacity, significant improvements in the ductility

and energy dissipation capacity of the shear wall can be achieved, which contribute to improving the seismic performance of the wall.

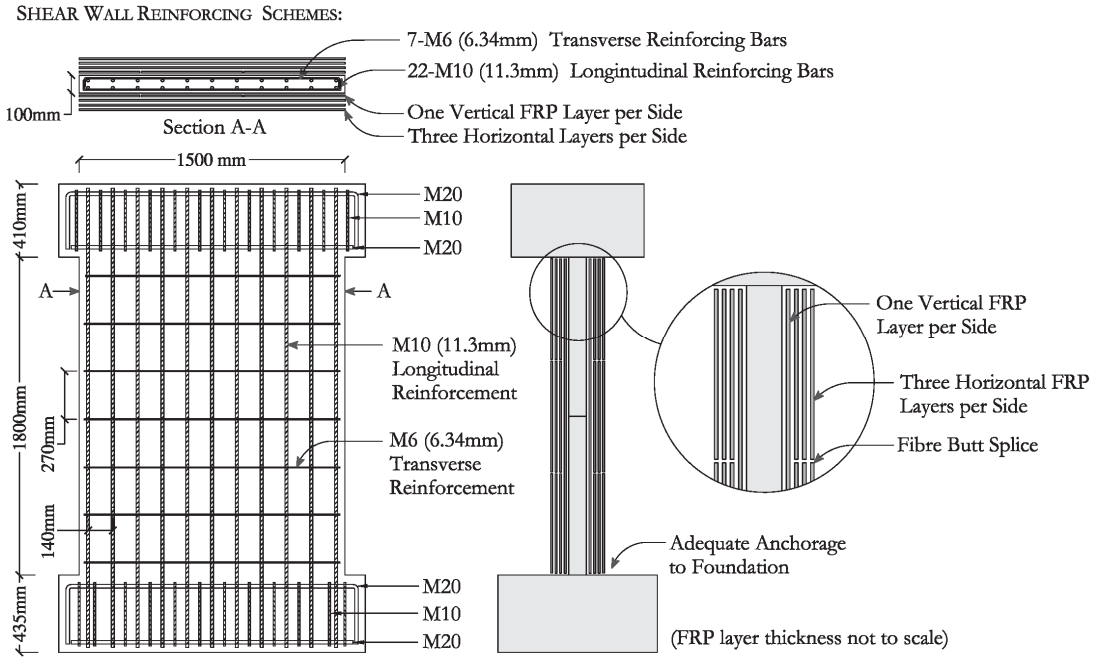

Figure 2-1: Steel and FRP Reinforcing Schemes.

To simulate the drift demand and damage effects on a reinforced concrete shear wall during a major seismic event, the wall specimens are tested under quasi-static cyclic load up to failure. The walls are secured to the laboratory strong floor and a hydraulic actuator applies the cyclic load to the top of the wall specimens. Axial load is not applied to the wall specimens because the primary focus of this study is on the shear dominant behaviour of the walls. The application of axial load would result in increased shear strength and reduce the need for shear strengthening, thus reducing the impact of the FRP retrofitting system. The wall specimens are first tested in load control by applying two successive cycles at 25%, 50%, 75% and 100%

of the estimated yield load. The estimated yield load is determined according to finite element models of the walls presented in a study by Shaheen (2014). The test is then continued in displacement control by increasing the target displacement ductility level up to failure. A typical cyclic load sequence for a wall specimen is shown in Figure 2-2. At each target displacement ductility level, the load cycle is repeated twice to simulate any softening effects the recursive load cycles may have on the strength and stiffness of the shear wall specimen. The load sequence is the same as those used in studies by Lombard (1999) and Hiotakis (2004) to be able to compare and contrast results from each study. Out-of-plane deformations of the wall specimen are minimized through the use of two one-way hinges located on either side of the hydraulic actuator, as shown in Figure 2-3. The hinges allow free rotation in the in-plane direction of the cantilevered wall specimen. Out-of-plane deformation are also limited by a lateral restraint frame located around the wall specimen which ensures that the load is applied to the test specimen in the in-plane direction.

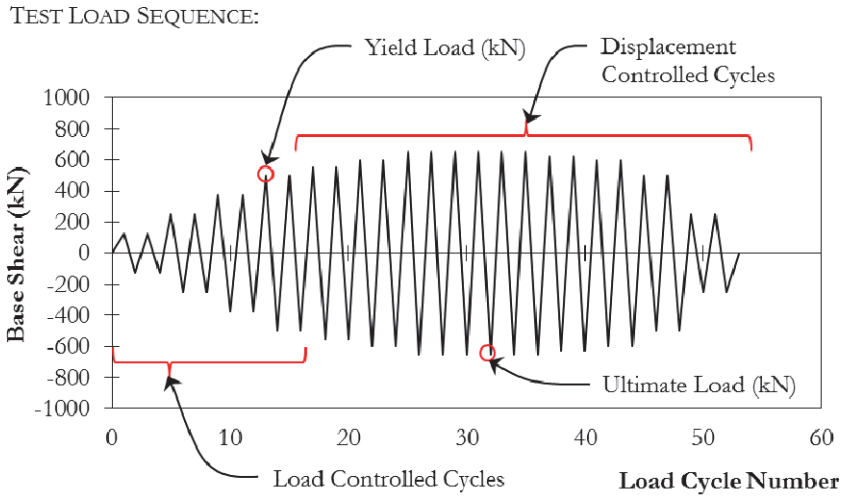

Figure 2-2: Typical Cyclic Lateral Load Sequence.

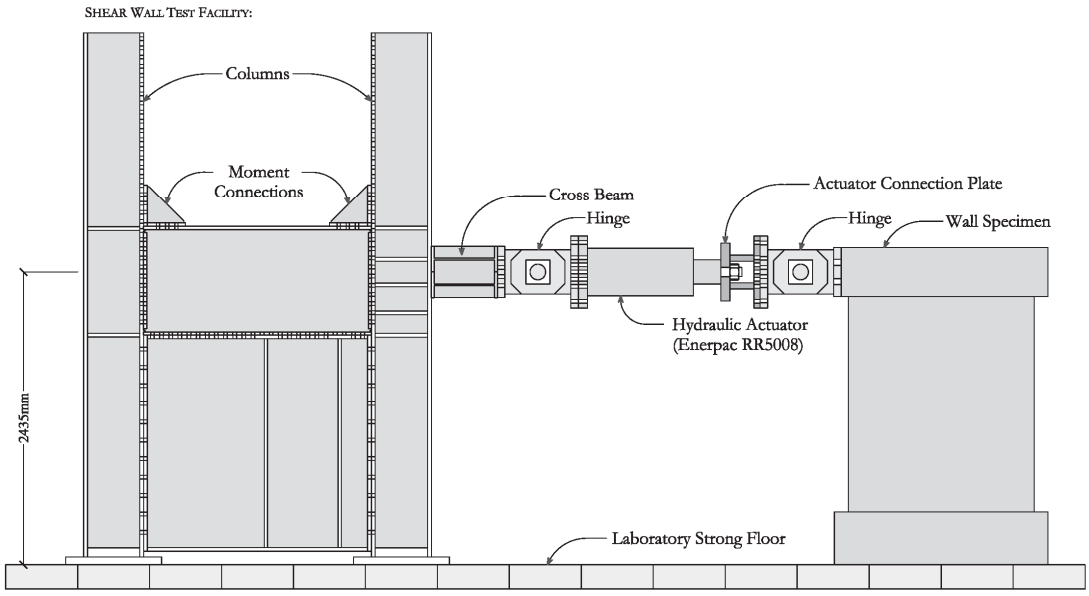

Figure 2-3: Shear Wall Test Setup.

2.2 MATERIAL PROPERTIES

The wall specimens are constructed with a lower strength concrete typically used in construction during the 1960s and 1970s. The concrete strength of the test specimens is determined according to concrete cylinder compression tests and results range between 15 and 25 MPa. The 28-day concrete compressive strength as well as the compressive strength on the day of each test are shown in Table 2-1. Grade 400 rebar is used for the vertical and horizontal reinforcement. Results from the average of three coupon tests for each size of reinforcing bar are shown in Table 2-1. Material specifications for the carbon fibre-reinforced polymer (CFRP) provided by the manufacturer (Tyfo SCH-41 CFRP) list the ultimate strength of the dry fibre as 4000 MPa, and has an ultimate strain of 1.7%. Material properties of the gross

composite laminate are determined by tests of FRP coupons measuring 50.8 mm (2 in) by 305 mm (12 in). The coupons are tested in an MTS universal testing machine using flat hydraulic grips and an extensometer is used to measure the elongation of the FRP coupon, as shown in Figure 2-4. Results of the tests show the CFRP laminate has an ultimate strength of 986 MPa, an ultimate strain of 1.0%, and an average young's modulus of 84,000 MPa. The lower strength of the gross laminate section is attributed to the brittle nature of the epoxy matrix, which effectively reduces the strength of the dry fibre. Average material strengths are summarized in Table 2-1 and typical stress-strain curves for the reinforcing bars, concrete cylinders and FRP coupons are shown in Figure 2-5. More detailed information on the materials used in the experimental program are available in Appendix A.

2.3 Shear Wall Instrumentation

The lateral load applied to the top of the wall specimens is measured using two pressure transducers for push and pull cycles. At the end of each load cycle, the test is stopped to record the progression of crack distributions and FRP debonding patterns. Each of the wall specimens has 30 strain gauges, as illustrated in Figure 2-6, to measure the strains along the horizontal and vertical reinforcement at the base, mid-height and top of the wall specimen. Displacements of the wall specimen are measured using 16 linear voltage differential transformers (LVDTs), which are also illustrated in Figure 2-6. Lateral displacements and rotations are measured at the base, middle, and top of the wall. Shear deformations are measured using two diagonally mounted LVDTs on the face of the wall specimen. Out-of-

Table 2-1: Average Material Properties for each Wall Specimen.

Concrete Properties		Steel Reinforcement Properties			FRP Properties		
Test Time	Compressive Strength (MPa)	Bar Size	Yield Strength (MPa)	Ultimate Strain (με)	FRP State	Ultimate Stress (MPa)	Ultimate Strain (%)
28 Day	24.0	6M	415	0.02	Dry Fibre	4000	1.7
SLCW	21.9	10M	440	0.141			
SLRW	20.6	15M	450	0.115	Gross Laminate	986	1.0
SLSW	19.7	20M	480	0.137			

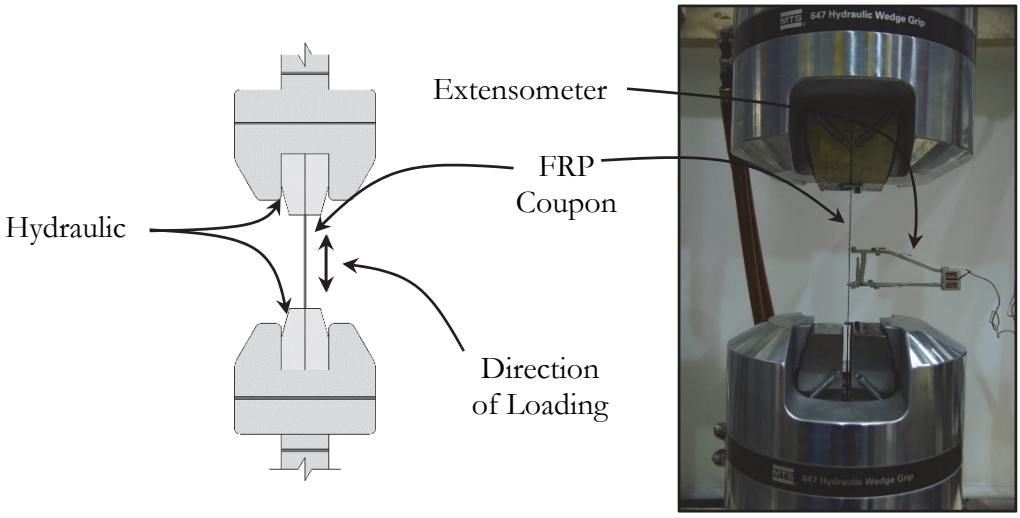

Figure 2-4: Typical FRP Coupon Test Setup

STRESS-STRAIN RESPONSE OF TEST MATERIALS:

(a)

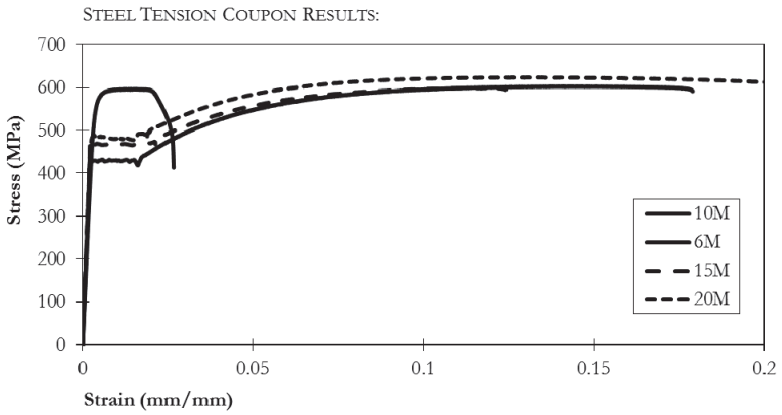

(b)

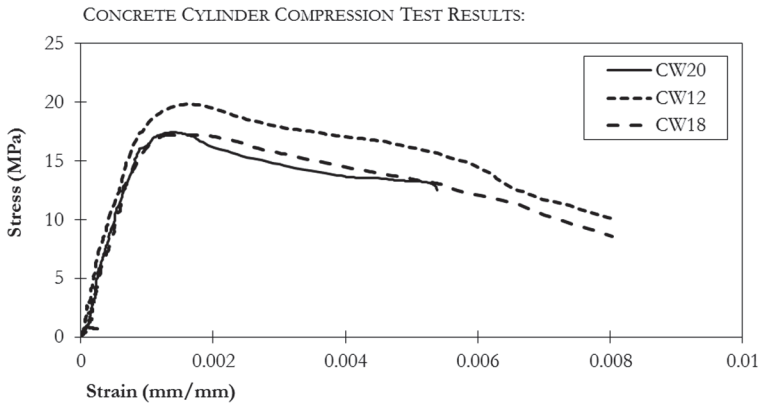

(c)

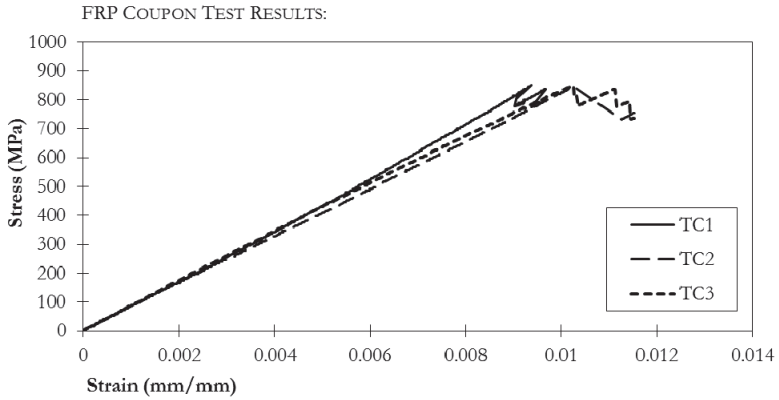

Figure 2-5: (a) Reinforcing Bar Stress-Strain Response; (b) Typical Concrete Cylinder Stress-Strain Response; (c) FRP Tension Coupon Stress-Strain Response.

plane displacement is monitored by two LVDTs attached to the cap beam on top of the wall specimen. The strain gauges are used to determine the propagation of yielding throughout the test specimen and the measured displacements can be analyzed to separate the shear and flexural behaviour of the wall. The spread of yielding throughout the steel reinforcement and displacement contributions from shear and flexural deformations are important factors for understanding the response behaviour and deformation mechanisms for comparing the ductility and energy dissipation characteristics of the test walls.

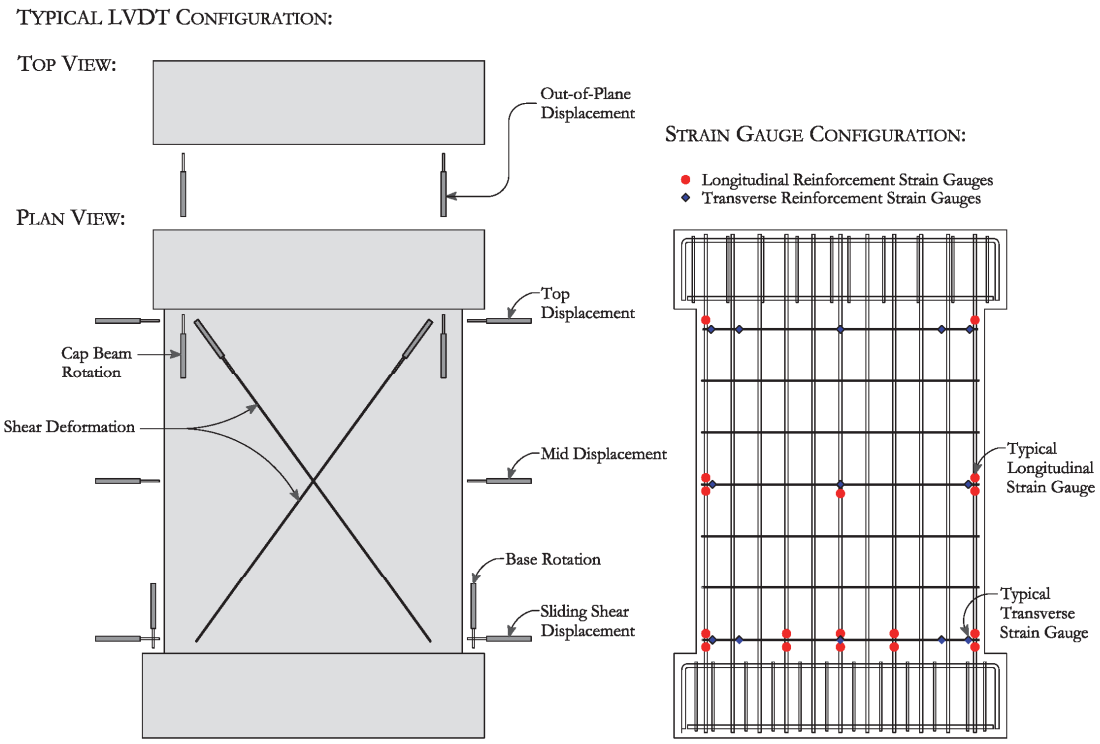

Figure 2-6: Typical Shear Wall LVDT and Strain Gauge Configuration.

2.4 Distributed Fibre Optic Sensor Strain Measurement

In this study, a new measurement technique is used to capture the strain distribution throughout the FRP sheet. The measurement system is a distributed fibre optic sensor (DFOS) based on the Broullion optical frequency domain reflectometry (OFDR) technique, which can measure strain at any point along the length of the optical fibre (Soller et al., 2005). A new polarization maintaining fibre (PMF), coupled with the latest advances in OFDR is used in the experimental program which allows a high resolution measurement of the flexural and shear strains in the FRP during the test. In the fibre optic measurement, location-dependent measurement sensitivities along the PMF are compensated by cross and auto-correlation measurements of the spectra. Simultaneous temperature and strain measurement accuracy in the order of 1 micro-strain and 0.1°C is achieved with 2.5mm spatial resolution in the use of a fibre 180m long. In this study, the fibre is first installed on the front side of the wall specimen in the horizontal direction and then continues to the back of the wall where it is applied to the FRP in the vertical direction (Figure 2-7). The fibre is oriented in separate horizontal and vertical directions on opposite sides of the wall to avoid interference between vertical and horizontal strain measurements. Results on the performance of the distributed fibre optic sensor system are presented in Section 5-3.

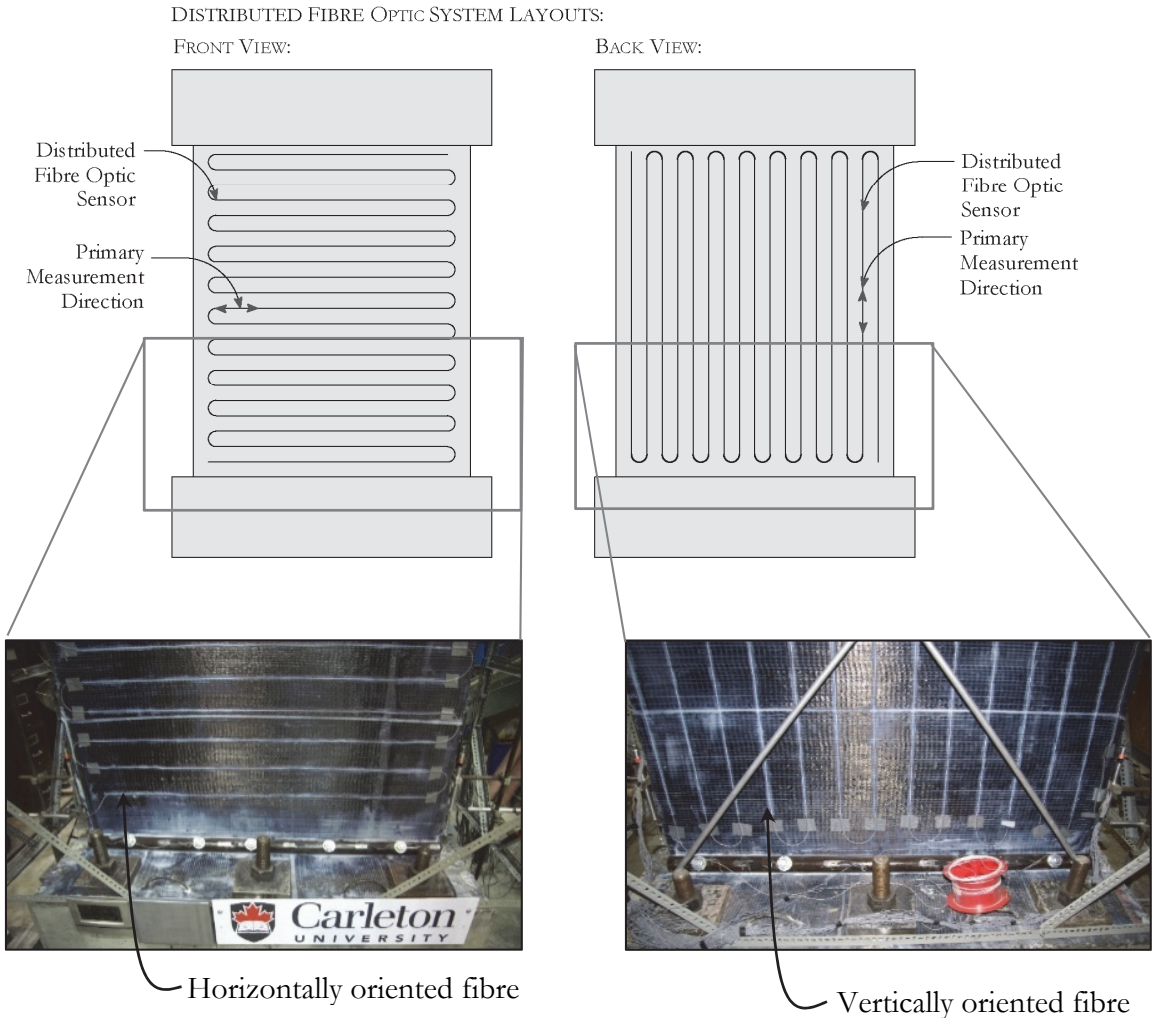

Figure 2-7: Primary Fibre Orientation on either Side of the Shear Wall Specimen.

CHAPTER 3: ANCHOR SYSTEMS

The use of fibre-reinforced polymer (FRP) composites for repair and strengthening of existing reinforced concrete (RC) elements has increased dramatically over the past two decades. Specifically, FRP has been used in retrofitting applications to increase the stiffness and strength of RC elements leading to improvements in ductility and energy dissipation capacity. All of these factors contribute to improving the seismic performance of the RC element and the safety of the structure. When externally bonded FRP sheets are utilized in the strengthening or retrofit of reinforced concrete members (such as beams, columns, and walls) the optimal mode of failure is controlled by crushing of the concrete and/or rupture of the FRP sheets after yielding of the steel reinforcement (Grelle and Sneed 2011). However, it is commonly recognized that in many cases, failure of the FRP strengthening system through debonding of the FRP sheets from the concrete substrate occurs prior to the FRP material reaching its ultimate tensile capacity, preventing the member from reaching its design strength (Lombard et al., 2000; Teng et al., 2002; Cruz et al., 2014). In studying FRP reinforcing systems, various FRP anchor systems have been developed in an attempt to eliminate or at least minimize FRP-concrete debonding before the FRP reaches its ultimate tensile strength. Early studies on the use of FRP anchor systems focused on the strengthening of RC beams and slabs and found that optimal design performance can be achieved when effective anchor systems are implemented (Triantafillou, 1998; Smith and Teng, 2003). More recent studies on

reinforced concrete shear walls by Lombard et al. (2000), Hiotakis (2004), and El-Sokkary et al. (2013) on the strengthening and repair of RC shear walls using FRP sheets each conclude that special attention should be taken to providing adequate anchorage of the FRP reinforcement, especially in preventing premature debonding failures. This thesis presents a brief review of several FRP anchor systems available in the seismic strengthening and retrofit of RC members and discusses in more detail two mechanical anchor systems developed and tested at Carleton University, including a steel angle anchor and an innovative tube anchor system. Based on insights gained from observations of the anchor systems in reversed cyclic tests of reinforced concrete shear walls, this thesis presents the development of an innovative tube anchor that eliminates premature debonding failures associated with many other anchor systems. Detailed finite element (FE) analyses are conducted on the mechanical anchor systems. Results of the FE simulations of the two anchor systems used in the seismic retrofit of RC shear walls using externally bonded FRP sheets are compared with measured data from experimental testing in the next chapter.

3.1 Debonding Mechanisms

The performance of FRP anchor systems is a crucial component in the design of an FRP strengthening system. By allowing the FRP laminate to reach its ultimate tensile capacity without premature failure, such an anchor system is able to enhance the efficiency of the FRP strengthening system. However, premature failure of the FRP strengthening system characterized by debonding or peeling of the FRP sheet(s) from the concrete substrate leading to rupture of the FRP fibres prior to reaching its ultimate capacity is a commonly reported

problem identified as a challenging performance issue in many investigations (Lombard, 1999; Grelle and Sneed, 2011). Several failure modes for FRP-strengthened members have been identified in previous experimental investigations which are summarized by Kalfat et al. (2013). In that study, the authors identify concrete crushing and/or rupture of the FRP sheets after yielding of the steel reinforcement as the optimal failure mode in RC elements strengthened with externally bonded FRP sheets. After the steel reinforcement yields, additional load applied to the member is carried by the FRP sheets, resulting in the spread of inelastic behaviour throughout the remaining longitudinal steel reinforcement. The applied load on the member will continue to increase causing crushing of the concrete and rupture of the FRP at its ultimate tensile capacity. Rupture of the FRP sheets propagates along the length of the member until a significant drop in load carrying capacity occurs. This is considered the optimal failure mode because the full strength of the FRP material is utilized prior to failure of the member, resulting in the maximum efficiency of the retrofitting scheme. Other common failure modes in RC members strengthened using FRP include intermediate crack (IC) debonding, critical diagonal crack (CDC) debonding, and end interfacial delamination, as illustrated in Figure 3-1. These failure modes are those associated with premature failure of the FRP-strengthening system, which is attributed to FRP-concrete debonding mechanisms. The IC and CDC debonding mechanisms originate from a flexural crack or an inclined shear crack which then propagates parallel to the FRP-concrete substrate interface leading to debonding of the FRP material (Pham & Al-Mahaidi, 2004). End interfacial delamination is attributed to a lack of anchorage force in regions where the force carried by the FRP cannot be fully developed leading to delamination of the FRP sheet from the concrete substrate. End

interfacial delamination is the most common failure mode observed in experimental investigations of FRP-strengthening systems (Pham & Al-Mahaidi, 2004). However, through the implementation of an appropriately designed and detailed anchor system, end interfacial delamination can be avoided resulting in an increase in force sustained by the FRP sheet. Therefore the adoption of an anchor system can prevent end interfacial delamination and lead to more desirable failure modes in FRP reinforced members. In the seismic strengthening of RC elements, these desirable, typically flexural failure modes result in an increase in strength and ductility when compared to brittle failures associated with shear. This results in improved seismic performance of the retrofitted element, improving the safety of the structure during an earthquake.

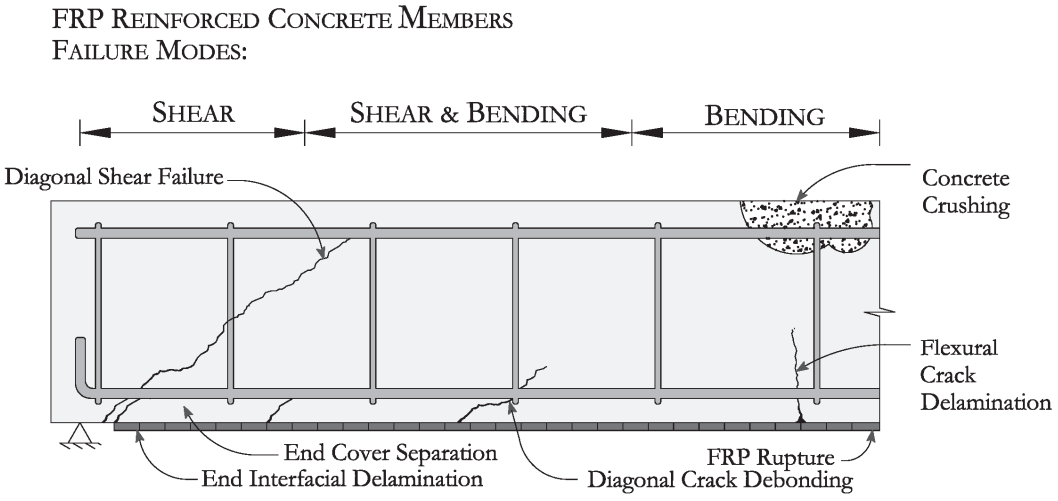

Figure 3-1: FRP Debonding Mechanisms.
(Adapted from Pham & Al-Mahaidi, 2004)

3.2 Conventional FRP Anchor Systems

To date, various anchorage systems have been developed with the goal of preventing premature debonding failure in RC members repaired or strengthened using externally bonded FRP sheets. These anchor systems have all been designed with the performance objective of allowing the FRP sheet to rupture without premature slippage/peeling from the concrete substrate. Anchor systems aim to achieve this performance objective through one or more of the following design principles: 1) preventing premature debonding failure by resisting tensile forces developed within the FRP; 2) reducing the required development length to within appropriate lengths; or 3) transferring the full force from the FRP laminate to adjacent supporting structural elements (Grelle & Sneed, 2011). As discussed by Kalfat et al. (2013), the wide variety of existing anchor systems can be grouped into three general categories: FRP anchors, U-shaped anchors, and mechanical anchorage systems, as shown in Figure 3-2. Fibre-reinforced polymer anchors, referred to in some cases as spike or fan anchors, are fabricated from strands of bundled composite fibres. At one end, the fibres are splayed and embedded within the composite matrix; at the other end the fibres are bundled together into a dowel and inserted into a predrilled hole within the adjacent supporting structural element (Figure 3-2). Although it has been shown in tests by Zhang and Smith (2012) and Lam and Teng (2001) that FRP anchors are capable of increasing slip capacity of FRP-concrete joints significantly, the failure of RC elements strengthened using FRP sheets anchored with fan or spike anchors is sudden and brittle in nature upon rupture/slippage of the FRP dowel prior to the laminate sheet reaching its rupture capacity. Alternatively, U-anchors aim to increase the capacity of RC

elements in FRP repair or strengthening schemes through an increase in FRP-to-concrete bond length. U-anchors are installed by forming a groove at or near the termination of an FRP sheet. The FRP material is then fitted into the groove which is subsequently filled with an epoxy resin. In some instances, a steel or FRP rod is placed inside the groove after placing the FRP sheet, as illustrated in Figure 3-2. The U-shaped anchor system increases the anchorage force in an FRP strengthening system by providing additional concrete-FRP bond length along the surface of the groove. Although U-anchors have been shown to be effective in delaying premature debonding in tests by Khalifa et al. (1999) and Ceroni et al. (2008), failure of such an anchor system is brittle and non-ductile once the FRP material begins to peel from the concrete groove prior to the FRP sheet reaching its ultimate tensile capacity (Kalfat et al., 2013). Alternatively, mechanical anchor systems are designed to increase the capacity of FRP repair and strengthening systems through the use of a structural section at the termination of an FRP sheet. The most common structural sections used in anchorage applications include steel plates, angles and tubes, as illustrated in Figure 3-2. In most cases, a steel structural section is bolted into adjacent supporting structural elements to transfer tensile stresses from the FRP sheets. For construction purposes, the use of steel sections as an FRP anchor is an attractive option because the anchor can be readily fabricated (Grelle & Sneed, 2011). Mechanical anchorage systems can also be designed to fail in a ductile manner, to give warning of impending failure and assist with energy dissipation. Research conducted by Kanakubo et al. (2000), Hall et al. (2002) and Hiotakis et al. (2004) has demonstrated that a mechanical anchor system implemented in the repair or strengthening of RC shear walls improved the performance of the wall and the efficiency of the retrofitting system by fully utilizing the tensile

strength of the FRP material. It is also reported that mechanical anchor systems provide higher anchorage strength when compared to non-metallic anchor systems including FRP and U-shaped anchor systems (Kalfat et al. 2013). Given the comparatively better performance of mechanical anchor systems, this study focuses on the behaviour and performance of mechanical anchorage devices to evaluate their effectiveness and develop design guidelines for their application in FRP-strengthening systems. The application of a mechanical anchor system allows the member to exhibit ductile behaviour through yielding of the reinforcing steel before rupture of the FRP sheets, resulting in good seismic performance of the retrofitted RC structure.

3.3 Angle Anchor System

Mechanical anchor systems can be configured to meet design requirements in a wide range of applications due to their common availability in an array of sizes, materials and geometries. One of the most common mechanical anchor systems is a steel angle anchor system in which one flange of the steel angle is bonded to the vertical FRP sheet(s) while the other is bolted to adjacent structural elements using steel anchor rods. The angle anchor system is designed to transfer stresses from the FRP sheet to the walls foundation through the flange of the steel angle which is epoxy-bonded to the FRP. Observations by Lombard et al. (2000) and Kanakubo et al. (2000) show that the steel angle anchor system tends to facilitate debonding of the FRP material from the concrete wall prior to the FRP material reaching its ultimate capacity. Failure of the steel angle anchor system occurs as a result of an eccentricity

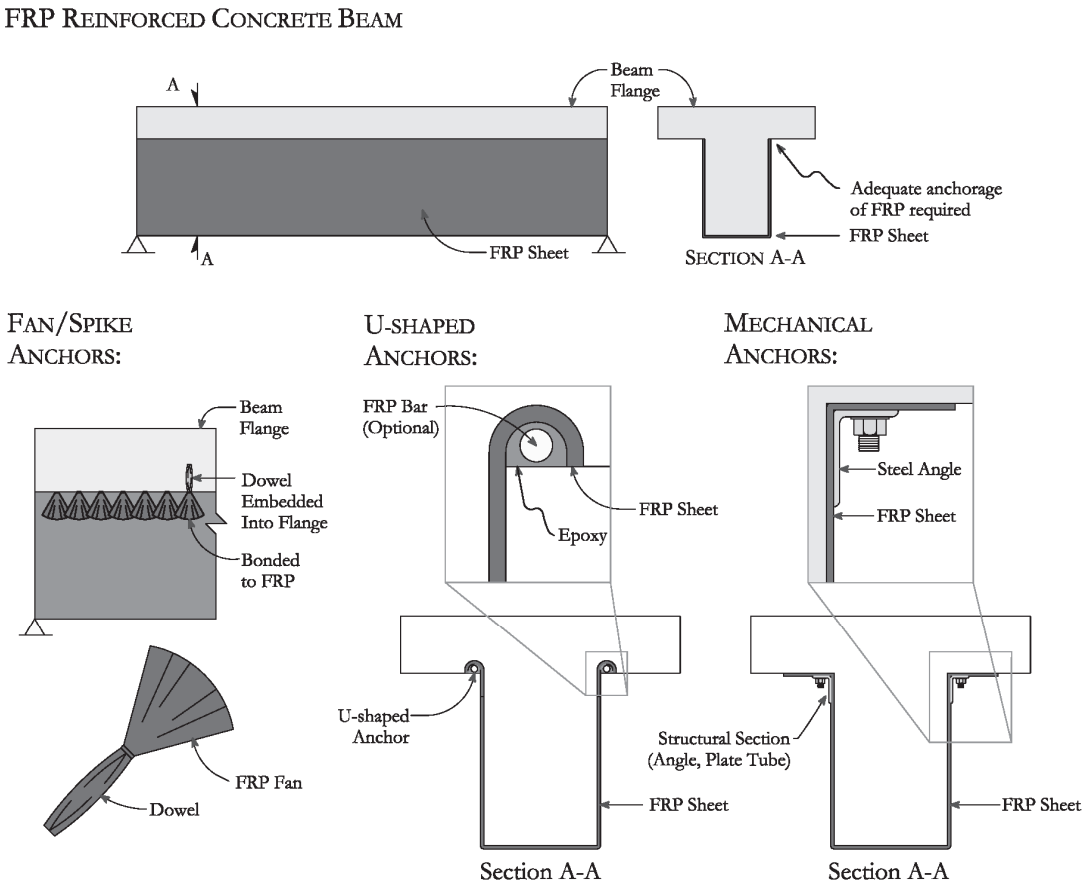

Figure 3-2: Different Types of Systems used to Anchor FRP Sheets.

between the tensile force carried by the FRP sheet and the tie-down reactions of the anchoring bolts, as illustrated in Figure 3-3(a). As the FRP is loaded in tension, the eccentricity between these two forces causes a moment which leads to rotation of the steel angle, also referred to as "prying" action, which is illustrated in Figure 3-3(b). During the cyclic response of the wall specimen, the prying or rotation of the steel angle leads to debonding as the flange of the angle pulls away from the surface of the wall, shown in Figure 3-4. When the load is reversed, the debonded FRP sheet buckles in compression in the polymer matrix between high strength fibres. Buckling of the debonded FRP sheets leads to fracture of the hardened epoxy matrix leaving a sharp edge along the fractured FRP sheet, which can easily cut the FRP fibres before they reach their ultimate rupture capacity, as shown in Figure 3-4. This observed behaviour effectively reduces the load carrying capacity of the FRP sheet, rendering the reinforcing scheme less efficient and lowering the ultimate load resistance capacity of the retrofitted/strengthened member.

3.4 TUBE ANCHOR SYSTEM

Motivated by the observed behaviour of the commonly used steel angle anchor system, in which the prying action between the anchor and the FRP sheet(s) leads to premature debonding of the FRP material from the concrete substrate, this thesis presents an innovative anchor system fabricated of a cylindrical hollow section (CHS), around which the FRP sheet is wrapped and anchored to the adjacent supporting structural element. The tube is bolted into the supporting concrete element by placing several steel anchor rods at a 45 degree along the

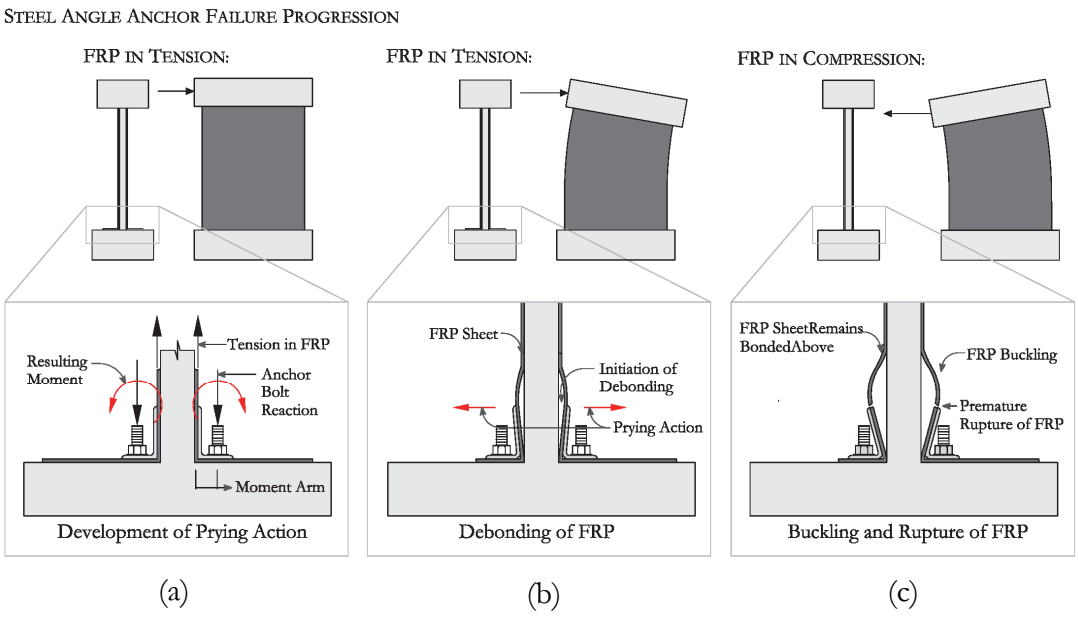

Figure 3-3**:** Steel Angle Anchor Failure Progression.

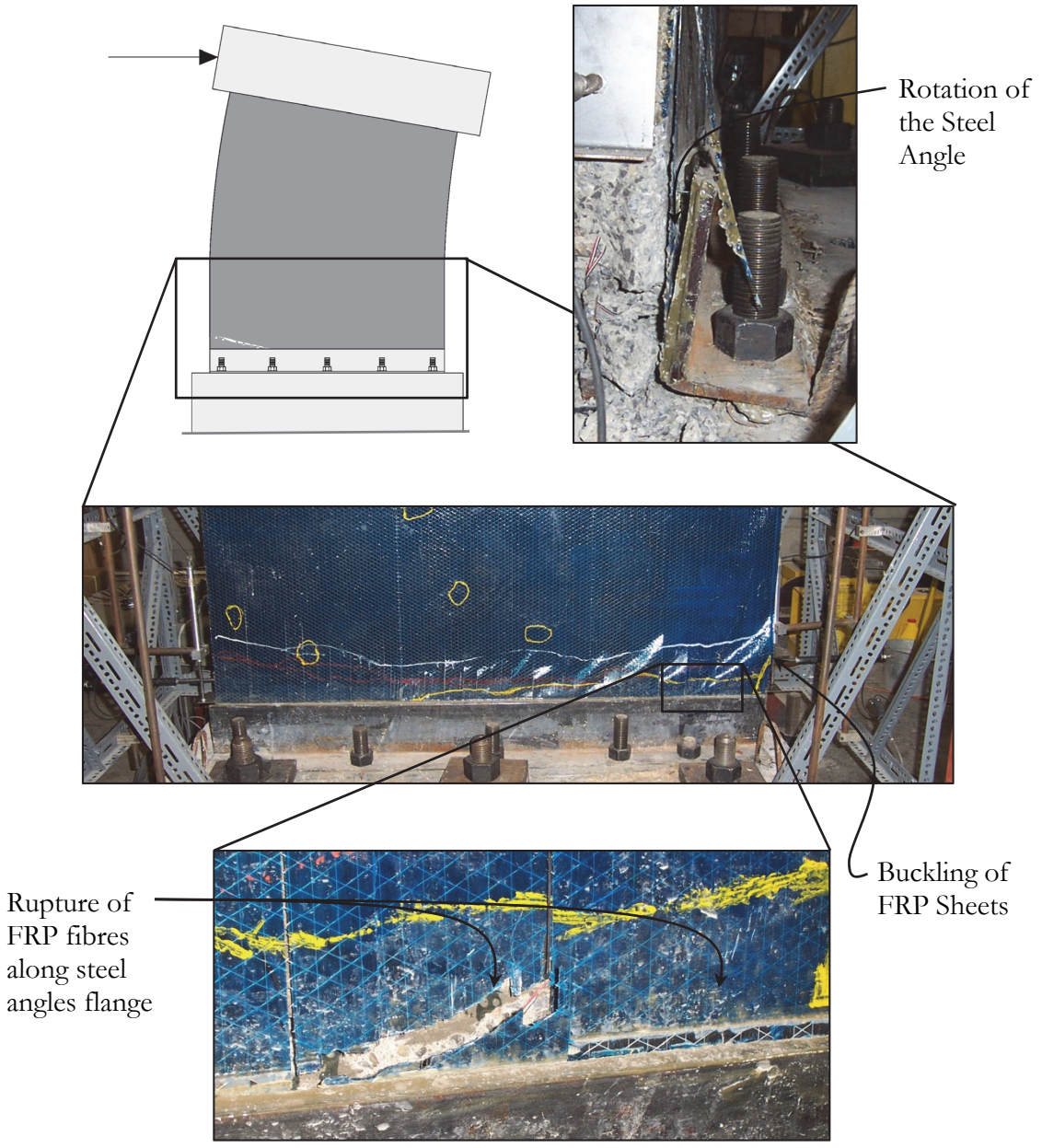

Figure 3-4: Rotation of the Steel Angle, Debonding, and Rupture of the FRP Fibres. (Images from Lombard, 1999)

length of the anchor, as illustrated in Figure 3-5. The design of the anchor is based on the pulley principle: as the FRP sheet is loaded in tension, the vertical force in the FRP sheet(s) is equated by the tension in the horizontal portion of the FRP sheet(s) which must be provided with the appropriate development length (Figure 3-5).

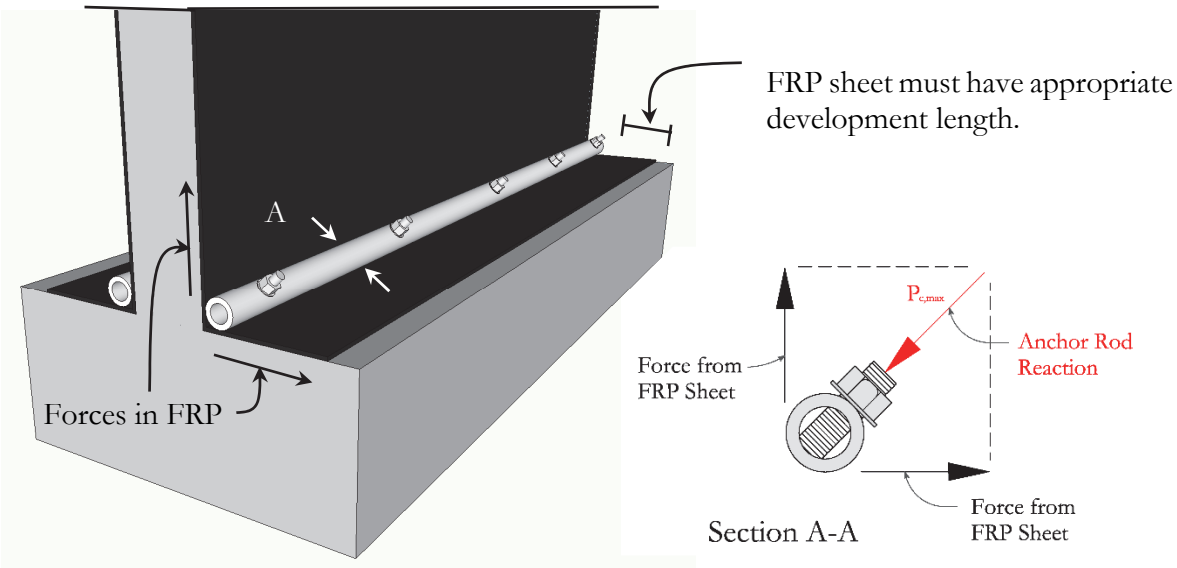

Figure 3-5: Forces acting on the Tube Anchor System.

As outlined in the ACI440.2R-08 guidelines for the application of externally bonded FRP systems, it is recommended that to develop the effective FRP stress at a section, a minimum length of the FRP sheet must be bonded to the concrete element (l_{df}), as determined by Equation 1

$$l_{df} = \sqrt{\frac{n_s E_f t_s}{\sqrt{f'_c}}} \qquad (1)$$

where n_s represents the number of FRP sheets requiring development, E_f is the modulus of elasticity of the FRP composite, t_s is the thickness of the FRP sheet and f'c is the compressive

strength of the concrete to which the FRP is bonded (Teng et al., 2001). The threaded anchor rods installed at a 45 degree angle transfer the resultant component of the load from the FRP sheets into the concrete foundation. By wrapping the FRP sheet around the tube and placing the anchor bolts in the direction of the resultant load, the eccentricity between the forces carried the FRP sheets and the anchor bolts is eliminated. Experimental results and observations by Hiotakis (2004) shows that the anchor system performs well in transferring the load between the FRP laminate and adjacent supporting structural elements. The FRP sheet is capable of reaching its ultimate tensile strength without premature debonding of the FRP sheets from the concrete. Preliminary observations suggest that the tube anchor system eliminates the previously discussed deficiencies associated with other anchor systems and allows the FRP material to reach its full tensile capacity before rupture, shown in Figure 3-6, thus maximizing the efficiency of the FRP repair or strengthening scheme. The increase in efficiency can be clearly identified by comparing the hysteretic response of two shear wall specimens with identical steel and FRP reinforcement details tested by Lombard (1999) and Hiotakis (2004), one of which is implemented with the steel angle anchor system and the other with the tube anchor system (Figure 3-7). It is shown that through implementation of the tube anchor system, significant improvements in strength, ductility and energy dissipation capacity in reinforced concrete shear walls is achieved when compared to the same wall with the angle anchor system. These factors contribute to an increase in the efficiency of the retrofitting scheme and better seismic performance of the wall. This study aims to improve the design of the tube anchor system when compared to the previous study by Hiotakis (2004) through an optimization study of the tube anchor system to ultimately develop a more efficient design.

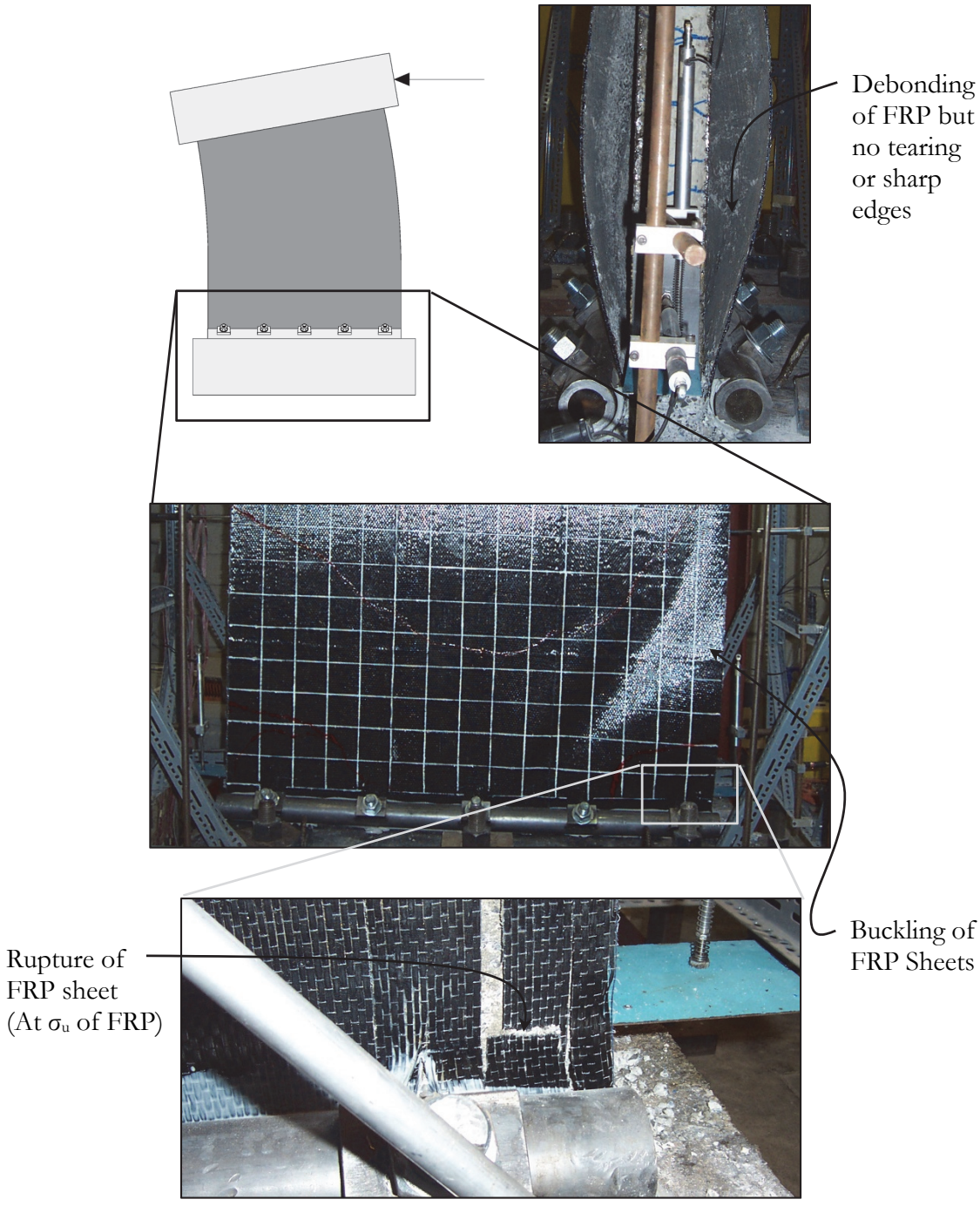

Figure 3-6: Tearing of FRP Fibres in Tube Anchor System.
(Images from Hiotakis, 2004)

COMPARISON OF ANGLE AND TUBE ANCHOR SYSTEMS:

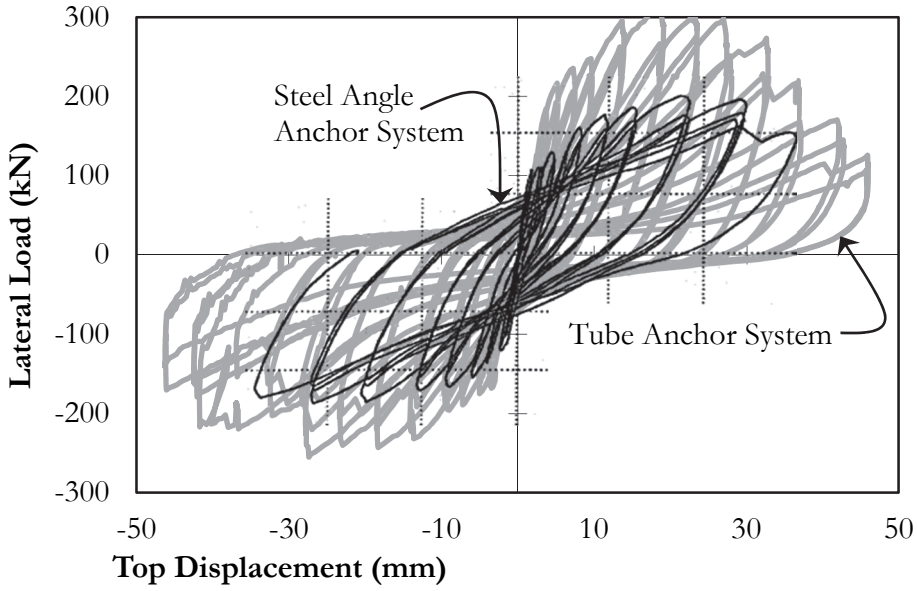

Figure 3-7: Wall Hysteretic Response with Angle and Tube Anchor Systems.
(Results from Lombard, 1999 and Hiotakis, 2004)

CHAPTER 4: ANALYTICAL MODELLING OF MECHANICAL ANCHOR SYSTEMS

In previous studies by Lombard (1999) and Hiotakis (2004) the performance of the angle and tube anchor systems in experimental tests on reinforced concrete shear walls retrofitted with FRP sheets is observed. Results show that the tube anchor system performs better than the angle anchor system by allowing full utilization of the high strength capacity of the FRP sheets without premature failure due to debonding of the FRP sheets from the concrete substrate. However, the studies by Lombard (1999) and Hiotakis (2004) lack analytical results to confirm the behaviour of the systems observed during experimental tests. To gain a better understanding of the behaviour and performance of the angle and tube anchor systems and to assist in the design of the tube anchor system the finite element (FE) computer package ABAQUS v6.10 is used to analyze both anchor systems under simulated seismic load demands.

4.1 IDEALIZED SEISMIC LOAD PATTERN

An assumed load distribution pattern is applied to the tube anchor system based on an idealized loading condition in a laterally loaded reinforced concrete shear wall strengthened with externally bonded FRP reinforcement. When a reinforced concrete shear wall is cyclically loaded by a horizontal force applied at the top of the wall, the tensile forces carried by the FRP sheet increases with the increase in the applied load until the ultimate tensile strength is reached at the edge of the wall. It is assumed that the load applied to the FRP sheet follows a

linear distribution up to the neutral axis of the wall specimen, as illustrated in Figure 4-1, which has been shown through finite element simulations by Hassan et al. (2013) to be a reasonable assumption. However, it is assumed that minor variations in the load distribution would not have a significant impact on the overall performance of the anchor system. Based on previous studies by Hassan et al. (2013) and Cruz-Noguez et al. (2014), it is assumed that the neutral axis lies at approximately 85% of the shear walls length.

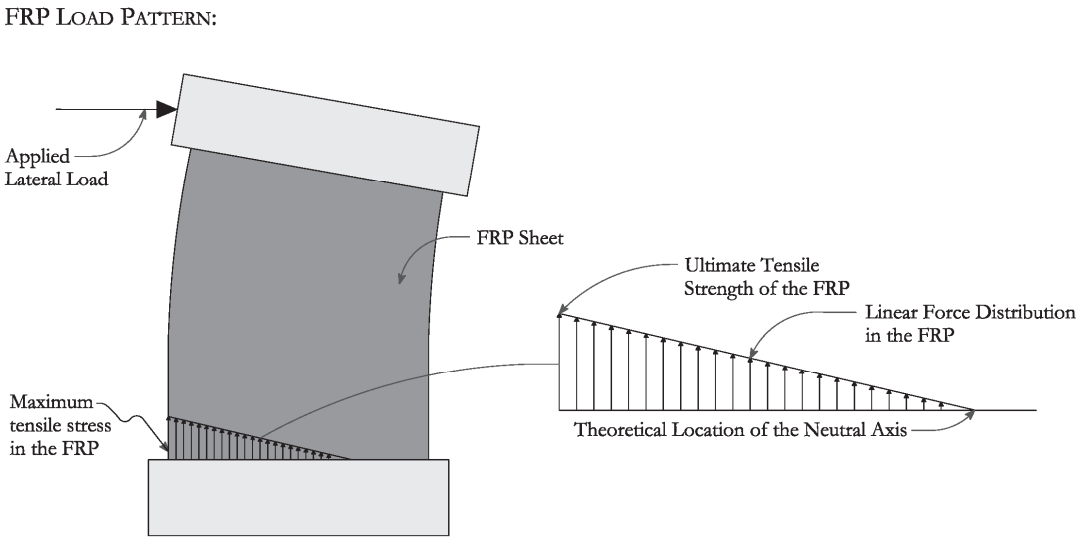

Figure 4-1: Idealized Seismic Force Distribution acting on the Anchor System.

The force carried by the FRP sheet is then transferred to the anchor system and into adjacent structural elements through several anchor bolts located along the anchor. At regions between adjacent anchor bolts, the load from the FRP sheet is resisted by the anchors structural section.

The load carried by the FRP sheet is distributed as a pressure over the area of steel in contact with the FRP sheet. The maximum resultant load ($P_{c,max}$) carried by the FRP sheets can be determined using Equation 2 as follows

$$P_{c,\max} = \sqrt{2}\sigma_u t_s n_s \tag{2}$$

where σ_u is the ultimate tensile capacity of the FRP material. Depending on the type of structural section used for the anchor, the resultant load must be converted into a pressure acting over the area of steel in contact with the FRP. This is computed for the steel angle and tube anchor systems in Sections 4-2 and 4-3.

4.2 Modelling of Steel Angle Anchor

A study on the application of the angle anchor system has been conducted by Lombard et al. (2000). In that study, the angle anchor system is tested in the seismic retrofit of RC shear walls. The system is shown to be deficient due to a prying action which results in rotation of the steel angle, causing debonding of the FRP sheets from the concrete substrate and early rupture of the FRP sheet prior to reaching its ultimate tensile capacity. This behaviour reduces the efficiency of the retrofitting scheme by not being able to utilize the full capacity of the FRP, which leads to lower strength, ductility and energy dissipation capacity in the shear wall resulting in a lower level of seismic performance. In this study, the steel angle anchor is modelled to capture the behaviour of the anchor system and to verify the observed experimental performance by Lombard (1999). The angle anchor system is fabricated using a

150x100x10mm off-the-shelf steel angle. The anchor bolts of 31.75mm diameter are spaced along the length of the angle, as shown in Figure 4-2(a).

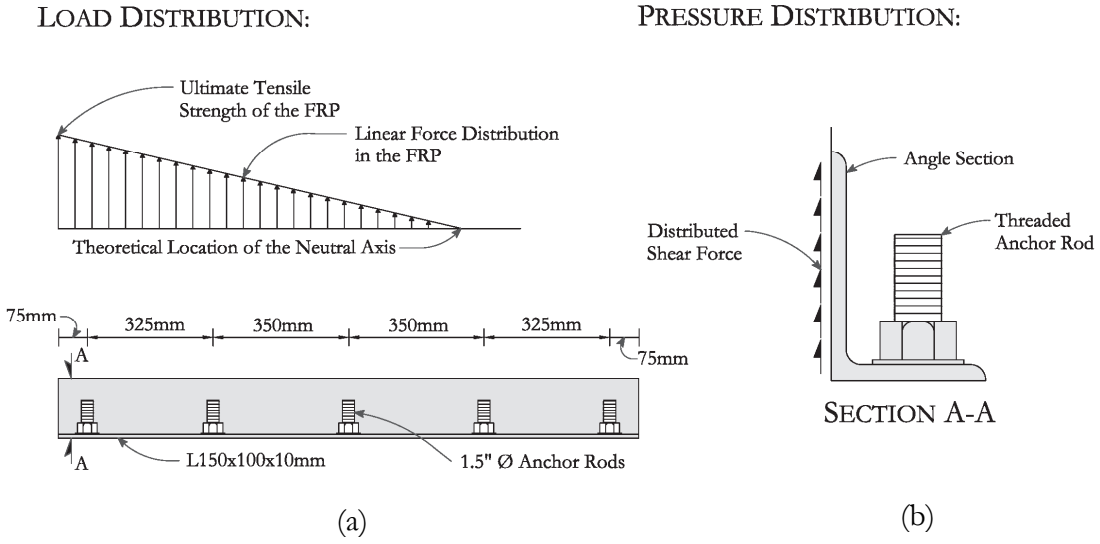

Figure 4-2: (a) Geometry of Angle Anchor; (b) Applied Force on Angle Anchor.

The behaviour and performance of the angle anchor system is analyzed using a finite element model. The steel materials are modelled by a bi-linear stress-strain relationship in which the material behaves linearly up to the yield stress after which the material reaches a constant yield plateau. Material properties for the components of the angle anchor system are shown in Table 4-1. Finite elements of 8 node solid brick elements (CD3D8R) are used to model the steel components of the angle anchor system. A mesh refinement analysis is conducted to determine the optimal mesh size to improve the efficiency of the model and hourglass control is used to prevent warping of the rectangular elements, a requirement for linear reduced integration elements.

Table 4-1: Steel and FRP Material Properties for Steel Angle Anchor Modelling.

Steel Properties	Elastic Modulus (MPa)	Yield Stress (MPa)	Ultimate Stress (MPa)	Poisson's Ratio	Grade
Steel Angle	200,000	400	500	0.3	CSA G40.21
Anchor Rods	200,000	558.5	827.4	0.3	Grade 5
FRP Properties	Tensile Modulus (MPa)	Tensile Strength (MPa)	Ultimate Elongation (me)	Density (g/cm^2)	Weight (g/m^2)
Master Builders CF150	230,000	3480	1.5%	1.74	20.0

The idealized load pattern acting on the steel angle anchor system is determined based on the methodology presented in Section 4-1. The resultant load carried by the FRP sheet ($P_{c,max}$) is distributed as a shear force acting over the angle's flange (Figure 4-2(b)) which is bonded to the FRP. This force varies linearly from the end of the anchor to the theoretical neutral axis location. The maximum shear stress acting on the flange of the steel angle can be determined as follows

$$\tau_{\max} = \frac{\sigma_u n_s t_s}{d_f} \tag{3}$$

where d_f represents the height of the flange of the steel angle. The load acting on the angle is determined based on the material properties of a single FRP sheet, which results in a maximum shear stress of 2.55 MPa applied as a linear distribution of shear force along the area of flange in contact with the FRP. It is assumed for modelling purposes that the FRP sheet remains perfectly bonded to the flange of the angle. This force is assumed to decrease linearly to zero

at the assumed location of the neutral axis 1275mm from the end of the anchor (85% of the anchors length) (Hassan et al., 2013; Cruz-Noguez et al., 2014).

The deformation behaviour of the steel angle anchor model correlates well with the observed behaviour during experimental tests discussed by Lombard (1999). Analytical results confirm that the eccentricity between the force applied to the angle from the FRP and the reaction force within the anchor bolts results in the prying or rotation of the flange of the angle, as shown in Figure 4-3.

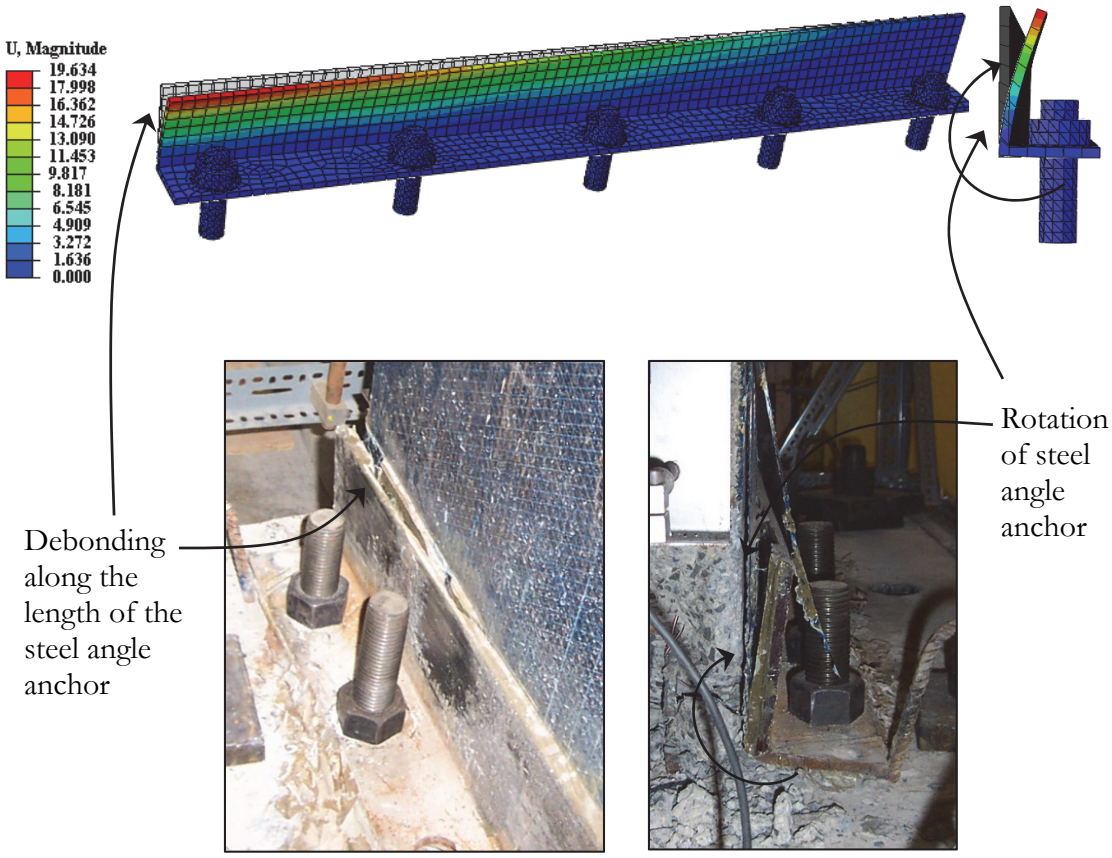

Figure 4-3: Analytical and Experimental Behaviour of Angle Anchor.
(Images from Lombard, 1999)

The observed rotation of the steel angle in experimental tests and analytical models leads to premature failure of the strengthening scheme due to large rotation of the angle causing debonding of the FRP sheet from the concrete substrate. Maximum displacement of the angles flange occurs at the edge of the wall, where the highest load is carried by the FRP sheet, and is approximately 20mm when the fibres rupture according to experimental observation reported by Lombard et al. (1999). The analytical model predicts an ultimate displacement of 19.6mm at the point in which the FRP sheet reaches 60% of its ultimate tensile capacity, as shown in Figure 4-4, which shows the relationship between the force applied to the angle in a percentage of the ultimate capacity of the FRP sheet and the displacement of the tip of the angle. This correlates well with experimental observations and confirms that there is a significant loss in efficiency of the FRP retrofitting system as a result of the prying action of the steel angle anchor system, as the FRP sheet is only able to reach 60% of its ultimate capacity prior to debonding from the concrete substrate. Separation of the FRP from the concrete leads to premature rupture of the FRP sheet during subsequent load cycles as the FRP buckles in compression, fracturing the polymer matrix between fibres and rupturing the high strength fibres along the top of the angles flange. Experimental observations on the performance of the steel angle anchor by Lombard (1999) leads to the development of a new tube anchor system by Lau, Hiotakis, and Londono (Hiotakis, 2004), with the ability to eliminate premature failure of the FRP fibres and allow the FRP sheet to reach its ultimate tensile strength. By ensuring rupture of the FRP material only after it reaches its full tensile capacity and yielding of the steel reinforcement, maximum strength and ductility

is achieved in the retrofitted RC member. Improving the seismic performance of the retrofitted RC member results in a reduction in seismic risk to the structure and its occupants.

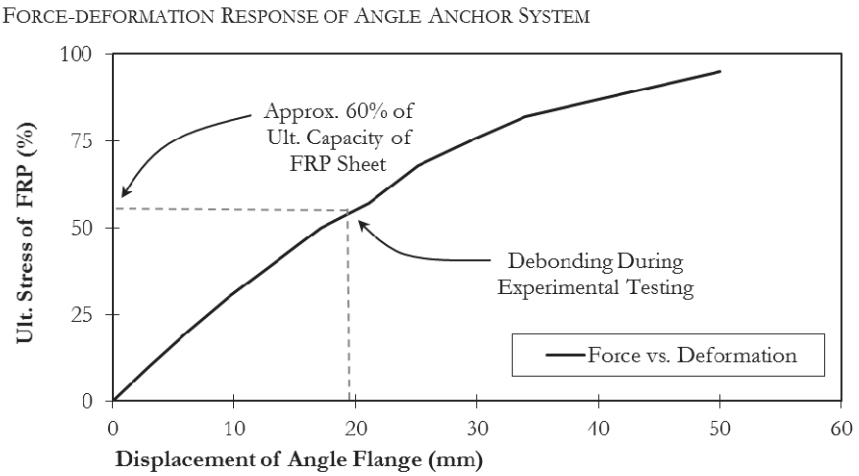

Figure 4-4: Force-deformation Response for the Flange of the Steel Angle Anchor.

4.3 MODELLING OF TUBE ANCHOR SYSTEM

Motivated by the observed behaviour of the steel angle anchor system, a new tube anchor system which eliminates premature failure of the FRP retrofitting system, resulting in an increase in efficiency of the retrofitting system is developed at Carleton University. To study the response of the tube anchor system under varying loads, boundary conditions and different geometric configurations, a rigorous finite element (FE) model of the tube anchor system is developed. A feasibility study of the tube anchor system has been conducted by Hiotakis (2004). In this study, the tube anchor system is tested in the seismic retrofit of RC shear walls. In earlier versions of the anchor, the tube is designed to remain elastic under the applied loading, determined by FE analysis. Based on these analyses, the tube anchor is fabricated

using a 76.2mm (3.0 in.) diameter cylindrical hollow section (CHS) with a wall thickness of 12.7mm (0.5 in.). The anchor bolts of 38.1mm (1.5 in.) diameter are placed at five locations along the length of the tube, spacing for which is shown in Figure 4-5(a). Specially fabricated convex washers are placed on the anchor rod under the head of the anchor bolt to minimize the high stress concentration at the contact zone between the anchor rod nut and tube anchor, as illustrated in Figure 4-5. The steel materials are modelled by a bi-linear stress-strain relationship in which the steel material behaves linearly up to the yield stress, at which point the material reaches a constant yield plateau. Material properties of the components of the tube anchor system are shown in Table 4-2.

Table 4-2: Steel Material Properties for Analytical Modelling.

Steel Properties	Elastic Modulus (MPa)	Yield Stress (MPa)	Ultimate Stress (MPa)	Poisson's Ratio	Grade
Tube Section	200,000	400	500	0.29	CSA G40.21
Anchor Rods	200,000	400	515	0.3	Grade 316
FRP Properties	Tensile Modulus (MPa)	Tensile Strength (MPa)	Ultimate Elongation (me)	Density (g/cm^2)	Weight (g/m^2)
MRL-T7-200W Reno CFRP	235,000	4800	1.7%	1.74	20.0

The contact between the base of the convex washer and the curved pipe and the contact between the threaded anchor rods and steel pipe is modelled by a surface-surface contact algorithm. Steel on steel tangential contact is modelled using a penalty friction model

with the coefficient of friction of 0.2. Small variations in the coefficient of friction did not have a significant impact on the results of the analysis. Finite elements of 10-node linear tetrahedral solid 3D stress elements (C3D10) are used to model the steel components of the tube anchor system. In regions with cylindrical contact surfaces, such as under the convex washer or around the anchor rods, a finer mesh is adopted to allow a smoother stress transfer over the contact surface area. Once again, a mesh refinement analysis is conducted to improve the efficiency of the model while maintaining an appropriate level of accuracy. Boundary conditions applied to the anchor model included fully fixed conditions at the base of the anchor rod, assuming that sufficient embedment length into the concrete is provided to prevent pullout. Out of plane deformation of the anchor system is prevented.

The total resultant load carried by the vertical FRP sheets ($P_{c,max}$) is determined based on the methodology described in Section 4-1. The resultant load is distributed over the area of steel tube in contact with the FRP, as shown in Figure 4-5, and can be calculated using Equation 4 as follows

$$p_{c,\max} = \int_0^{\frac{\pi}{2}} p_c \cos\left(\frac{\pi}{4} - x\right) r_o d\theta \tag{4}$$

where p_c is the pressure over the curved surface, x is the distance along the radius of the CHS, and r_o is the outer radius of the tube. The solution to this integral can be converted into an expression for the maximum uniform pressure ($p_{c,max}$) acting over the area in which the FRP sheet is in contact with the tube anchor by using Equation 4 as follows

$$p_{c,\max} = \frac{\sigma_u t_s n_s}{r_o} \tag{5}$$

It is assumed that the maximum uniform pressure determined from Equation 5 varies linearly from the end of the anchor to the neutral axis of the shear wall, as shown in Figure 4-5. By using these relationships, an idealized load pattern acting on the anchor system can be determined based on the material properties of the FRP sheet (Table 4-2). Assuming that the design force is based on one sheet of externally bonded FRP, a maximum uniformly distributed pressure of 10.94 MPa is applied in the FE model at the end of the tube decreasing linearly until the assumed location of the neutral axis, 1275mm from the anchors end (85% of the anchors length), as illustrated in Figure 4-5.

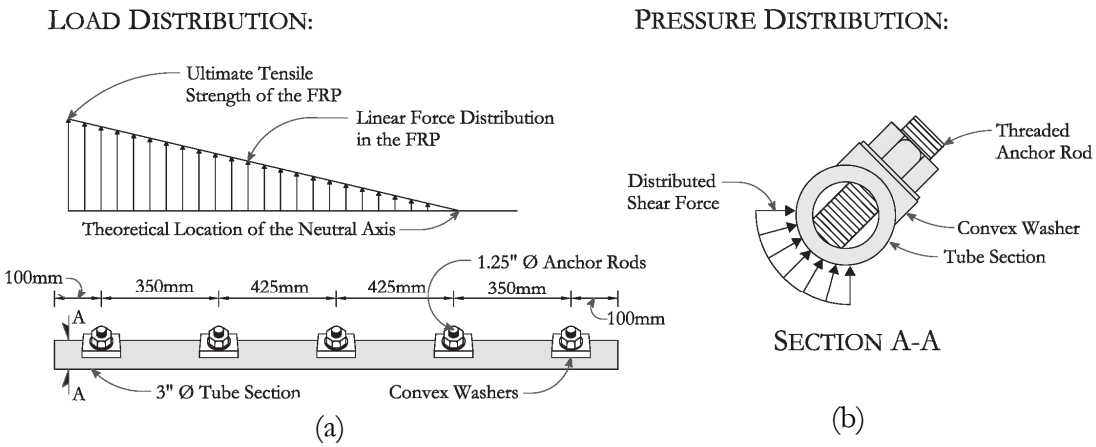

Figure 4-5: (a) Geometry of the Tube Anchor System (b) Forces on the Tube Anchor.

Anchor deformations perpendicular to the longitudinal axis of the tube are shown in Figure 4-6. A maximum displacement of 0.35mm occurs between the first and second anchor bolts, regions which are subject to the largest pressure. The maximum stress in the tube is approximately 40% of the yield strength of the material while the two outermost anchor bolts

anchor bolts experience a maximum stress of approximately 230MPa (58% of yield). The lateral displacement of the anchor systems is shown for 20%, 50% and 100% of the ultimate capacity of the FRP along half of the anchors length in Figure 4-7. Results obtained from the analytical model confirm experimental observations discussed by Hiotakis (2004) that the anchor system experiences very little displacement and no inelastic deformation under the applied load from a single sheet of FRP. In this study, the optimization design procedure for the tube anchor system is developed to further improve the design and cost-efficiency. The combination of an anchor system which allows the FRP to reach its rupture capacity without premature failure and maximizes cost-efficiency by reducing the total required material will improve the efficiency of the FRP retrofitting scheme and make the tube anchor system an even more attractive alternative to other anchor systems for repair and strengthening of RC elements using FRP sheets.

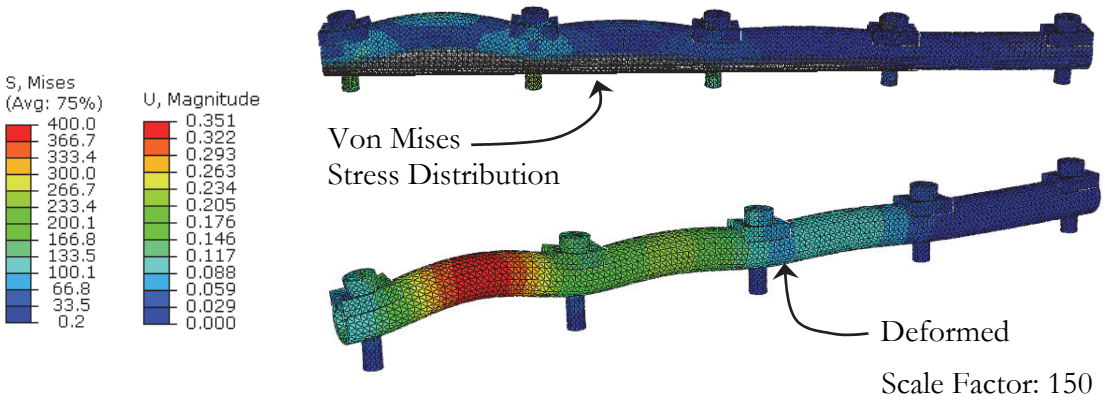

Figure 4-6: Analytical Results for Tube Anchor Model.

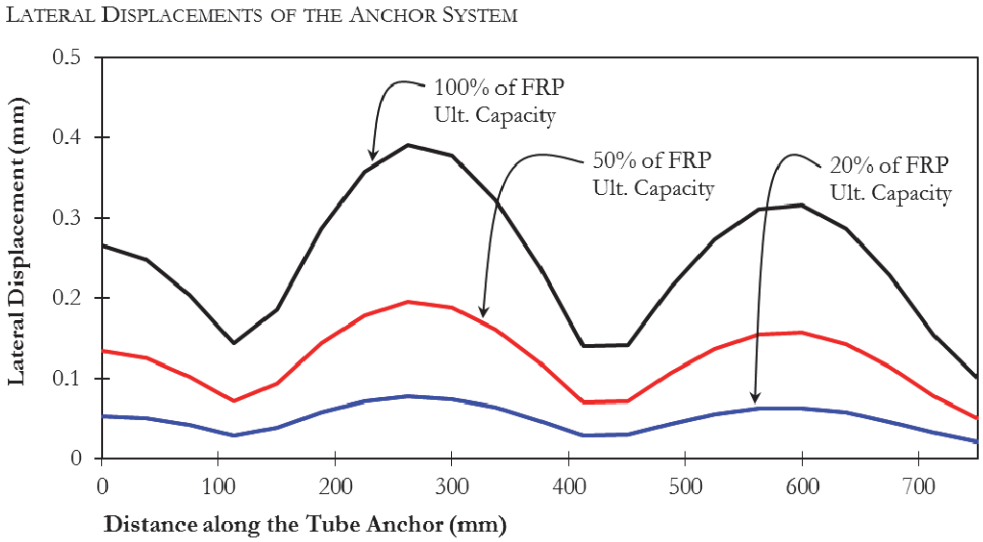

Figure 4-7: Lateral Displacement along Half of the Tube Anchor System.

4.4 Optimization of Tube Anchor System

The tube anchor is a crucial component of the FRP retrofitting system used in this study. The previous work by Lombard (1999) and Hiotakis (2004), shows through experimental tests conducted on reinforced concrete shear walls that the tube anchor system is effective in transferring the force carried by the FRP and is an improvement over the conventional steel angle anchor system. The tube anchor has been shown to perform well in achieving its performance objective of fully utilizing the tensile capacity of the FRP sheets (Hiotakis et al. 2004). In the present study, improvements to the tube anchor systems cost efficiency while maintaining the same level of performance are investigated. Through the use of FE models, an optimized design procedure for the tube anchor system is developed to improve its performance and simplify the fabrication process. By comparing tube anchor

models with and without the convex washer located beneath the head of the anchor rod, as shown in Figure 4-8, it is shown that there is negligible difference between the performance of the two anchor systems (<10% difference in lateral displacement results). It is also shown that any stress concentrations under the head of the anchor rod without the convex washer are not significant enough to cause local damage when the washer is not present. Therefore it is determined that the convex washers under the head of the anchor bolts can be replaced by a conventional flat washer without significant effect on the performance of the system. By eliminating the convex washer, a significant reduction in fabrication time and cost of the tube anchor system is achieved.

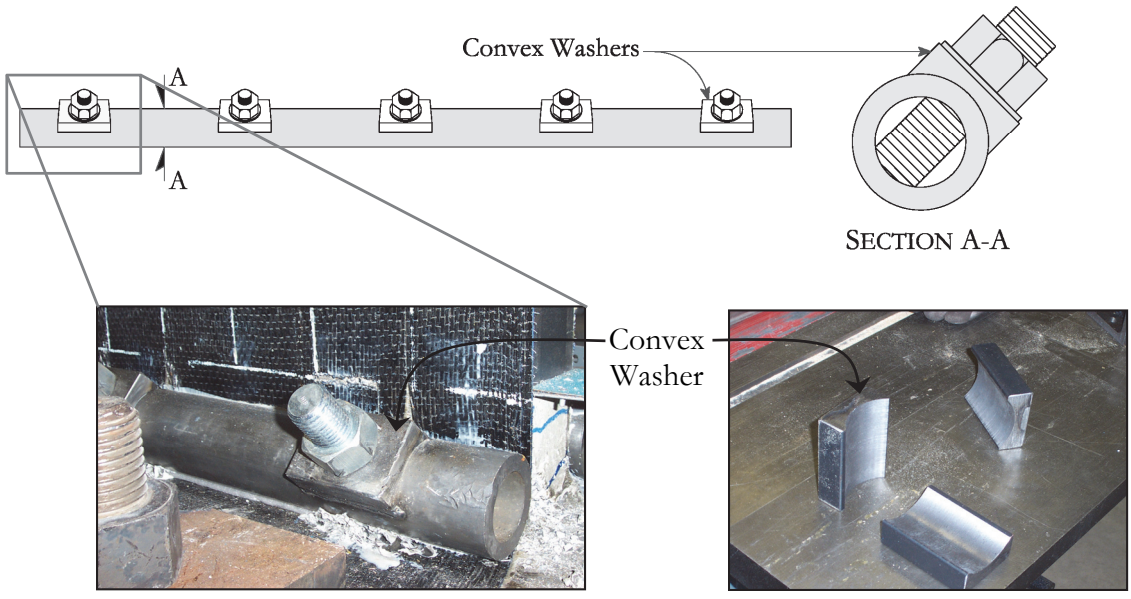

Figure 4-8: Convex Washers for the Tube Anchor System.
(Images from Hiotakis, 2004)

The next step in the optimization process is to modify the geometry of the tube and the anchor bolt spacing to achieve the most efficient design. To do so, the finite element

modelling procedure outlined in Section 4-2 is used to determine the optimal tube size and anchor bolt spacing. Prior to completing the parametric study for the optimization of the tube anchor system, refinement of the modelling procedure is carried out to ensure the models performance is accurate and also efficient. During the first stage in the optimization process, it is determined that based on an embedment depth of 305 mm (12 in.), five 25.4 mm (1 in.) diameter anchor bolts are required to effectively transfer the load from one sheet of FRP into the concrete foundation. Capacities of the anchor rods are determined according to the manufacturer's guidelines in conjunction with CSA A23.3 Annex D, which describes design provision for anchor rods in reinforced concrete. The anchor bolts are placed at 100, 425 and 750 mm from the end of the tube. The second anchor rod, located 425 mm from the end of the tube coincides with the location of the resultant load carried by the FRP sheet, located at the centroid of the triangular load distribution shown in Figure 4-5(a). Based on this preliminary bolt layout, FE analysis on the optimal tube size for the application is conducted by varying outer diameters ranging from 38.1 mm (1.5 in.) to 101.6 mm (4 in.) and wall thicknesses from 6.35 mm (0.25 in) to completely solid tubes. Results of the analyses are shown in Figure 4-9(a). Analytical results show that tubes with slightly more area at a smaller wall thickness perform better due to a higher moment of inertia, which results in higher bending stiffness. Conclusions from the analysis indicate that the optimal tube size is a 50.8 mm (2 in.) outer diameter tube with a wall thickness of 6.35 mm (0.25 in.). With these dimensions, the least amount of displacement coincides with the smallest area of tube, resulting in a tube anchor design which is more cost effective by using less material. This size of tube also maintains the same level of performance as previously implemented tube anchor

systems, one of the main goals of the optimization procedure, by ensuring that the deformation experience in the tube is not significant enough to cause debonding which can lead to premature failure of the FRP strengthening system. Although that it is not explicitly known what level of deformation of the anchor system results in debonding, it is assumed that displacement less than 2.5mm will not have a significant effect on allowing the FRP to reach its ultimate tensile strength. Based on the preliminary bolt layout, an analysis on the optimal edge distance for the furthermost anchor bolt is conducted, results of which are shown in Figure 4-9(b). The results clearly show the optimal edge distance is 125mm from the end of the tube. This gives the smallest deformation in the tube anchor system when subject to the design load pattern. By placing the first anchor rod a small distance from the edge of the wall, this reduces the unsupported length between anchor rods in the adjacent bay, which is typically the critical bay for the design of the anchor, as it is the bay with the highest unsupported length and is under the highest uplift pressure. Therefore by reducing the unsupported length in this bay, an improvement in the performance of the anchor system can be achieved.

For the experimental test program, a tube 57.15mm (2.25") in diameter with a 9.525mm (0.375") wall thickness is used for the tube anchor system. The final design of the anchor system used in the experimental program is shown in Figure 4-10 and the numerical results from the finite element model for this particular anchor system design is shown in Table 4-3, and the fabrication of the tube anchor system is discussed in more detail in the following section. Due to material availability, the dimensions of the tube were selected as close as possible to those from the optimization study.

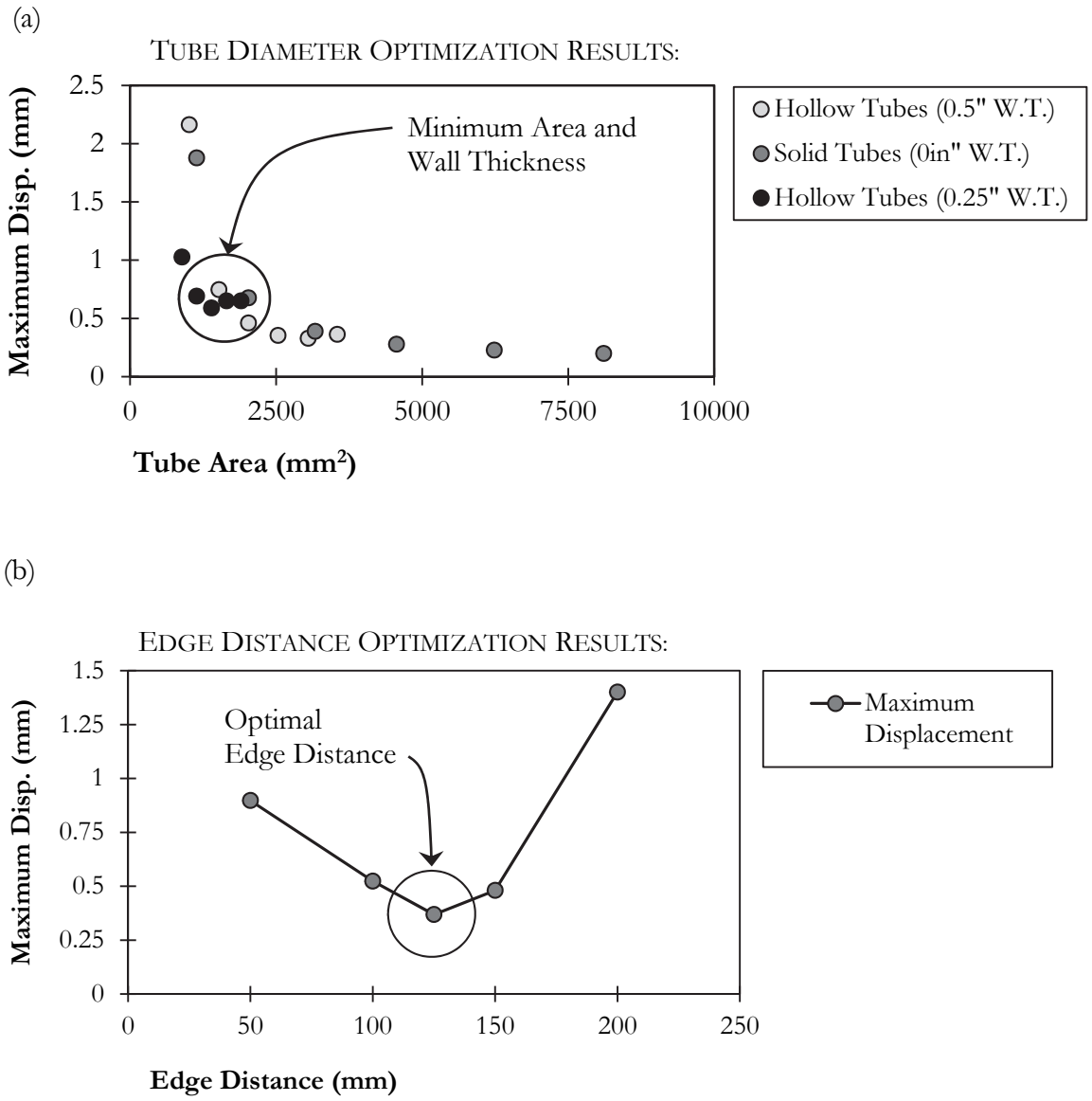

Figure 4-9: Results from Analytical Studies on the Tube Anchor System.

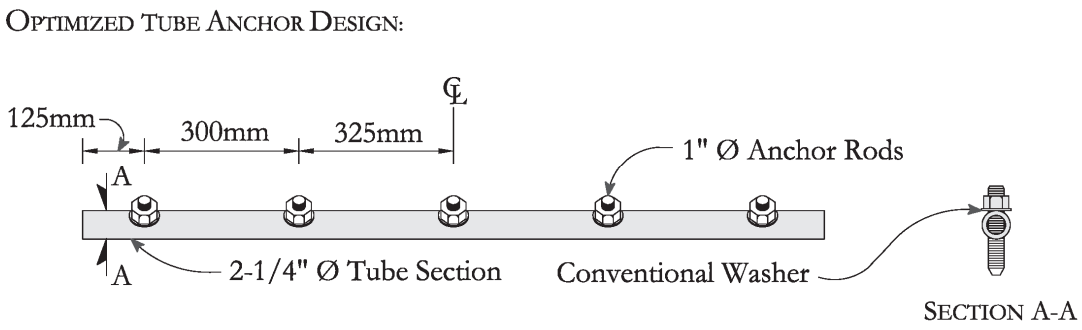

Figure 4-10: Tube Anchor System Design for Deficient RC Walls.

Table 4-3: Modelling Results for As-built Anchor System.

Anchor System	Max. Pressure (MPa)	Max. Displacement (Tube) (mm)	Max. Stress (Tube) (MPa)	Max. Stress (Anchor Rods) (MPa)
57.15mm (2-1/4") O.D. 9.525mm (0.375") W.T	13.4	0.439	195 (37.9%)†	365 (50.3%)†

†Represent the stress as a percentage based on the tabulated yield stress of the materials.

4.5 Construction of the Tube Anchor System

The tube anchor system used in this study is optimized through FE simulations to have an anchor system which is cost-effective, while maintaining the same performance levels as previous tube anchor designs. The tube anchor system is constructed from a 57.15 mm (2.25 in.) rolled-over-mandrel steel seamless pipe with a 9.5 mm (0.375 in.) wall thickness. Upon casting of the reinforced concrete shear wall specimens, five 30.75mm (1.25in.) holes are drilled into the foundation of the wall at a 45 degree angle for the installation of the 400 mm (16 in.) long adhesive anchor rods. The stock sections of pipe are cut to length and five 25.4 mm (1 in) holes are drilled in the pipe at the predetermined locations along the pipes length. Material properties for the anchor rods and steel pipe are shown in Table 4-4. Upon completion of the steel tubes, the anchor rods are installed in the concrete foundation and the tube is installed. Epoxy is placed behind the anchor to fill any voids between the base of the steel tube and the FRP sheet. The installation process for the tube anchor system is outlined in Figure 4-11.

Table 4-4: Mechanical Properties for the Anchor Rods and Steel Pipe.

Anchor Component	Yield Stress (MPa)	Ultimate Tensile Strength (MPa)	Percent Elongation (me)
Steel Tube	590	667	32.2%
Hilti Steel Anchor Rods	724	862	32.2%

PRIOR TO TUBE ANCHOR INSTALLATION:

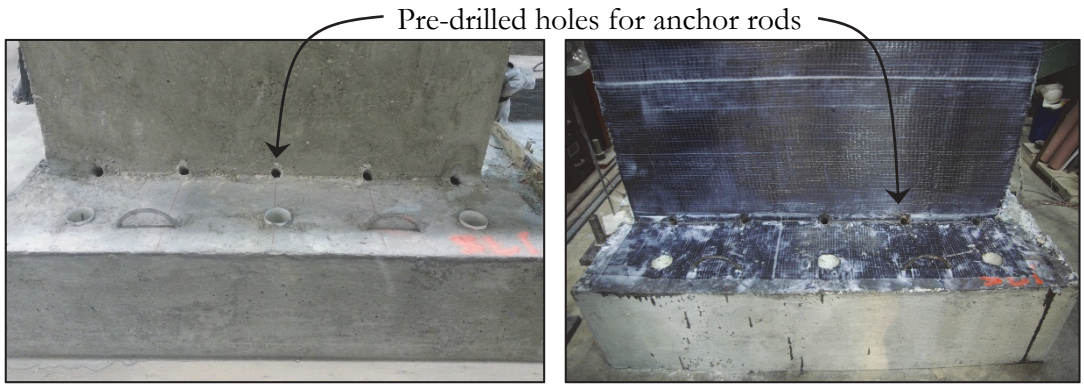

TUBE ANCHOR FABRICATION:

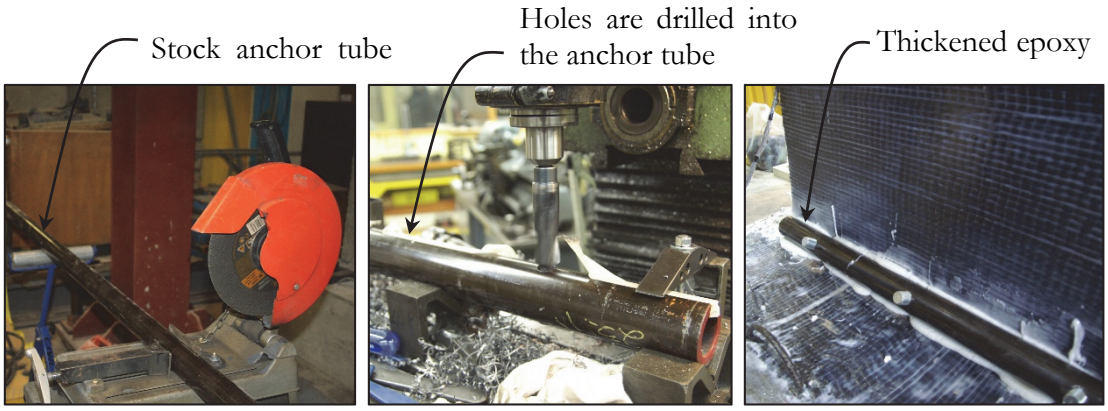

COMPLETED TUBE ANCHOR SYSTEM:

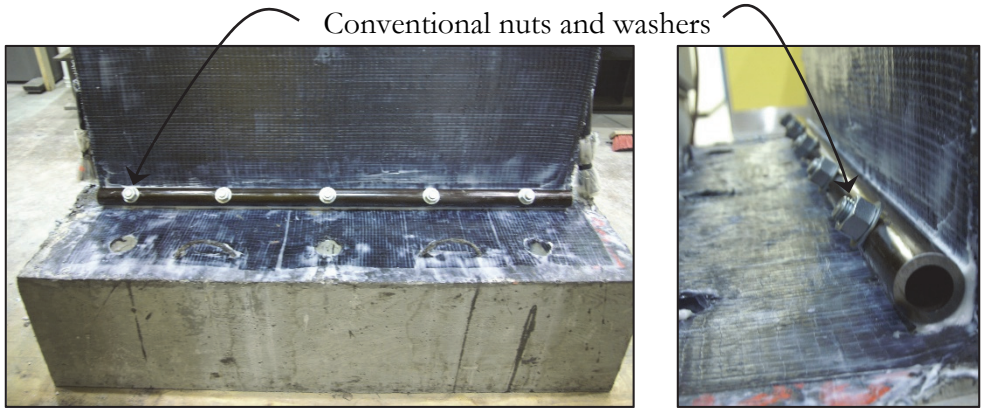

Figure 4-11: Construction Steps for the Tube Anchor System.

CHAPTER 5: EXPERIMENTAL RESULTS

The experimental program in this study is focused on the behaviour of RC shear walls with poor seismic detailing typically associated with older design standards. These walls are expected to behave in a brittle manner with little to no warning of impending failure, posing a significant risk to the safety of the structure and its occupants. Wall specimens of this nature typically lack strength, ductility, and energy dissipation capacity leading to poor seismic performance of the walls. To improve the performance of these older shear walls, a retrofitting system consisting of externally bonded FRP sheets is used to increase the strength, ductility, and energy dissipation capacities. These enhancements contribute to better seismic performance and reduce the seismic risk associated with old shear wall structures.

5.1 CONTROL WALL SPECIMEN

The control wall specimen (SLCW) is tested first to assess the performance of shear walls designed according to older design standards without FRP and also serves as a baseline for later comparison with the FRP retrofitted wall specimens. Failure criterion for the control wall specimen is set at a 10 to 15% drop in ultimate capacity as an attempt to limit the damage to the wall and not reach the collapse state. However, due to the extremely brittle nature of the wall specimen, it is difficult to precisely control the level of damage during the test.

The control wall is subject to a total of 8.5 load cycles prior to failing in brittle diagonal tension shear. The first 8 load cycles are applied in load control, at 25%, 50%, 75% and 100% of the estimated yield load. During the first two load cycles (25% of yield), diagonal cracking appears first near the middle of the wall. At 50% of the yield load, short flexural cracks along the boundary elements of the wall occur, propagating upwards during successive load reversals, as shown in Figure 5-1(a). The yield load of the wall specimen, which occurs when the reinforcing bars near the edges of the wall yield in tension, first occurs at an average load of 242 kN and an average drift of 0.29%. During the 9th load cycle, attempting to reach a target displacement ductility level of 1.5, two large diagonal shear cracks located 75.0 mm apart at approximately 45 degrees along the diagonal of the wall specimen enlarge significantly when compared with adjacent crack widths, as shown in Figure 5-1(b).

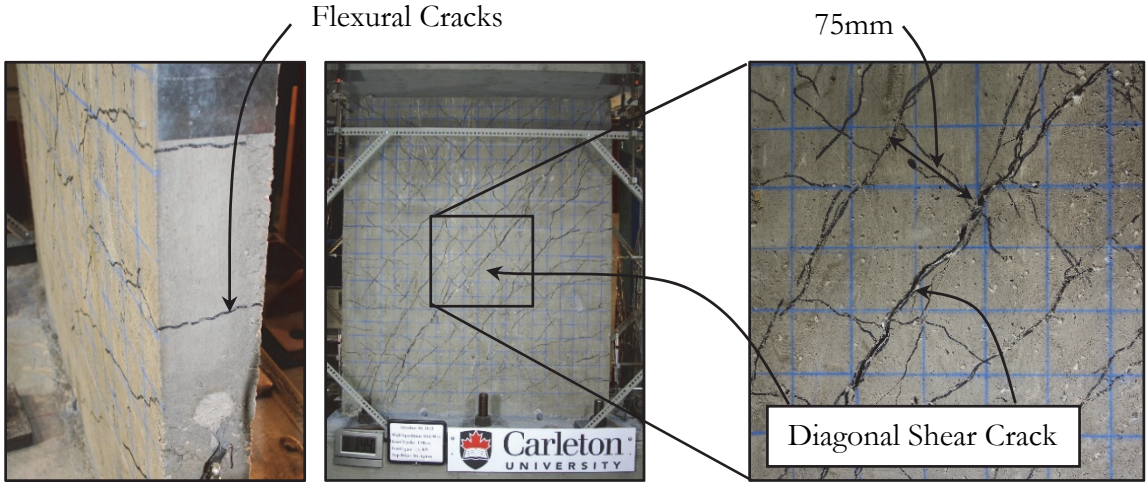

Figure 5-1: (a) Flexural Cracking; (b) Formation of Diagonal Tension Failure.

At an ultimate load of 346 kN, failure of the wall specimen due to rupture of the transverse steel reinforcement results in a significant drop in load carrying capacity of the wall (to 40% of the ultimate capacity). Only a small portion of the toe of the wall experiences concrete crushing at the time of failure. The ultimate displacement of the control wall specimen during the test is 13.2 mm prior to failing in diagonal tension shear, which results in a maximum drift ratio of 0.73%. To determine the displacement ductility of the wall specimen, a bilinear idealization of the force-displacement envelope is used to identify the yield load and yield displacement by the mean area balancing method (Cruz-Noguez et al. 2014). The maximum load carrying capacity of the wall specimen is defined as the point when the load drops to 80% of the ultimate load. Displacement ductility, μ_Δ is determined using Equation 6, where Δ_u is the ultimate displacement achieved by the wall specimen at the maximum load carrying capacity, and Δ_y is the yield displacement of the wall specimen.

$$\mu_\Delta = \frac{\Delta_u - \Delta_y}{\Delta_y} \tag{6}$$

The average displacement ductility of the control wall specimen is 1.2, which shows the lack of ductility in walls detailed according to older design standards. This behaviour is confirmed by examining the hysteretic response of the test specimen (Figure 5-2) which shows minimal energy dissipation in the response, typical behaviour of non-ductile walls. The asymmetric response of the control wall specimen is attributed to minor variations in the placement of the longitudinal reinforcing bars during construction. Figure 5-2 also shows the

crack pattern at different stages of loading during the test. In the response sequence, diagonal cracks occur first at 25% of the yield load followed by small flexural cracks at the edges of the wall at 50% of the yield load. During subsequent load cycles, the number of diagonal cracks increases significantly up to the yield load of the wall. After yield, the diagonal cracks become considerably wider leading to rupture of the transverse reinforcement and failure of the wall in diagonal tension. The average crack width prior to failure is approximately 0.1 mm, showing little to no warning of impending failure. The observed behaviour clearly identifies the susceptibility of walls designed according to older design standards to collapse failure during a moderate to large seismic event. It is evident that these deficient walls require retrofitting to reduce their seismic risk by improving the ductility and energy dissipation performance.

Further analysis of the strain gauge data shown in Figure 5-3 indicates that only the longitudinal reinforcing bars closest to the edges of the wall yield prior to the failure of the wall in diagonal tension. Reinforcing bars located on the interior of the wall remain elastic, which is also shown in Figure 5-3 and contributes to a lack of energy dissipation capacity of the wall specimen. The limited yielding in the longitudinal reinforcement localized along the base of the wall is attributed to the lack of transverse reinforcing steel in the wall specimen. Insufficient transverse reinforcement leads to a brittle shear dominant failure mode, with little to no ductility or energy dissipation capacity. These results clearly identify the need to have an effective means for the strengthening existing walls with deficiencies associated with older design standards to improve their seismic performance and safety. Additional plots from the response of the control wall specimen are available in Appendix B.

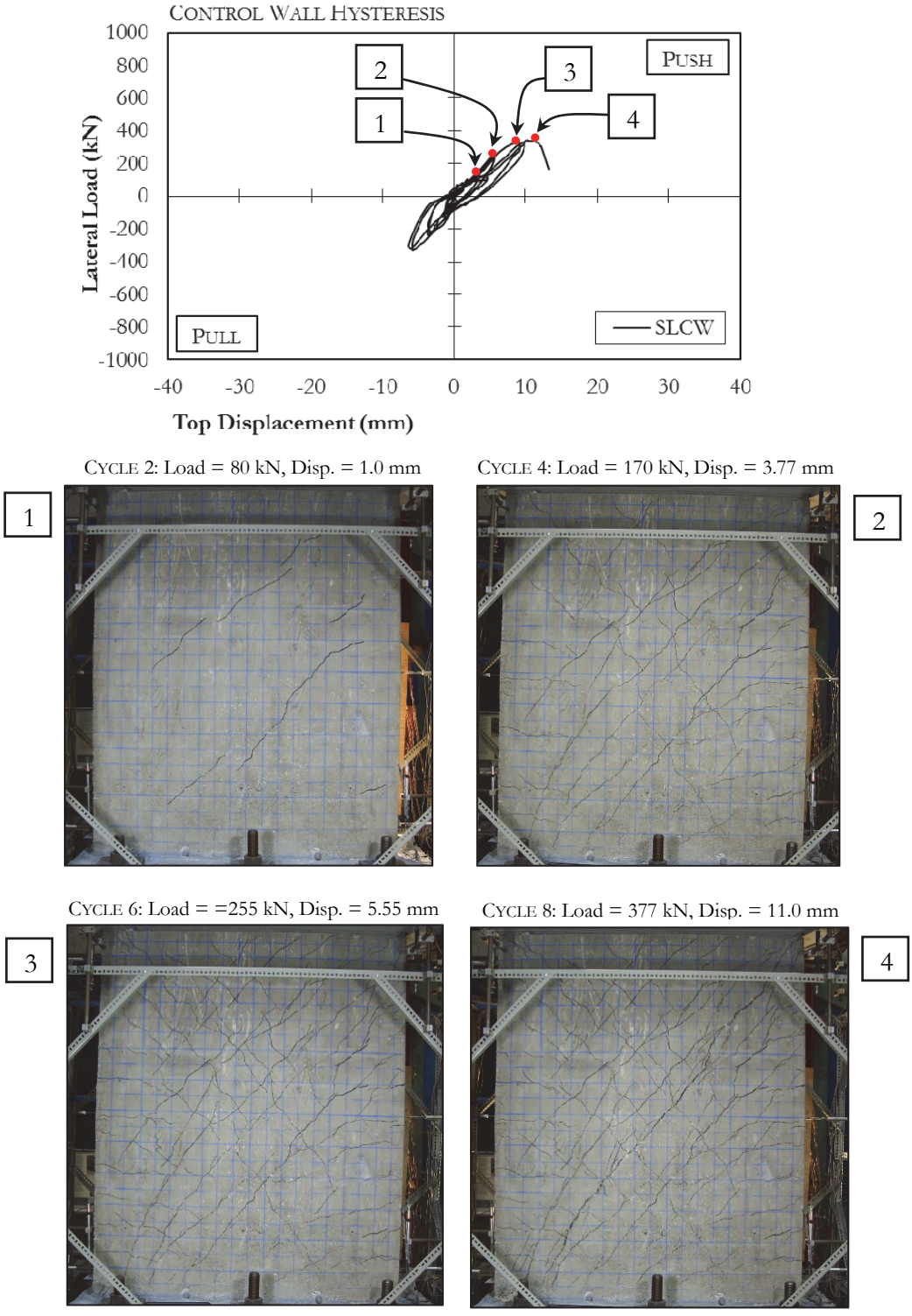

Figure 5-2: Hysteretic Response of the Control Wall and Crack Distributions.

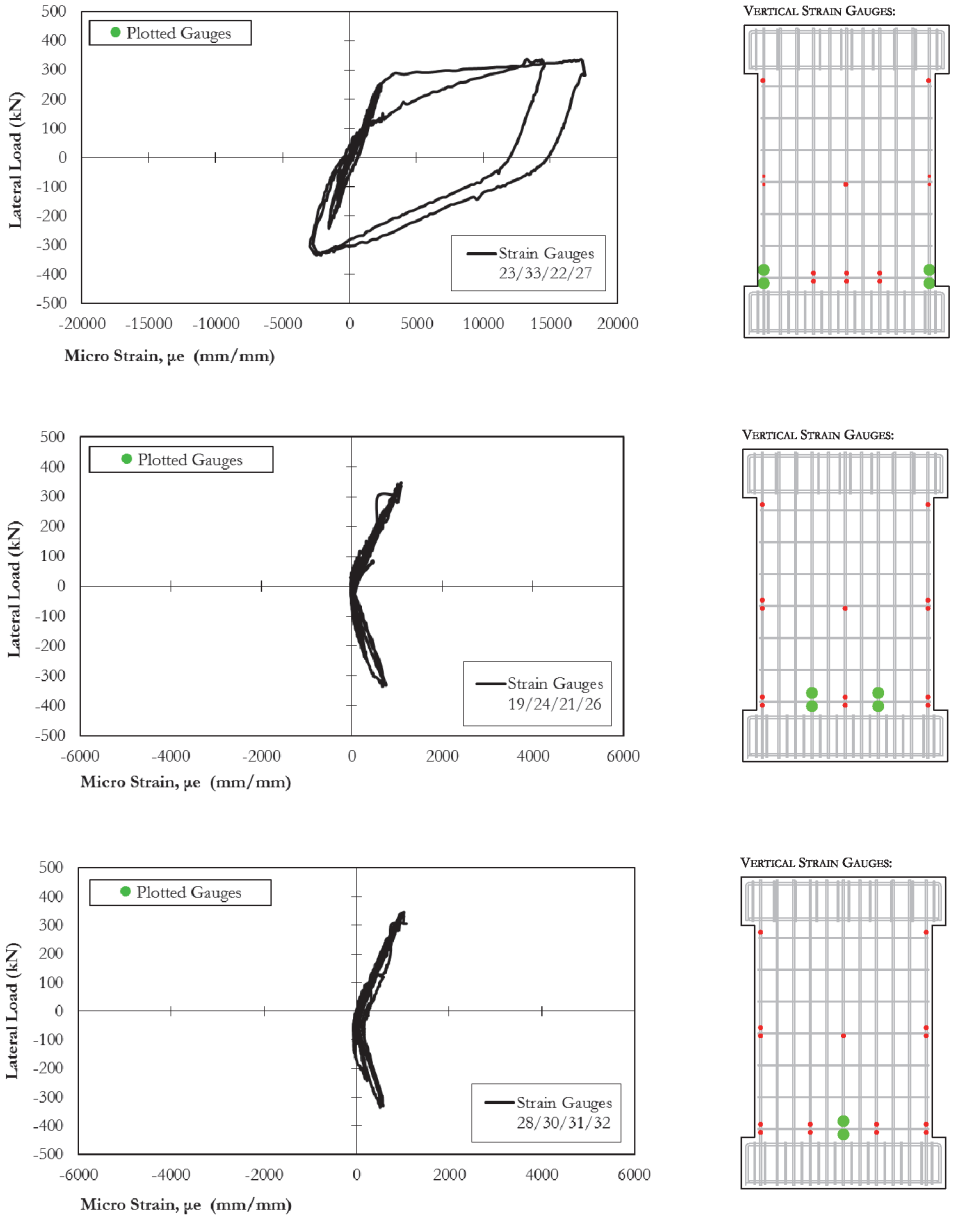

Figure 5-3: Longitudinal Reinforcement Hysteretic Response (SLCW).

5.2 Repaired Wall Specimen

Following the initial test, the control wall specimen is repaired using a combination of epoxy and patching mortar. Loose concrete is removed and significant cracks (0.25-5mm) are injected with a low viscosity epoxy. A thicker epoxy resin is then used to seal any remaining cracks (>5mm). Prior to the installation of the FRP, areas of spalled concrete are patched using mortar to provide a level bonding surface for the FRP sheets. The surface of the wall is then lightly ground to expose the concrete substrate for the application of the FRP. The three stages of the concrete repair process are shown in Figure 5-4. The wall specimen is retrofitted using a single layer of vertical FRP in combination with three horizontal FRP layers. In contrast to previous studies (Antoniades et al. 2003; Paterson and Mitchell 2003; Khalil and Ghobarah 2005), the FRP composite is not wrapped around the shear wall to account for the fact that in the field, the sides of a RC shear wall are typically not exposed. The FRP retrofitting system attempts to increase the shear strength, restore the initial stiffness and increase the ductility of the wall specimen. All of which contribute to improving the seismic performance of the wall when compared to the control wall and ensure the wall has the appropriate capacity to survive a significant seismic event.

The repaired wall specimen is subject to a total of 23 load cycles, the first 8 of which are in load control at 25%, 50%, 75%, and 100% of the estimated yield load. Initial debonding of the FRP layers occurs in the centre of the wall specimen at 50% of the yield load and an average drift ratio of 0.20%. Debonding of the FRP sheets in this region is attributed to the damage sustained during the earlier test. Further debonding occurs significantly later in the

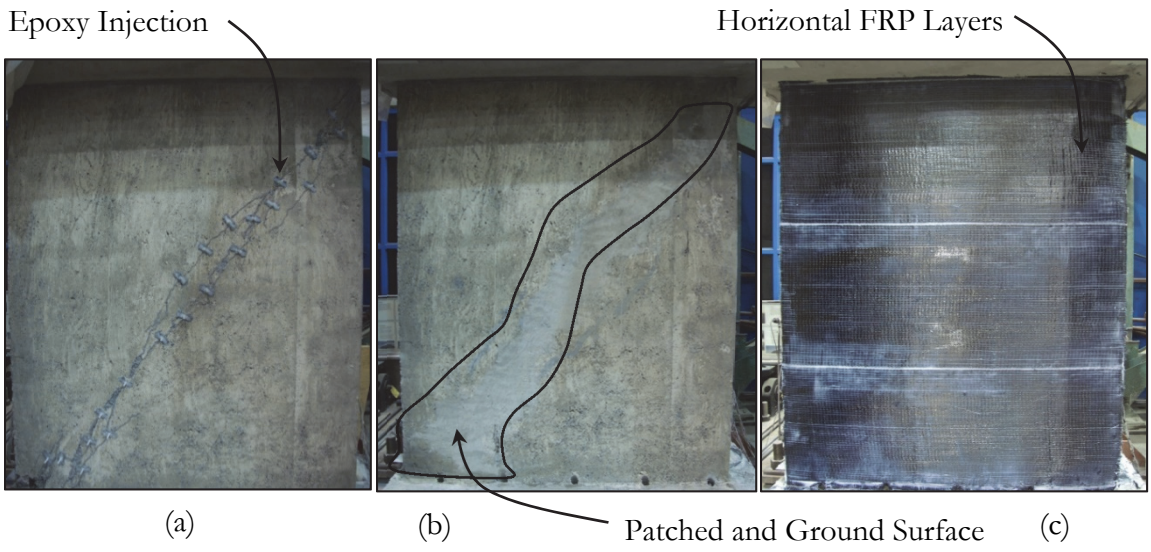

Figure 5-4: (a) Epoxy Crack Injection; (b) Patched Wall Specimen (c) Repaired Wall.

test at 100% of the yield load when debonding is also observed along the base of the wall, as shown in Figure 5-5. Debonding along the base of the wall is attributed to the intermediate crack (IC) debonding mechanism. The IC debonding mechanism is initiated by cracking in the concrete beneath the FRP layers which results in separation of the FRP sheets from the concrete substrate. The IC debonding phenomenon in RC members strengthened using FRP has been previously described and investigated by Teng et al. (2002) and Cruz-Noguez et al. (2014). At the maximum load-carrying capacity of the wall, fracture of the vertical FRP is observed at the base near the edges of the wall. Failure of the wall is attributed to diagonal compression failure, when concrete crushes in the compression zone at the toes of the wall. The FRP sheets in the compression zone debond due to extensive concrete cracking. During subsequent load cycles, the FRP is no longer bonded to the concrete in the compression zone which causes out-of-plane buckling of the FRP sheets in compression, as shown in Figure 5-6.

Concrete crushing and FRP buckling extends into the interior of the wall due to degradation provoked by the load reversals eventually leading to a significant drop in the load carrying capacity of the wall specimen. Complete debonding of the FRP sheets along the base of the wall occurs during the 23rd load cycle, which corresponds to a target displacement ductility level of 4.0. Complete debonding of the FRP sheets results in out-of-plane buckling of the longitudinal steel reinforcement between transverse steel layers near the edges of the wall, as shown in Figure 5-6. The average ultimate load of the repaired wall specimen is 610 kN, and the average drift at failure is 1.29%. The hysteretic response of the repaired wall is shown in Figure 5-5. Asymmetry in the hysteretic response is attributed to the higher level of damage sustained in the earlier test in one load direction (push) compared to the other direction (pull). The response of the repaired wall in the less damaged direction shows a higher strength, ductility and energy dissipation capacity when compared to the damaged direction. However, even in the damaged direction, the retrofitting system is capable of restoring the initial stiffness, increasing the energy dissipation capacity and ductility of the wall specimen. The ductility in the repaired wall specimen is 3.5 in the less damaged direction and 2.7 in the damaged direction. This demonstrates the ability of the FRP retrofitting system to dramatically improve the seismic performance in walls with minor damage. Additionally, these results also show the ability of the FRP retrofitting system to restore the initial stiffness and increase the strength, ductility and energy dissipation capacity even in severely damaged wall specimens. These results demonstrate that the repair of RC shear walls using FRP is a viable retrofitting technique for existing deficient RC structures.

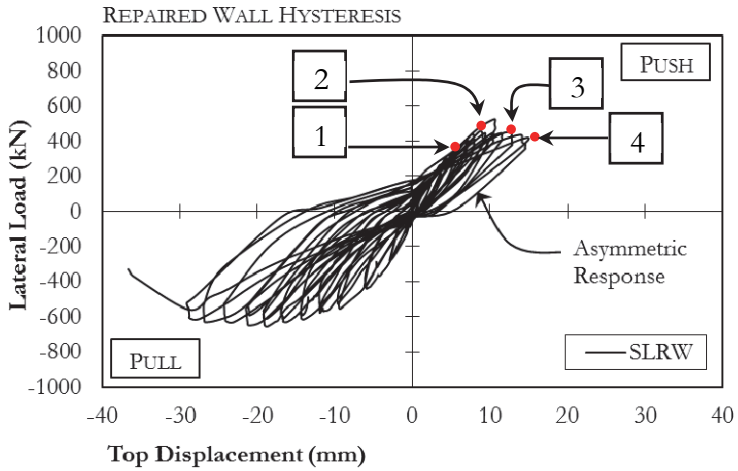

CYCLE 8: Load = 301 kN, Disp. = 4.5 mm

CYCLE 16: Load = 458 kN, Disp. = 9.0 mm

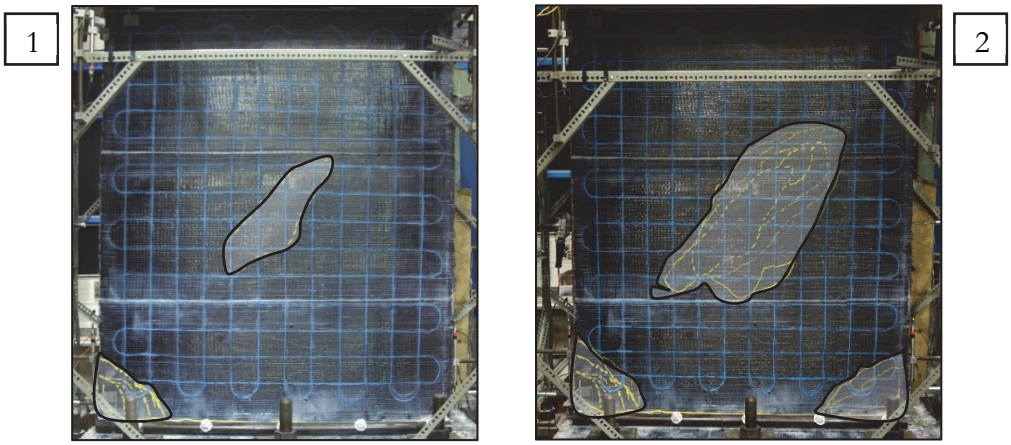

CYCLE 22: Load = 416 kN, Disp. = 14.6 mm

CYCLE 23: Load = 377 kN, Disp. = 16.2 mm

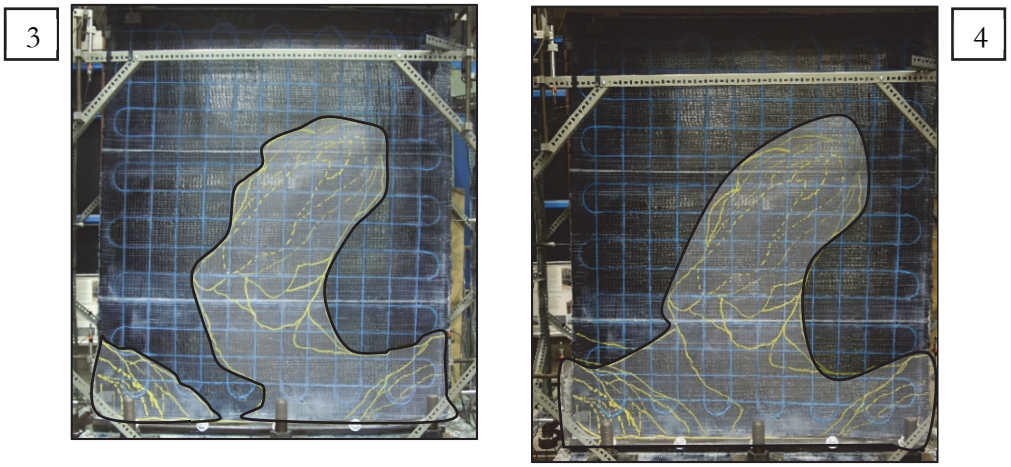

Figure 5-5: Hysteretic Response and Debonding Patterns for Repaired Wall.

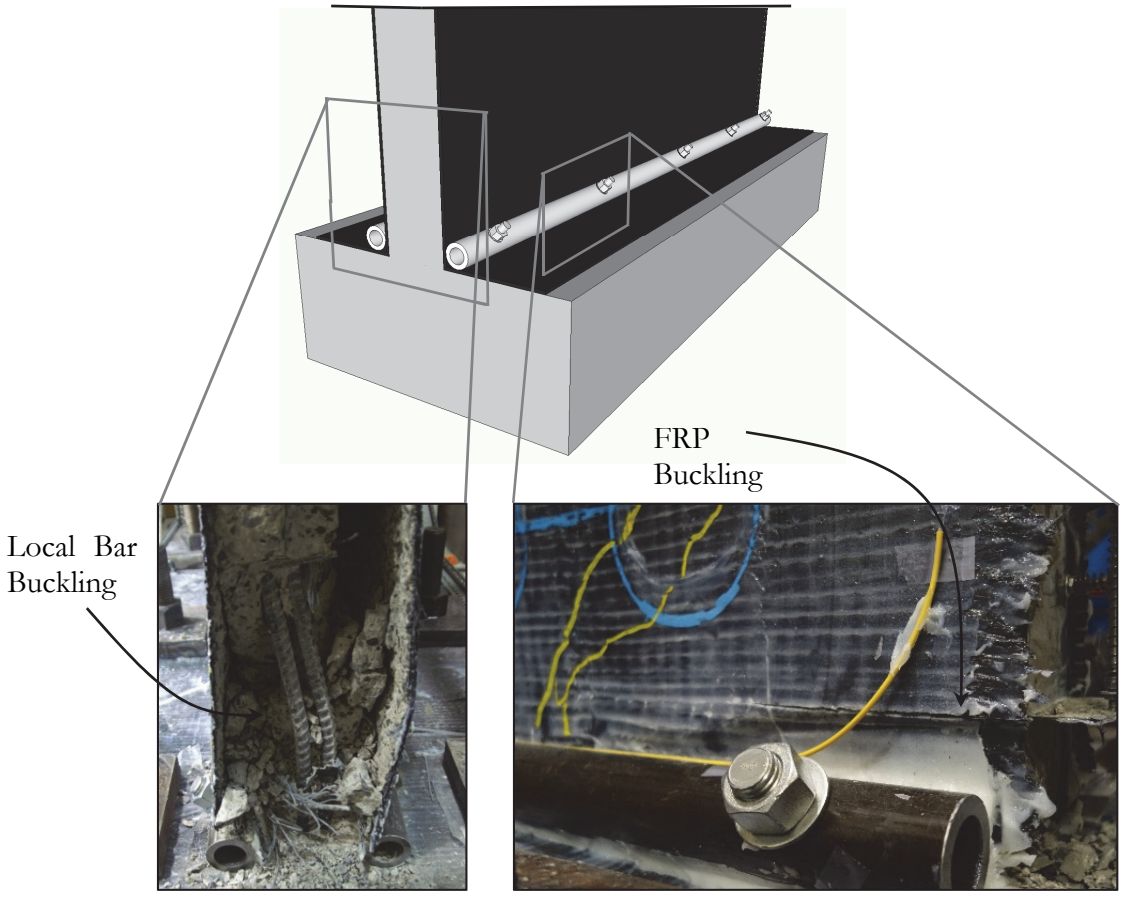

Figure 5-6: Concrete Crushing and Reinforcement Buckling.

5.3 STRENGTHENED WALL SPECIMEN

The FRP retrofitting system for the strengthened wall is identical to the repaired wall to compare the effectiveness of the retrofitting system in repair and strengthening scenarios. Prior to the application of the FRP sheets, the surface of the concrete is lightly ground to expose the concrete substrate to facilitate a better bond between the concrete and the FRP sheets. By strengthening the wall using FRP, it is expected that the wall specimen will exhibit a higher stiffness, strength and ductility when compared with the control and repaired walls.

The strengthened shear wall specimen is subject to a total of 26 load cycles before a significant drop in load carrying capacity. The resistance of the wall at high levels of lateral load shows the ability of the strengthened wall specimen to sustain a higher lateral drift when compared with the control wall. The average yield load of the strengthened wall specimen is 341 kN at an average top displacement of 3.89 mm. Debonding of the FRP sheets first occurs at the toes of the wall specimen in the compression zone which then progresses inward in a v-shaped pattern as the cyclic load increases, as shown in Figure 5-7. It is noted that the debonding is first observed at a much later stage during the test (cycle 12) when compared with the repaired wall due to the lack of pre-existing damage in the wall. Debonding first appears at a load of 606 kN and a drift of 0.88%, after the wall specimen has reached its ultimate load carrying capacity. Debonding along the base of the wall specimen is once again attributed to the opening of large cracks in the concrete resulting in debonding of the FRP sheets by the intermediate crack (IC) debonding mechanism, similar to the debonding mechanism discussed in Section 3.2. At the ultimate load carrying capacity, fracture of the

vertical FRP sheets is observed at the toes of the wall. The maximum load carrying capacity of the wall is 633 kN and the maximum top lateral displacement is 29.1 mm. This results in an average displacement ductility of 4.1 and an average maximum drift of 1.91%, which is a significant increase over the control wall specimen.

In a similar manner to that of the repaired wall discussed earlier, ultimate failure of the strengthened wall is a result of diagonal compression, which causes a significant amount of concrete crushing at the toes of the wall specimen, as shown in Figure 5-8. During successive load cycles, crushing of the concrete in the toes of the wall results in separation of the FRP sheets from the concrete substrate in a v-shaped pattern (Figure 5-7). Under multiple cyclic load reversals, concrete crushing and FRP debonding spreads towards the centre of the wall which leads to a significant drop in load carrying capacity. Extensive concrete crushing and a lack of confinement of the reinforcing bars located near the edges of the wall results in out-of-plane buckling, as shown in Figure 5-8. The hysteretic response of the strengthened wall specimen in Figure 5-7 shows a similar behaviour in the push and pull directions, with only minor differences in the two directions of the response likely attributed to the slightly off-centre placement of the reinforcing steel during construction of the wall. Through the use of externally bonded FRP sheets, it is shown in the hysteretic response of the wall that dramatic improvements can be achieved in terms of strength, ductility and energy dissipation capacity in poorly detailed wall specimens. This demonstrates that strengthening using FRP is a viable retrofitting technique which can be used to improve the performance of RC shear walls designed according to older design standards.

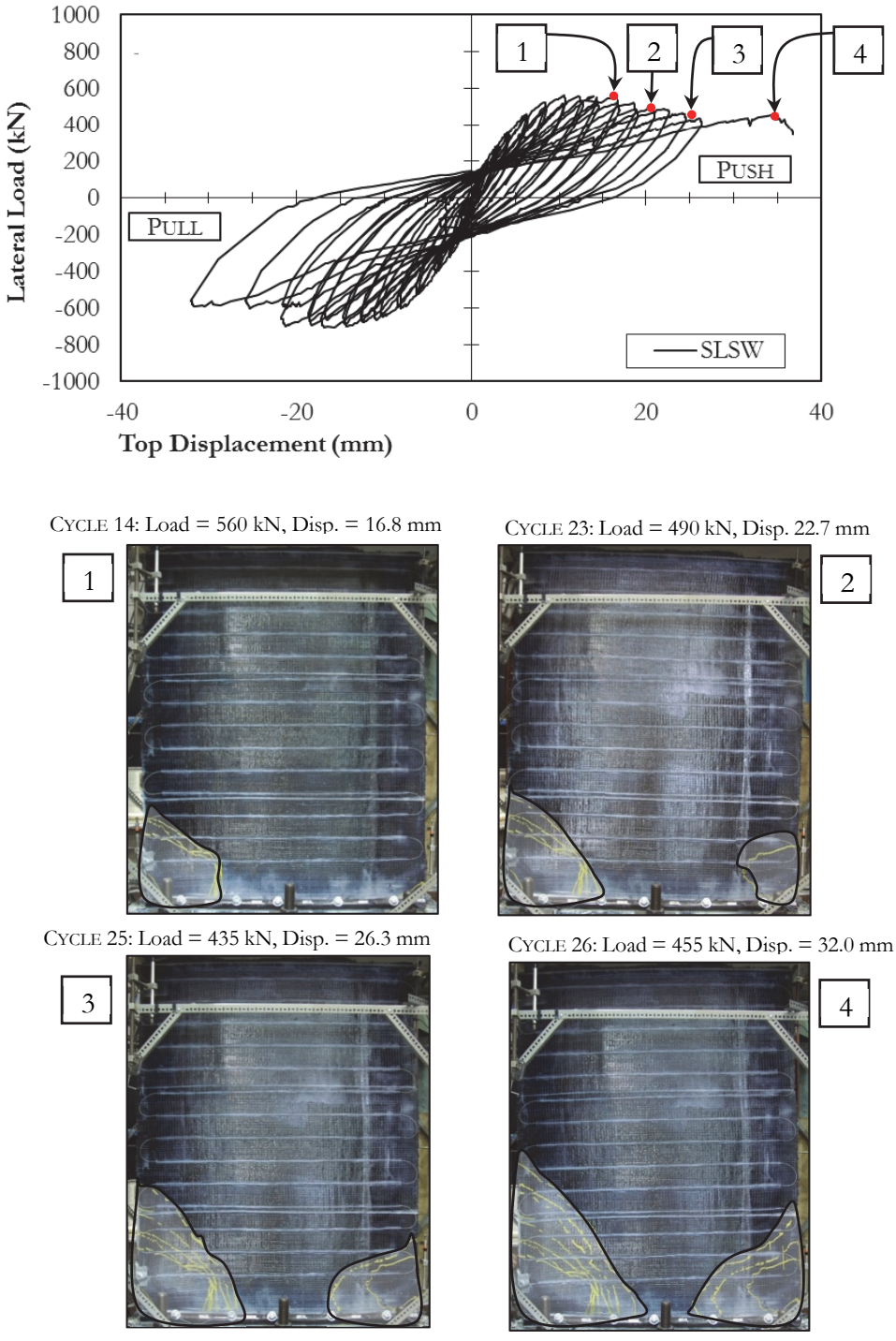

Figure 5-7: Hysteretic Response and Debonding Patterns for Strengthened Wall.

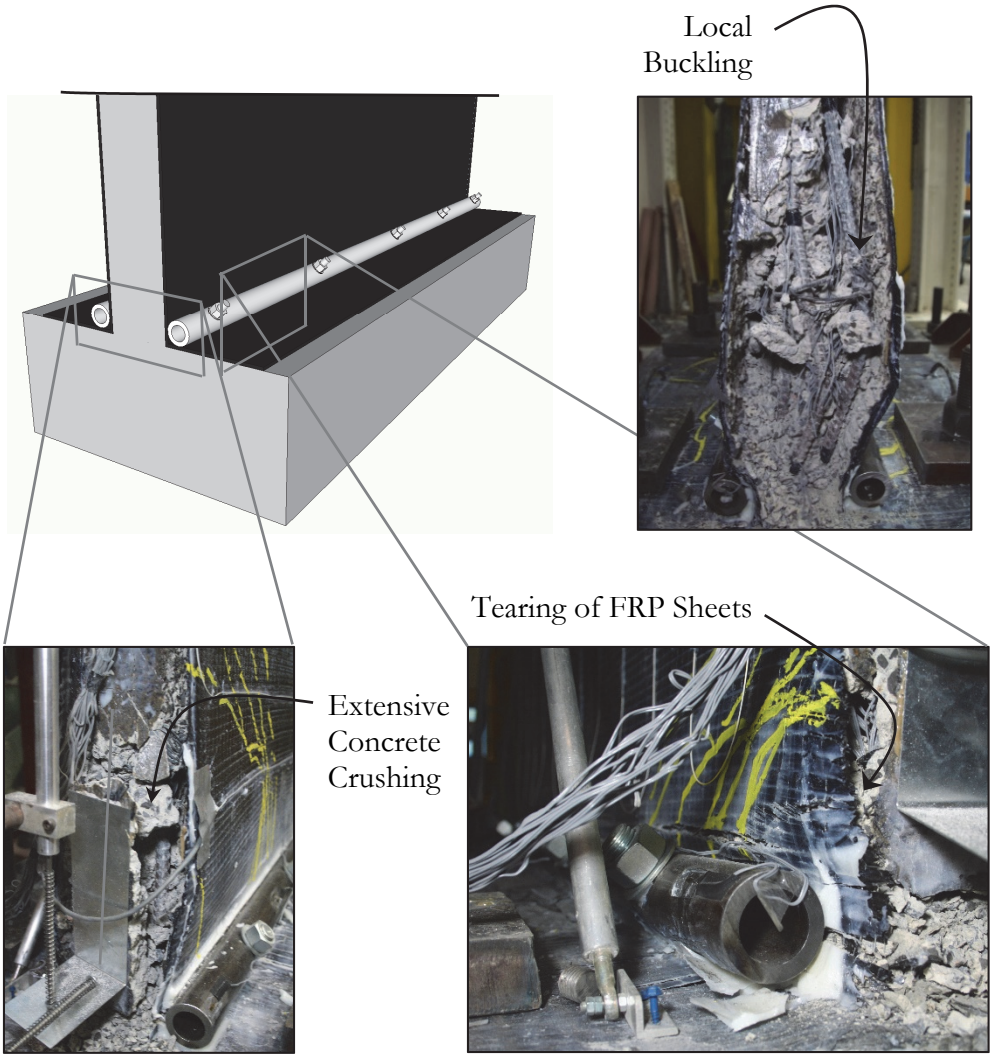

Figure 5-8: Damage to Wall Specimen and Reinforcement Buckling.

Analysis of the data from strain gauges placed on the longitudinal reinforcement shows that considerable yielding of the vertical reinforcing bars occurs at the outer edges and spreads towards the interior region of the wall, as shown in the Figure 5-9. This is a significant improvement when compared to the control wall specimen which experiences very limited yielding in the vertical steel reinforcement prior to failure. It is noted that in the strengthened wall specimen, yielding also spreads to the mid-height level of the reinforcing steel located at the edges of the wall, as shown in Figure 5-9. The increase in the spread of inelastic behaviour throughout the wall specimen is attributed to the addition of horizontal FRP layers which increases the shear capacity and prevents a brittle premature shear failure resulting in a more ductile flexural behaviour. The flexural behaviour of the wall results in an increase in ductility, drift, and energy dissipation capacity when compared to that of the control wall. Thus, these results show that by strengthening an existing deficient shear wall using FRP, significant improvements to the seismic performance of the wall can be achieved.

5.4 Results from the Distributed Fibre-optic Strain Measurement

As described in Section 2.4, a distributed fibre optic sensor (DFOS) for strain measurement is installed on the FRP in the strengthened wall test specimen in an attempt to accurately capture the vertical and horizontal strain distributions in the FRP. Results from this new measurement system indicate that the DFOS performs well in adequately capturing the strain distribution in the FRP along the length of the fibre. A typical strain output from the DFOS at the cracking, yield and ultimate load of the wall are shown in Figure 5-10. It should

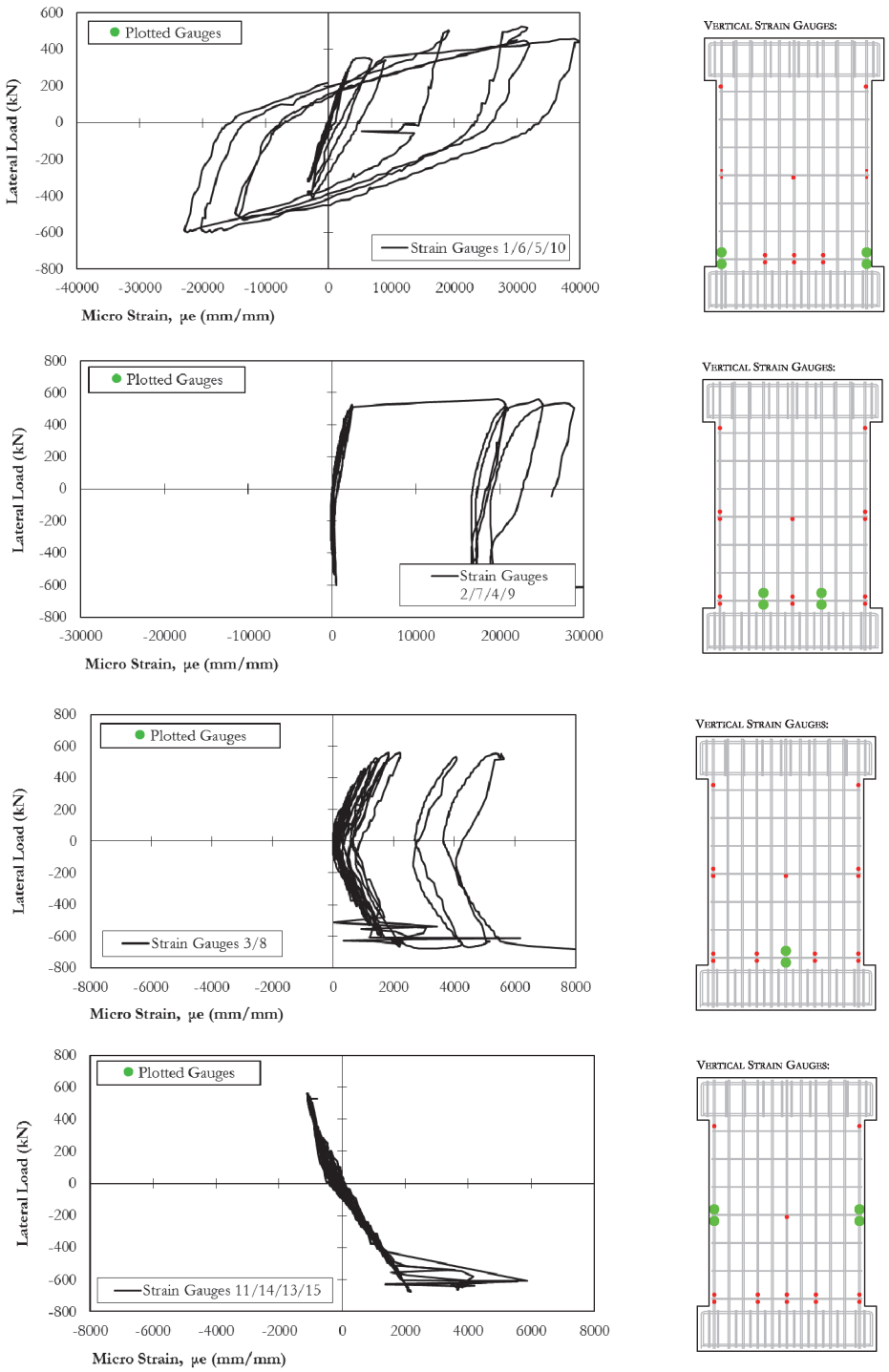

Figure 5-9: Longitudinal Reinforcement Hysteretic Response Behaviour.

be noted that the fibre is installed at a small distance above the base of the wall outside of the region where damage to the wall could lead to rupture of the fibre. Therefore, the vertical strain is not measured directly at the base of the wall. However, it is expected that the results nonetheless give a good representation of the vertical strain distribution in the FRP. Vertical strain profiles in the FRP at the base of the wall and horizontal strain profiles in the FRP at mid-height of the wall specimen are shown in Figure 5-11 for the cracking, yield and ultimate load. The strain profiles are determined based on the peak values from Figure 5-10. The horizontal strain profiles show that the shear strain at mid-height of the wall follows an approximately parabolic distribution, with the highest shear strain occurring close to the centre of the wall specimen. Results from the vertical strain profiles in the FRP agree with the design assumption that the neutral axis falls at a distance approximately equal to 2/3 times the length of the wall specimen and correlate well with analytical results from Hassan et al. (2013). This also verifies the idealization of the load applied to the anchor systems in Figure 4-1, where it is assumed that the stress in the FRP follows a linear stress distribution up to the location of the neutral axis. The DFOS can also be used to measure the strain contour in the FRP over the face of the shear wall. Vertical and horizontal strain contour plots shown in Figure 5-12 and Figure 5-13 demonstrate that the DFOS can adequately capture the strain distribution in the FRP sheet, something which has never been done in FRP strengthened members and is difficult to achieve with conventional strain gauge measurements. Although results from the strain distribution cannot be verified with conventional strain gauge measurements, the results nonetheless give a good representation of what is to be expected for the vertical and horizontal

stress distributions in the FRP. This includes high vertical stress in the FRP at the base of the shear wall, and large horizontal stresses located in the centre of the wall.

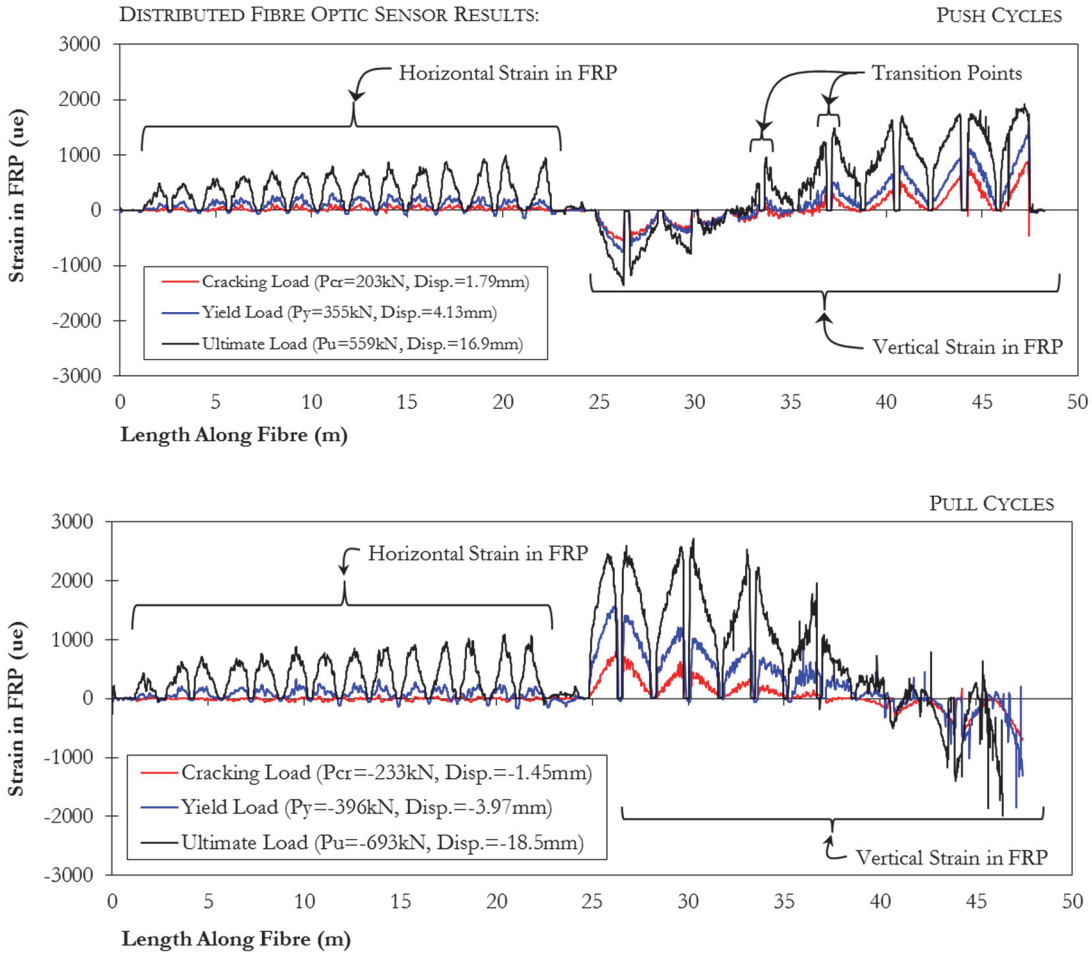

Figure 5-10: Strain in the FRP along the Length of the Fibre.

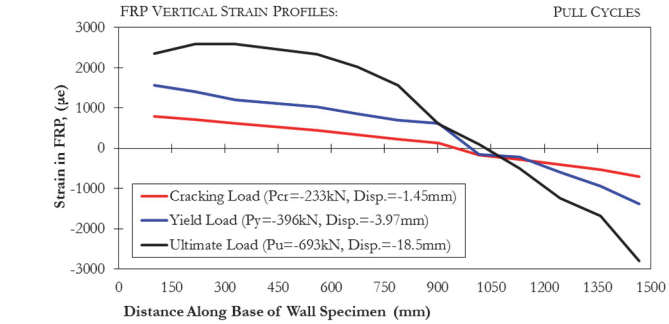

(a)

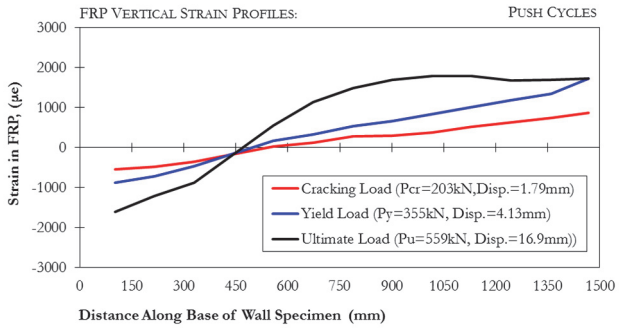

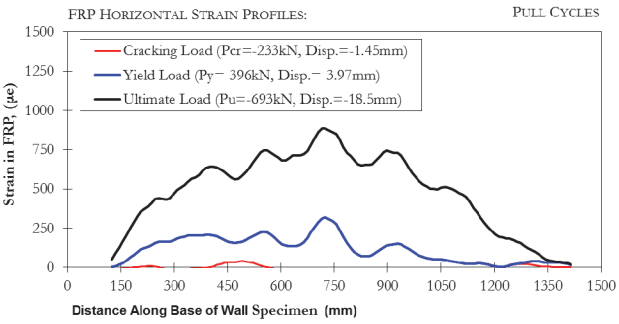

(b)

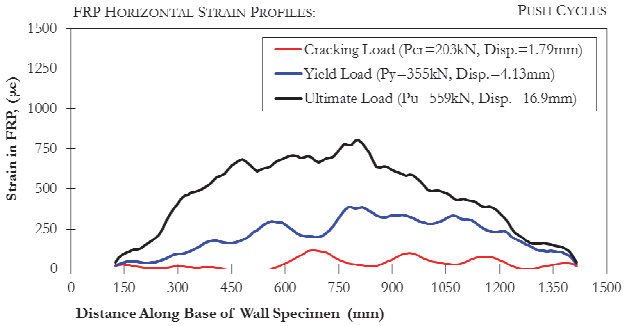

Figure 5-11: Strain Profiles: (a) Vertical Direction; (b) Horizontal Direction.

PUSH CYCLES PULL CYCLES

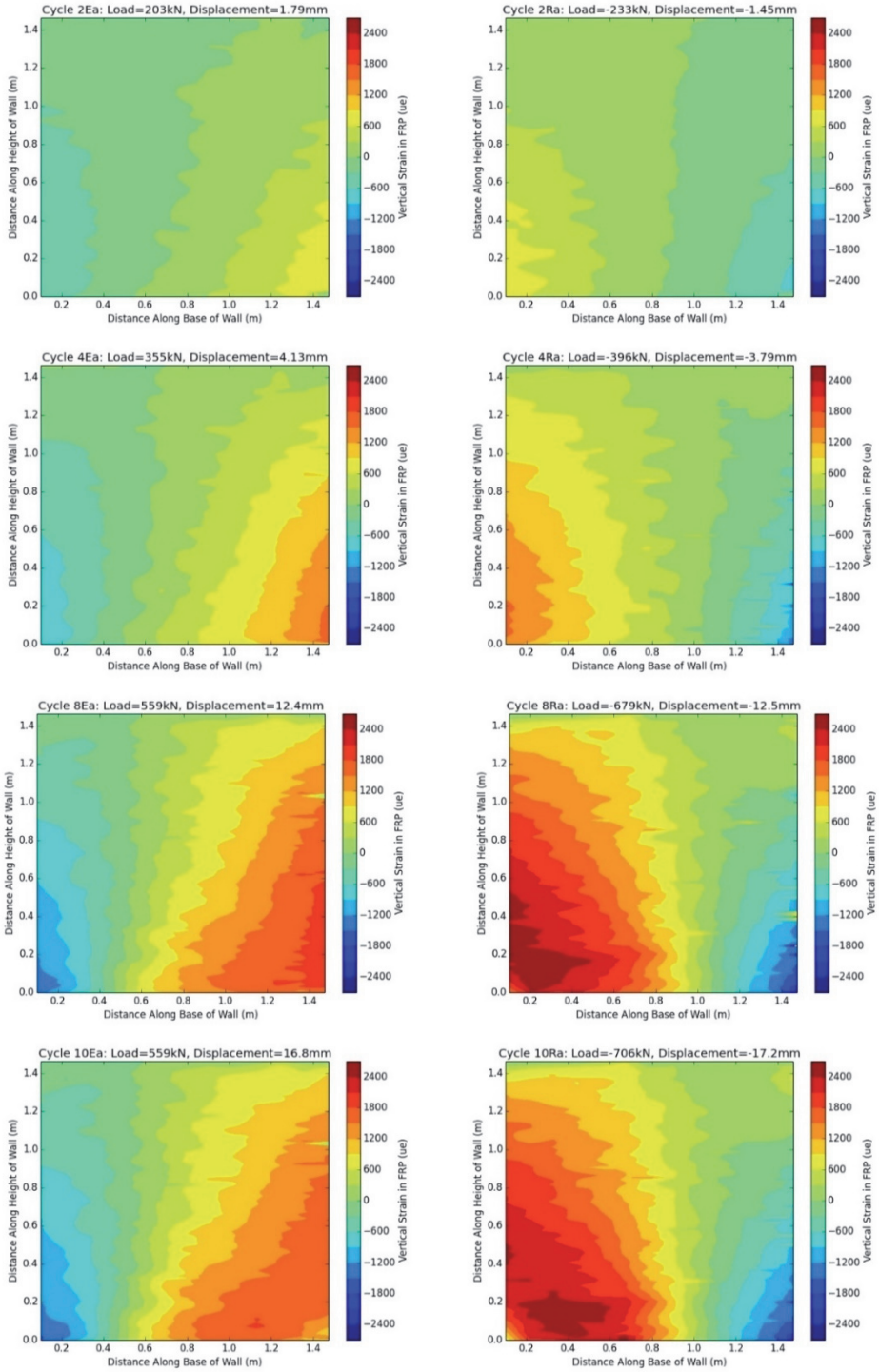

Figure 5-12: Vertical Strain Contour in the FRP.

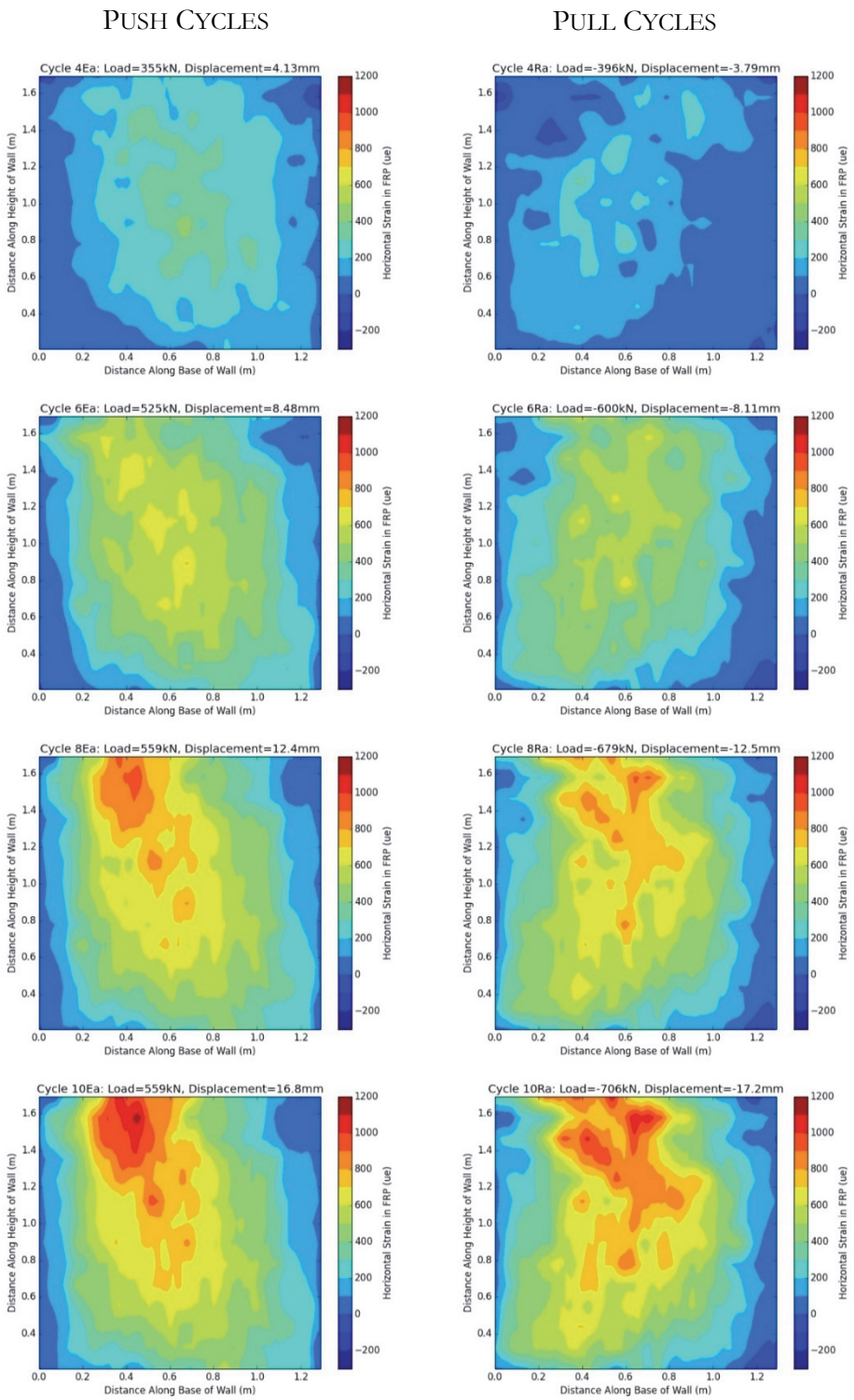

Figure 5-13: Horizontal Strain Contour in the FRP.

CHAPTER 6: DISCUSSION OF EXPERIMENTAL RESULTS

6.1 COMPARISON OF OVERALL SHEAR WALL RESPONSE

The results obtained from experimental testing on a deficient reinforced concrete shear wall have demonstrated that walls designed according to older design standards have a lack of ductility and energy dissipation capacity. The control wall specimen exhibits little to no yielding in the vertical reinforcement prior to brittle failure in diagonal tension. This shows the need to retrofit walls designed according to older design standards and the importance to improve their seismic performance and safety. Experimental results also show that shear walls reinforced with externally bonded FRP sheets in repair and strengthening applications significantly improves their ductility and energy dissipation capacities to promote flexural modes of failure when compared to the control wall. A summary of observations at the maximum load and failure for the three test cases are shown in Table 6-1. Results show that the first appearance of FRP debonding ranges drastically from 0.2-0.88% drift in the repaired and strengthened shear walls. The significant enhancement in the drift ratio observed in the strengthened wall clearly demonstrates the effectiveness of the FRP strengthening system in improving the seismic performance of the wall. The hysteretic response of the three wall specimens shown in Figure 6-1 shows the increase in strength, ductility and energy dissipation capacity of the repaired and strengthened wall specimens when compared to the control wall.

The pinched behaviour of the wall specimens is a phenomenon typically associated with sliding shear behaviour. Under multiple reversed load cycles, the opening and closing of large cracks along the base of the wall results in the "pinched" behaviour of the wall. The poor seismic performance of the control wall is reflected by the lack of energy dissipation in its hysteretic response. In comparison, walls reinforced with FRP sheets exhibit more energy dissipation, identified by the wide loops in the hysteretic response. The single exception to the significant increase in energy dissipation is in the repaired wall specimen in the direction which suffered a significant amount of damage during the previous test, which shows a less ductile hysteretic response when compared with the strengthened wall specimen. However, it still performs better than the control wall. The hysteretic response behaviour also shows that the compression softening effect in repeated load cycles at the same ductility ratio is minimal. To quantify and compare the energy dissipation among the wall specimens, the progress of energy dissipation during the three wall tests is calculated by dividing the total work of the wall specimen by the maximum load and displacement. The total amount of energy dissipated by each wall specimen is shown in Figure 6-2. Results indicate that the repair and strengthened wall specimens dissipate three to five times the energy of the control wall specimen, quantifying the conclusions drawn from observations on the hysteretic response of the wall specimens.

Table 6-1: Failure-modes Observed during Experimental Testing.

Wall Specimen	Drift at FRP Debonding	Observations at Maximum Load	Drift (%) at Ult. Load	Observations at Wall Failure	Drift (%) at Wall Failure
SLCW	-	Extensive diagonal cracking. Some flexural cracking along edges.	0.47	Wide diagonal shear crack. Some crushing at wall toe, longitudinal reinforcement exposed at wall base.	0.74
SLRW	0.2	Minor debonding at wall corner and along diagonal propagating from walls centre. Some flexural cracking and formation of significant sliding shear crack at wall base.	0.88	Major debonding along wall base and along diagonal in locations of pre-damage. Significant crushing at wall toes. Compressive buckling of longitudinal reinforcement and FRP.	1.48
SLSW	0.88	No visible debonding from concrete substrate. Large sliding shear crack along base of the wall specimen. Flexural cracking along wall boundaries.	0.78	FRP debonding at wall toes in v-shaped pattern. Significant crushing at wall toes. Compressive buckling of longitudinal reinforcement. Fracture and buckling of FRP in tension/compression.	1.62

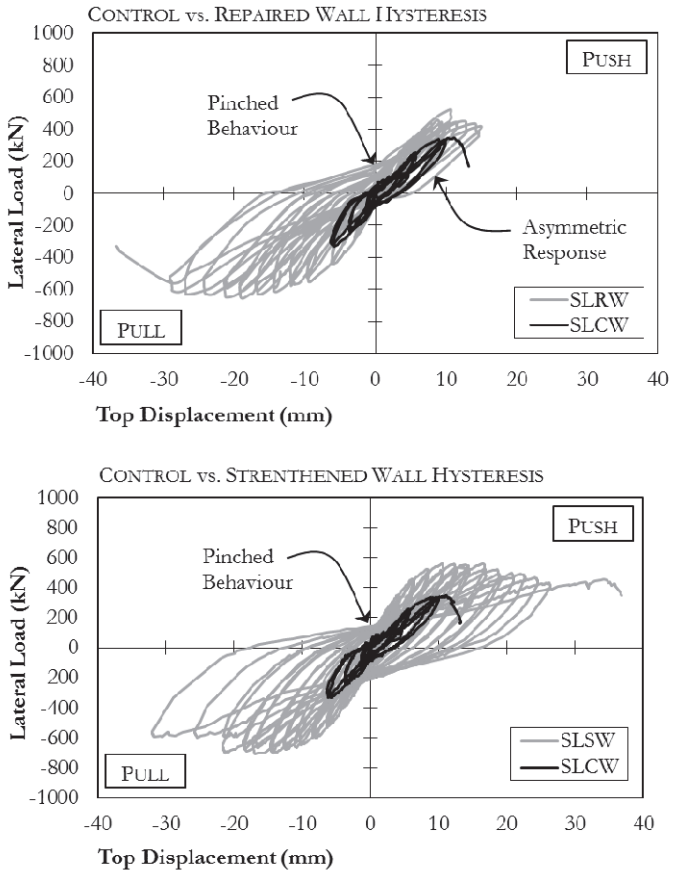

Figure 6-1: Comparison of the Hysteretic Response of the Wall Specimens.

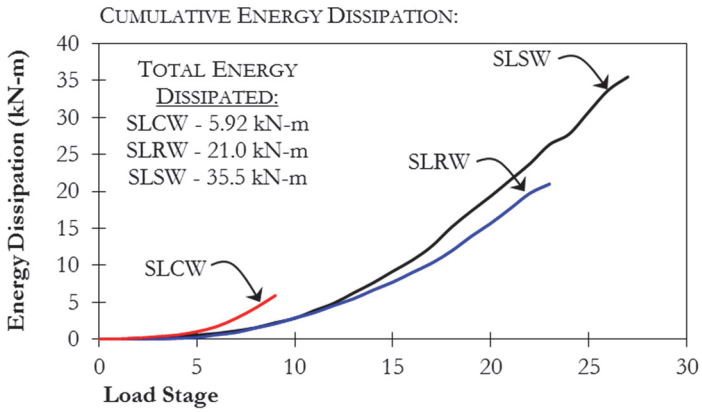

Figure 6-2: Comparison of the Cumulative Energy Dissipated for each Wall Specimen.

The strength envelopes for the three shear wall specimens (Figure 6-3) shows the ability of the FRP retrofitting system to increase the ultimate load carrying capacity and the ductility in repair and strengthening scenarios. The ultimate load carrying capacity is approximately 1.9 times larger for the strengthened wall specimen compared to the control wall and the ductility is increased by a factor of almost 3. This identifies the ability of the vertically applied FRP sheets to increase the flexural capacity of the wall specimen while the horizontal sheets provide additional shear capacity to promote a ductile failure mode resulting in an improved seismic performance of the shear wall.

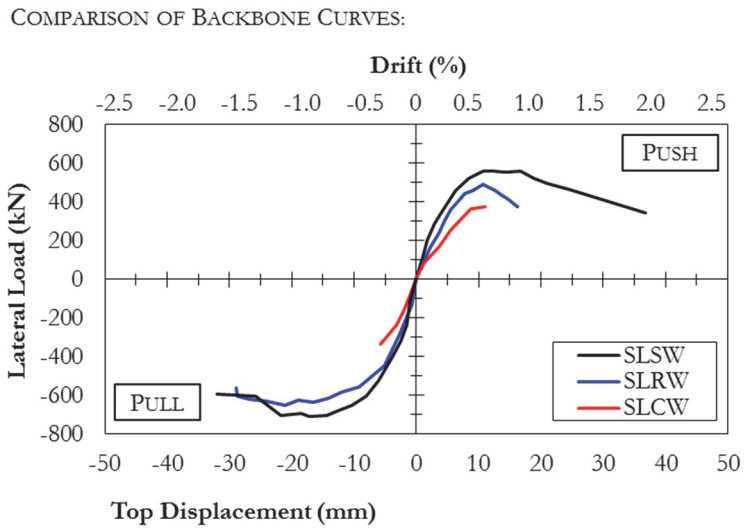

Figure 6-3: Backbone Curves for the Control, Repaired and Strengthened Walls.

Table 6-2 presents several structural performance indicators for the wall specimens including the initial stiffness, yield characteristics, ultimate strength and ductility. Values shown are the average of push/pull cycles. Results from the control and repair walls in Table 6-2 show that even in significantly damaged shear wall specimens (decrease to 40% of ultimate

load carrying capacity), the retrofitting scheme is capable of restoring the initial stiffness and increasing the lateral drift capacity of the wall specimen, demonstrating that the FRP reinforcing scheme is effective in repairing shear walls which may have experienced damage during moderate to large earthquakes. Although it could be argued that these walls would be too damaged to be repaired, typically after an earthquake has occurred not all of the shear walls in the structure would be damaged to this extent, and therefore the retrofitting system would be applicable in shear walls in other location or other stories which experienced less seismic damage.

Table 6-2: Comparison of Measured Structural Parameters for Each Wall Specimen.

Experimental Response Quantity	Shear Wall Specimen		
	SLCW	SLRW	SLSW
Cracking Load (kN)	83.3	N/A	N/A
Initial Stiffness (kN/mm)	73.4	125	117
Initial Stiffness Compared to SLCW	1.00	1.70	1.59
Yield Load (kN)	242	372	376
Yield Displacement (mm)	5.21	4.78	3.96
Yield Load Compared to SLCW	1.00	1.54	1.55
Yield Secant Stiffness (kN/mm)	22.4	40.6	51.4
Yield Stiffness Compared to SLCW	1.00	1.82	2.30
Maximum Load Carrying Capacity (kN)	341	610	633
Ultimate Displacement (mm)	13.2	26.6	29.1
Increase in Ultimate Load (kN) vs. SLCW	1.00	1.79	1.86
Displacement Ductility (mm/mm)	1.2	3.1	4.1
Maximum Drift (%)	0.54	1.48	1.91
Total Dissipated Energy (kN-m)	5.92	21.0	35.5
Dissipated Energy Compared to Control	1.0	3.5	6.0

6.2 Experimental Performance of Tube Anchor System

The experimental results show that the tube anchor system is capable of preventing premature debonding of the vertical FRP sheet and allows the FRP to reach its ultimate tensile capacity or rupture of the FRP sheet, as shown in Figure 6-4(a). Tearing of the FRP laminate occurred in the later stages of the tests after yielding of the steel reinforcement, resulting in a ductile flexural failure of both wall specimens. Although the size of the tube anchor system is significantly reduced compared to previous tests conducted by Hiotakis (2004) (43.7% reduction in steel area), excellent performance of the tube anchor system, characterized by little to no deformation in the tube between points of anchorage, is achieved. One shortcoming of the anchor system noted during the test is small deformation of the tube at the ends of the anchor, allowing small uplift of the FRP along the horizontal segment of FRP bonded to the foundation. This is a result of the fact that although the design drawings recommended an edge distance of 125mm, in some regions this cannot not be achieved due to the presence of reinforcing steel in the foundation of the wall. In cases where the final anchor rod could be located at the optimal edge distance as determined according to the parametric study presented in Section 4.4, uplift does not occur. This observation shows that proper anchorage of the FRP close to the edges of the wall is critical to prevent the slight uplift of the FRP by placing the final anchor rod at, or less than the optimal edge distance. The large shear crack located along the base of the wall also results in debonding of the FRP from the foundation underneath the anchor, as shown in Figure 6-4(b). However, even at the ends of the tube which experience some deformation, displacements do not result in a

significant loss in load carrying capacity of the wall specimen compared to those where anchorage is able to be placed at the design edge distance.

6.3 Comparison with Flexurally Dominant Wall Specimens

In this study, three experimental tests are conducted on two shear deficient reinforced concrete wall specimens to assess the seismic performance of shear walls detailed according to older design standards (ACI 1968; CSA A23.3-77). Results indicate walls detailed according to older design standards pose a significant risk to the safety of the structure due to insufficient shear strength, ductility and energy dissipation capacity leading to sudden and brittle failure of the wall under lateral loads representative of those induced by an earthquake. However, results also demonstrate that the FRP retrofitting system is capable of preventing brittle shear failures and increasing the flexural strength, stiffness and energy dissipation capacity of the wall specimen promoting a more ductile failure mode and improving the seismic performance of the wall. In previous studies by Lombard et al. (2000) and Hiotakis (2004), the efficiency of a similar retrofitting scheme is evaluated on shear walls designed according to modern design standards (CSA A23.3-94). Several comparisons can be made between the current study, and the one by Lombard (1999) and Hiotakis (2004) including the differences between modern and older design standards. The previously tested wall specimens have identical dimensions to those described in this study but with reinforcement ratios of 0.8 and 0.5% in the longitudinal and transverse directions, respectively. The wall specimens have good seismic details including confinement of the boundary elements, sufficient shear reinforcement and concrete strengths typical of modern construction practices. Steel and FRP reinforcing schemes for each of the

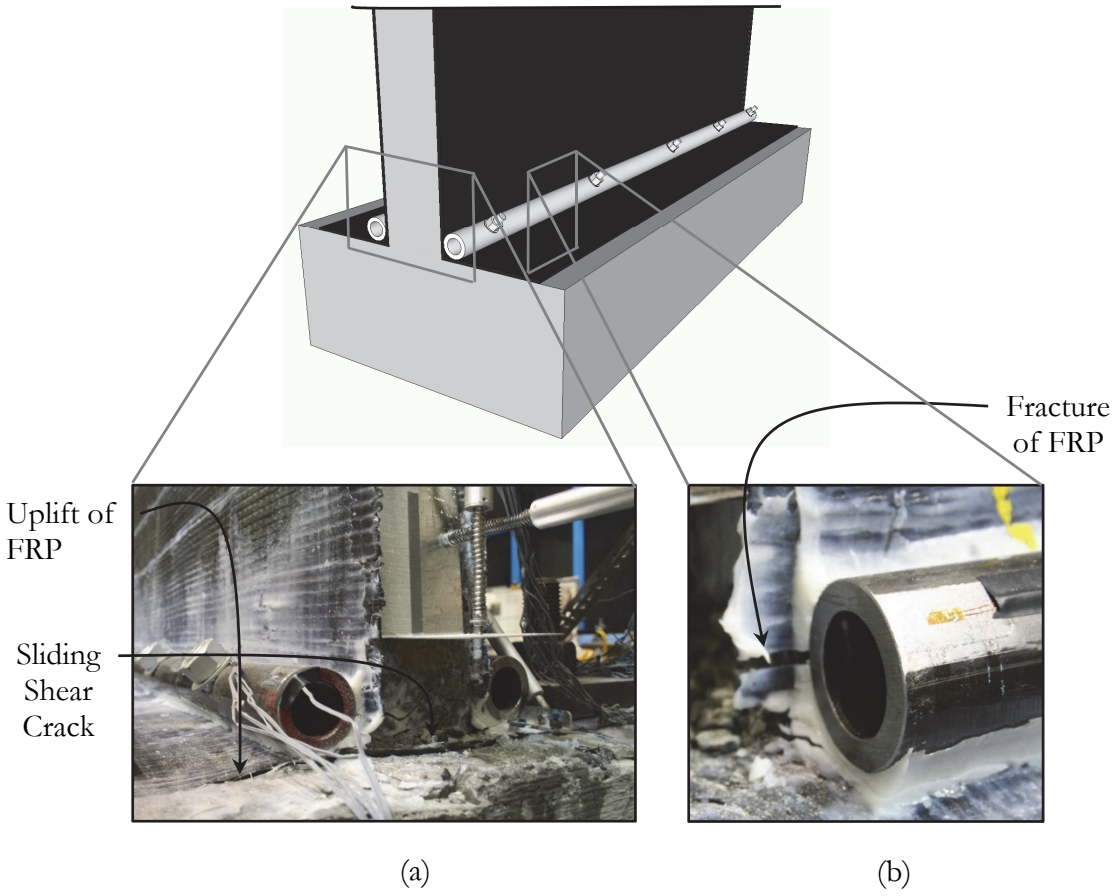

Figure 6-4: (a) Fracture of FRP Sheet at the Base; (b) Uplift of the FRP Sheet at Base.

wall specimens tested by Lombard (1999) and Hiotakis (2004) are shown in Table 6-3 and Figure 6-5. Lombard (1999) and Hiotakis (2004) conclude that by reinforcing shear wall specimens using externally bonded FRP sheets, the retrofitting system can recover the majority of the initial stiffness in damaged wall specimens and increase the initial stiffness in undamaged walls. The system is also capable of increasing the flexural capacity, ductility and energy dissipation capacity in repair and strengthening applications. Similar observations to those by Lombard (1999) and Hiotakis (2004) are made for deficient old shear walls in the current investigation. In this study, the FRP retrofitting system is shown to be capable of preventing premature shear failure and promoting a flexural failure mode resulting in an increase in strength, ductility and energy dissipation capacity of the walls in repair and strengthening scenarios. The FRP retrofitting system is also capable of restoring the initial stiffness in severely damaged walls.

Although results from the wall specimens in this study and those in the previous studies by Lombard (1999) and Hiotakis (2004) cannot be compared directly due to the differences in reinforcing schemes, comparisons can be made between the drift capacity, energy dissipation capacity, and ratio of the initial stiffness, yield displacement, yield load and ultimate load when compared to the control wall in each study. Results in Table 6-4 show the differences between walls designed according to older and modern design standards. The lack in drift and energy dissipation capacity in plain RC shear walls designed according to older design standards is clearly evident from the observed performance obtained in the two studies. Table 6-4 also shows that by strengthening or repairing a deficient wall using externally bonded

FRP sheets, the drift capacity of the deficient wall specimens (1.99 & 1.48%) can be increased to the level of walls designed according to modern design standards (2.0 & 1.99%). The comparison of drift and energy dissipation capacities shows that old shear wall structures are susceptible to collapse failure during moderate to large earthquakes and require retrofitting to meet the performance levels of modern design standards. The comparison of the three studies also shows that the FRP retrofitting scheme can significantly improve the performance of older shear wall structures to within acceptable levels defined by modern design standards. The differences in the performance levels of the wall specimens in the two studies can also be compared by examining the hysteretic response of the walls. Figure 6-6(a) shows the hysteretic response of one plain RC shear wall from the two studies. The results show that the deficient wall specimen has significantly less ductility and energy dissipation capacity when compared to the wall specimen designed according to modern design standards. The lack of confinement at the boundary regions and insufficient shear reinforcement in the walls designed according to older design standards results in poor seismic performance. A comparison of the hysteretic response behaviour of a strengthened wall specimen from each test in Figure 6-6(b) shows that deficient walls retrofitted using FRP sheets have the ability to reach the performance level of shear walls designed according to modern design standards and have the strength, ductility and lateral drift capacities required to resist a large earthquake without collapse. In the hysteretic response of the wall specimens, the deficient shear walls retrofitted using FRP have a more significant improvement in their seismic performance when compared to the walls detailed according to modern design standards retrofitted with FRP.

Table 6-3: FRP Reinforcing Schemes for Modern Shear Wall Specimens. (Lombard, 1999 and Hiotakis, 2004)

	Wall Specimen	Repair/Strengthening Scheme
Lombard (1999)	CW-1	-
	RW-1	1V
	SW1-1	1V
	SW2-1	2V+1H
Hiotakis (2004)	CW-2	-
	RW-2	1V
	SW1-2	1V
	SW2-2	2V
	SW3-2	3V+1H

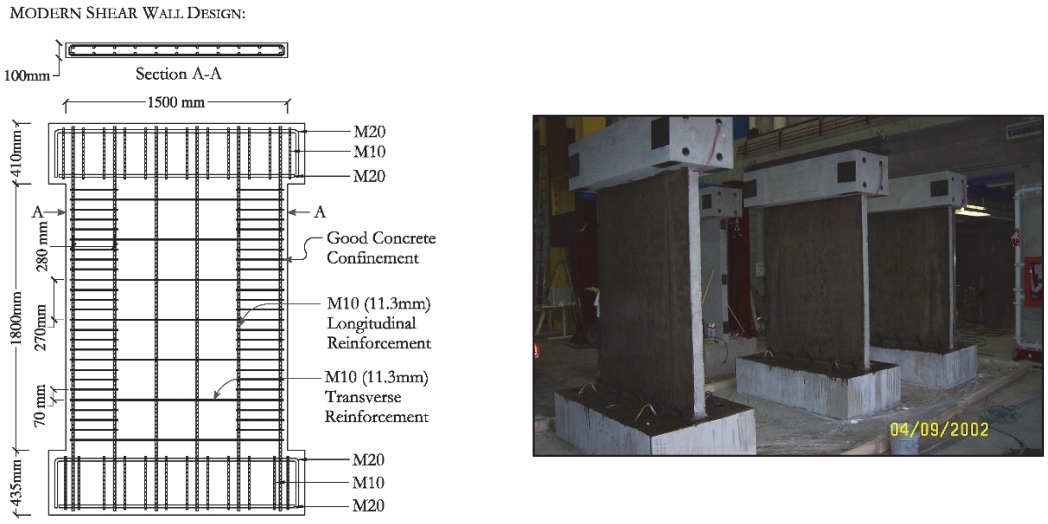

Figure 6-5: Steel and FRP Reinforcing Scheme for Modern Shear Wall Tests. (Image from Hiotakis, 2004)

Table 6-4: Comparison of Modern and Older Shear Wall Performance.
(Select results from Lombard, 1999 and Hiotakis, 2004)

	Specimen	Drift (%) At Wall Failure	Normalized Energy Dissipation (kN-m)	Initial Stiffness Compared to Control	Yield Stiffness Compared to Control Wall	Yield Load Compared to Control	Ultimate Load Compared to Control
Lombard (1999)	CW-1*	0.93	-	1.00	1.00	1.00	1.00
	RW-1	2.00	-	0.49	0.90	1.30	1.81
	SW1-1	1.36	-	1.64	3.19	1.24	1.46
	SW2-1	2.11	-	1.68	2.24	1.64	2.32
Hiotakis (2004)	CW-2*	1.47	20.5	1.00	1.00	1.00	1.00
	RW-2	1.99	23.8	0.47	0.83	1.15	1.44
	SW1-2	1.35	20.9	0.85	1.80	1.24	1.44
	SW2-2	1.20	15.9	2.58	2.12	1.67	2.15
	SW3-2	2.00	44.9	1.24	2.51	1.97	2.62
Woods (2014)	CW-1	0.54	5.92	1.00	1.00	1.00	1.00
	RW-1	1.48	21.0	1.70	1.82	1.54	1.79
	SW-1	1.99	35.5	1.59	2.30	1.55	1.86

* Control walls were not tested until failure.
Values are the maximum reached during the test.

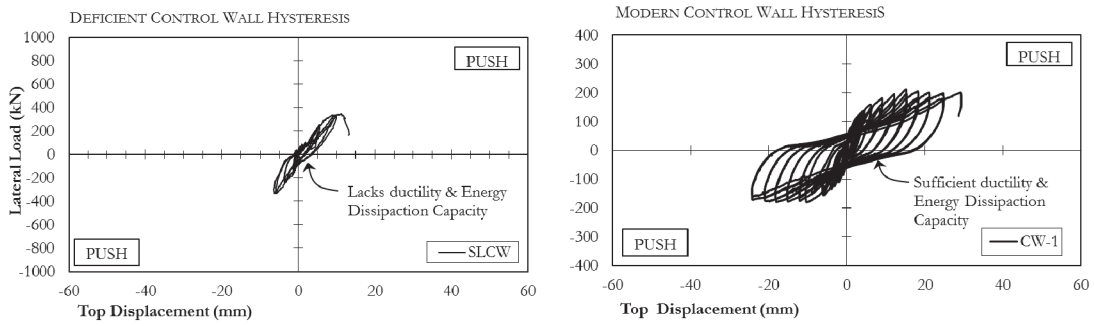

(a)

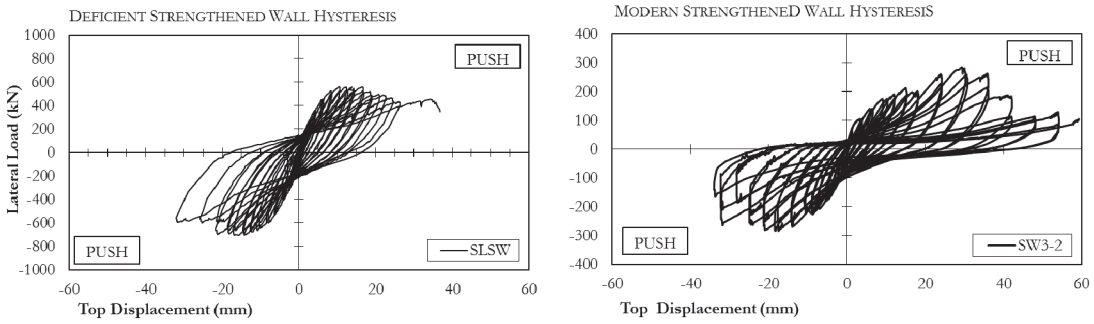

(b)

Figure 6-6: Hysteretic Response of Deficient and Modern Shear Wall Specimens. (Results in (b) from Hiotakis, 2004)

CHAPTER 7: CONCLUSIONS

7.1 SUMMARY OF RESEARCH

This thesis presents results of an ongoing study on the seismic retrofit of reinforced concrete shear walls using externally bonded FRP sheets. Based on previous research conducted by Lombard (1999) and Hiotakis (2004) on the seismic retrofit of reinforced concrete shear wall specimens designed according to modern design standards (CSA A23.3-94), this study expands on previous research and focuses on shear walls designed according to older design standards (ACI 318-68 and CSA A23.3-77). These shear wall specimens exhibit several common structural deficiencies including a lack of confinement in the boundary elements, insufficient shear reinforcement and lower concrete strength. These deficiencies are expected to result in a brittle shear dominant failure of the wall specimen in its unrepaired/un-strengthened state. The experimental program will then evaluate the use of externally bonded FRP sheets in both repair and strengthening applications to improve the seismic performance of the wall specimens. This includes improvements in strength, ductility, and energy dissipation capacity all of which contribute to a more ductile flexural failure of the wall specimen. The FRP sheets are not wrapped around the wall specimen to ensure the practicality of the retrofitting scheme, something which is unique to the FRP retrofitting system used at Carleton University. A significant portion of this study focuses on the optimization of an

innovative tube anchor system. The observations from Hiotakis (2004) on the preliminary experimental performance of the tube anchor system are carefully studied and taken into consideration in the development of an optimized design procedure for the tube anchor system using finite element simulations. Experimental observations on the performance of the tube anchor system by Hiotakis (2004) show the need to improve the efficiency of the tube anchor system, to improve practical applicability. The optimization aims to improve the efficiency of the tube anchor system while maintaining the same level of performance and to assist in the development of design guidelines for the tube anchor system.

7.2 CONCLUSIONS

This thesis presents results on the performance of reinforced concrete shear walls designed according to older design standards, in particular ACI 318-68 and CSA A23.3-77. Results of the study demonstrate that walls designed according to older design standards, specifically those detailed with insufficient shear reinforcement, poor confinement of the boundary elements and lower strength concrete are susceptible to sudden and brittle diagonal tension shear failure with little to no ductility or energy dissipation capacity. To address this issue, an innovative FRP retrofitting system is investigated. The system consists of uni-directional externally bonded FRP sheets applied in the vertical and horizontal directions to increase the flexural and shear capacity of the wall, respectively. Results of the strengthening system using FRP sheets in combination with an innovative tube anchor system show the ability of the retrofitting system to prevent premature shear failure and enhance the seismic response of the wall, including improvements to the in-plane stiffness, ultimate strength and

ductility of specimens with non-ductile details. The use of FRP sheets in the vertical and horizontal directions performs well in increasing ductility and energy dissipation capacity, even in severely damaged reinforced concrete shear walls. However, in the repaired wall specimen, premature debonding of the FRP composite from the concrete substrate due to the opening of pre-existing cracks within the concrete and FRP debonding in strengthened wall specimen at the formation of large cracks in the concrete continues to be a limiting factor in the overall behaviour of the wall specimen. Experimental results show that the shear strength of a wall specimen can be dramatically increased even without wrapping the FRP sheet around the wall. Experimental and analytical modelling of a steel angle anchor system confirms that the system has a deficiency due to an eccentricity which exists between the force in the FRP and the force in the anchor rods causing rotation of the angles flange and premature debonding from the concrete substrate. A new tube anchor system based on the pulley principle to transfer the load from the FRP to a shear walls foundation is shown to be a superior alternative to other mechanical anchor systems. Studies on the optimization of the tube anchor system design presented in this thesis show that the improved tube anchor system can achieve the performance objective with less material and simplified construction techniques, resulting in a more cost-effective design. Experimental results presented demonstrate that the use of tube anchor systems in the retrofit of RC elements with FRP has the potential to increase the stiffness and flexural strength of the specimen by preventing premature debonding between the FRP and concrete substrate.

7.3 SUGGESTIONS FOR FUTURE RESEARCH

This experimental investigation has focused on a small portion of a large area of research on the performance of reinforced concrete shear walls repaired or strengthened with externally bonded FRP sheets. The following include several topics/initiatives suggested for further investigation:

1. Testing multi-storey shear walls detailed according to modern and older design standards and repaired or strengthened using FRP.
2. Research the potential effects of the out-of-plane deformation response of RC shear walls to seismic excitation on the in-plane stiffness of the wall.
3. Testing of FRP-reinforced concrete shear walls loaded with a combination of in-plane cyclic lateral load and axial load, simulating the gravity load of the structure supported by the shear wall.
4. Research on the relative contribution of the FRP sheets on the deformation mechanisms related to shear, flexure, and sliding shear.
5. Development of design guidelines and simplified design aids for the application of the tube anchor system in real-world retrofit scenarios.
6. Application of the tube anchor system in the seismic retrofit of circular columns and curved walls as well as other RC members including beams and slabs.

REFERENCES

ACI 318. (1968). "Building Requirements for Structural Concrete." Detroit, Michigan, USA.: *American Concrete Institute.*

ACI Committee. (2002). "Guide for the Design and Construction of Externally Bonded FRP Systems for Strengthening Concrete Structures." *American Concrete Institute; 440.2R-02.*

Antoniades, K., Salonikios, T., and Kappos, A. (2003). "Cyclic tests on seismically damaged reinforced concrete walls strengthened using fibre-reinforced polymer reinforcement." *ACI Structural Journal,* 100(4), 510-518.

Ceroni, F., Pecce, M., Matthys, S., & Taerwe, L. (2008). Debonding Strength and Anchorage Devices for Reinforced Concrete Elements Strengthened with FRP Sheets. *Journal of Composites Part B: Engineering Vol. 39* , 429-441.

Cruz-Noguez, C. A., Lau, D. T., Sherwood, E. G., Lombard, J., & Hiotakis, S. (2014). "Seismic Behaviour of RC Shear Walls Strengthened for In-Plane Bending Using Externally Bonded FRP Sheets." *Journal of Composite Construction, ASCE.*

Canadian Standards Association (CSA). (1977). "Code for the Design of Concrete Structures for Buildings." *CAN3-A23.3-M77.* Rexdale, Ontario, Canada: *Canadian Standards Association.*

Canadian Standards Association (CSA). (2002). "Design and construction of building components with fibre-reinforced polymers." *CAN/CSA S806-02*, Rexdale, Canada, 177.

Canadian Standards Association (CSA). (1994). "Design of Concrete Structures." *Standard CAN/CSA A23.3-94,* Ottawa, ON, 240.

Elnady, M. (2008), "Seismic Rehabilitation of RC Structural Walls." PhD Thesis, McMaster University, Department of Civil and Environmental Engineering,.

El-Sokkary, H., Galal, K., Ghorbanirenani, I., Leger, P., & Tremblay, R. (2013). Shake Table Tests on FRP-Rehabilitated RC Shear Walls. *Journal of Composites for Construction* , 79-90.

European Committee for Standardization [CEN] (2004). *Eurocode 8 Design of structures for earthquake resistance, Part 1: General rules, seismic actions and rules for buildings.* EN 2004-1-1, Brussels: CEN.

FEMA, (1997). *NHERP Guidelines for the Seismic Rehabilitation of Buildings,* Federal Emergency Management Agency, FEMA 273 (and commentay FEMA 274), October 1997.

Fintel , M. P. (1995). "Performance of Buildings With Shear Walls in Earthquakes of the Last Thirty Years". *PCI Journal, Volume 40 (3)*, 62-80.

Grelle, S. V., & Sneed, L. H. (2011). An Evaluation of Anchorage Systems for Fibre-Reinforced Polymer (FRP) Laminates Bonded to Reinforced Concrete Elements. *Proceeding of Structures Congress* , 1-12.

Hall, J. D., Schuman, P. M., & Hamilton III, H. R. (2002). Ductile Anchorage for Connecting FRP Strengthening of Under-Reinforced Masonry Buildings. *Journal of Composites for Construction Vol. 3* , 3-10.

Hassan, A., Cruz-Noguez, C., Lau, D.T. (2013). Influence of FRP-Concrete Debonding Mechanisms on the Seismic Response of FRP-reinforced shear walls. *Proceedings from the 2013 CSCE General Conference.*

Hiotakis, S. (2004). "Repair and Strengthening of Reinforced Concrete Shear Walls for Earthquake Resistance Using Externally Bonded Carbon Fibre Sheets and a Novel Anchor System." Master's Thesis, Carleton University, Department of Civil and Envirnomental Engineering.

Kalfat, R., Al-Mahaidi, R., & Smith, S. T. (2013). Anchorage Devices Used to Improve the Performance of Reinforced Concrete Beams Retrofitted with FRP Composites: State-of-the-Art Review. *Journal for Composites for Construction 17:14* , 14-33.

Kanakubo, T., Aridome, Y., Fujita, N., & Matsui, M. (2000). Development of Anchorage System for CFRP Sheet in Strengthening of Reinforced Concrete Structures. *Proceeding of 12th World Conference on Earthquake Engineering* , 1831-1839.

Khalifa, A., Alkhrdaji, T., Nanni, A., & Lansburg, S. (1999). Anchorage of Surface Mounted FRP Reinforcement . *Concrete International: Design and Construction Vol. 21:10* , 49-54.

Khalil, A., & Gobarah, A. (2005). Behaviour of Rehabilitated Shear Walls. . *Journal of Earthquake Engineering 9:3* , 371-391.

Kuang, J.S., and Ho, Y.B. (2008). "Seismic behaviour and ductility of squat reinforced concrete shear walls with non-seismic detailing." *ACI Structural Journal*, 105(2), 225-231.

Lam, L., & Teng, J. G. (2001). Strength of RC Cantilever Slabs Bonded with GFRP Strips. *Journal of Composite Construction Vol. 5:4* , 221-227.

Layssi, H. and Mitchell, D. (2012), "Experiments on Seismic Retrofit and Repair of Reinforced Concrete Shear Walls", *Proceedings of the 6th International Conference on FRP Composites in Civil Engineering (CICE),* June 13-15, 2012. Rome, Italy.

Lombard, J. (1999). "Seismic strengthening of reinforced concrete shear walls using externally bonded carbon fibre tow sheets." *Master's Thesis*, Department of Civil and Environmental Engineering, Carleton University.

Lombard, J., Lau, D. T., Humar, J., Foo, S., & Cheung, M. (2000). "Seismic Strengthening and Repair of Reinforced Concrete Shear Walls." *Proceedings of 12th World Conference on Earthquake Engineering.*

Lu, X. Z., Ye, L. P., Teng, J. G., Huang, Y. L., Tan, Z., and Zhang, Z. X. (2004). "Recent research on interfacial behaviour of FRP sheets externally bonded to RC structures." *Proceedings from the 2nd International Conference on FRP Composites in Civil Engineering,* Adelaide, Australia, CRC Press, 389-398.

Paterson, J. and Mitchell, D. (2003). "Seismic Retrofit of Shear Walls with Headed Bars and Carbon Fibre Wrap." *Journal of Structural Engineering, ASCE, (129)5,*606-614.

Pham, H., & Al-Mahaidi, R. (2004). Assessment of Available Prediction Models for the Strength of FRP Retrofitted RC Beams. *Journal of Composite Structures Vol. 66* , 601-610.

Seible, F., Priestley, M. J. N., and Innamorato, D. (1995). "Earthquake retrofit of bridge columns with continuous carbon fibre jackets-Volume II, design guidelines." *Rep. No. ACTT-95/08*, Advanced Composites Technology Transfer Consortium, University of California, San Diego, CA.

Shaheen, I. (2014). "Seismic Retrofit and Strengthening of Deficient Reinforced Concrete Shear Walls Using Externally Bonded Fibre Reinforced Polymer Sheets". *Master's Thesis*. Department of Civil and Environmental Engineering, Carleton University.

Smith, S. T., & Teng, J. G. (2003). Shear Bending Interaction in Debonding Failures of FRP-plated RC Beams. *Advanced Structural Engineering Journal Vol. 6:3* , 183-199.

Smith, S. T., Hu, S., Kim, S. J., & Seracino, R. (2011). FRP-strengthened RC Slabs Anchored with FRP Anchors. *Engineering Structures Vol. 33:4* , 1075-1087.

Smith, T. S., Hu, S., Kim, S. J., & Seracino, R. (2011). FRP-strengthened RC slabs anchored with FRP anchors. *Journal of Engineering Structures Vol. 33* , 1075-1087.

Soller, B., Gifford, D., Wolfe, M., and Froggatt, M. (2005) "High resolution optical frequency domain reflectometry for characterization of components and assemblies." *Opt. Express Vol 33:666.*

Su, K. L. R., and Wong, S. M. (2007). "A survey on axial load ratios of structural walls in medium-rise residential buildings in Hong Kong." *HKIE Trans.*, 14(3), 40-46.

Teng, J. G., Chen, H.F., Smith, S. T., and Lam, L. (2002). *FRP-Strengthened RC Structures*, Wiley, London.

Triantafillou, T. C. (1998). "Shear strengthening of reinforced concrete beams using epoxy-bonded FRP composites." *ACI Structural Journal*, 95(2), 107-115.

Wood, S. L. (1990). "Shear strength of low-rise reinforced concrete walls." *ACI Structural Journals*, 87(1), 99-107.

Woods, J., Cruz-Noguez, C., Lau, D.T. (2014). An Innovative FRP Anchor System for the Seismic Retrofit of Reinforced Concrete Shear Walls. *Proceedings of the 10th National Conference in Earthquake Engineering,* Earthquake Engineering Research Institute, Anchorage, AK. Paper No. 913.

Zhang, H. W., & Smith, S. T. (2012). Influence of Fan Configuration and Dowel Angle on Anchor FRP Plates. *Journal of Composites Part B: Engineering Vol. 43:8* , 3516-3527.

APPENDIX A: MATERIAL PROPERTIES

REINFORCING STEEL

The reinforcing steel used in the design and fabrication of all wall specimens is grade 400 rebar. In the two walls, No. 15 bars are used for flexural reinforcement and M6.34 deformed bars are used for horizontal reinforcement. Detailed mechanical properties for the reinforcing steel are shown in Table A-1. Mechanical properties of the reinforcing steel are the average of three separate tension tests. A typical stress-strain curve for each of the four bar diameters is shown in Figures A-1 through A-4. Strains are measured through the use of an MTS extensometer which is clipped to the center of the reinforcing bar. The extensometer has an overall gauge length of 50.8mm (2 in.).

Table A-1: Mechanical Properties of Reinforcing Steel for each Bar Size.

Bar Designation	Yield Stress F_y (MPa)	Yield Strain ε_y	Elastic Modulus (MPa)	Strain Hardening Strain ε_{sh}	Ultimate Stress (MPa)	Ultimate Strain ε_u	Fracture Strain $\varepsilon_{fracture}$
6M	414.76	0.002968	139744	N/A	597	0.0120	0.025
10M	438.93	0.00218	201346	0.018	613	0.1410	0.18
15M	452.41	0.002414	187410	0.02	596	0.1149	0.12
20M	483.31	0.002825	171082	0.02	622	0.1374	0.27

Note: values shown in this table are an average from three separate coupon tests.

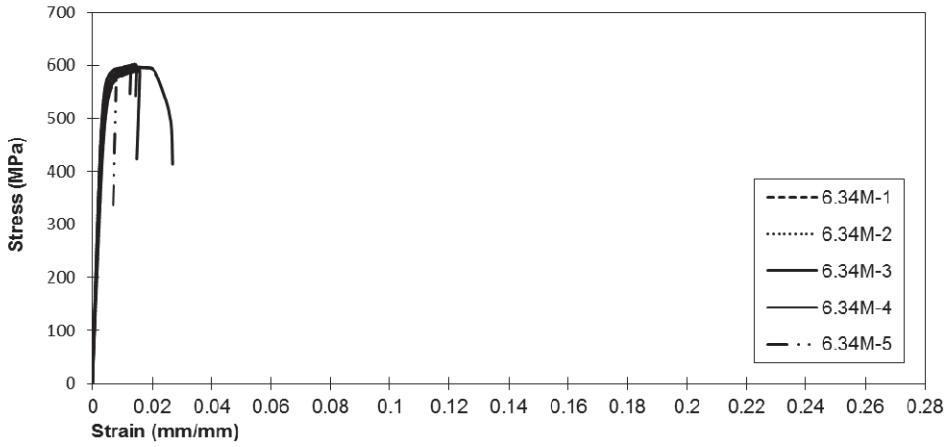

Figure A-1: Stress vs. Strain Relationship for 6.34M Reinforcement Tensions Coupons.

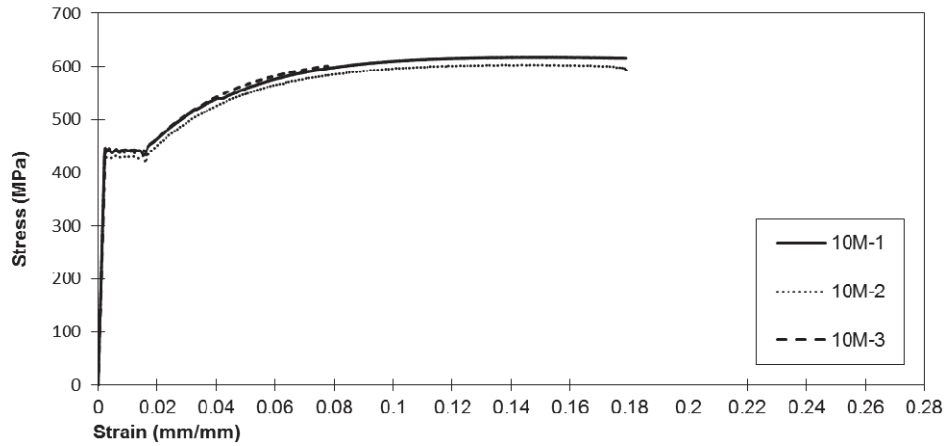

Figure A-2: Stress vs. Strain Relationship for 10M Reinforcement Tensions Coupons.

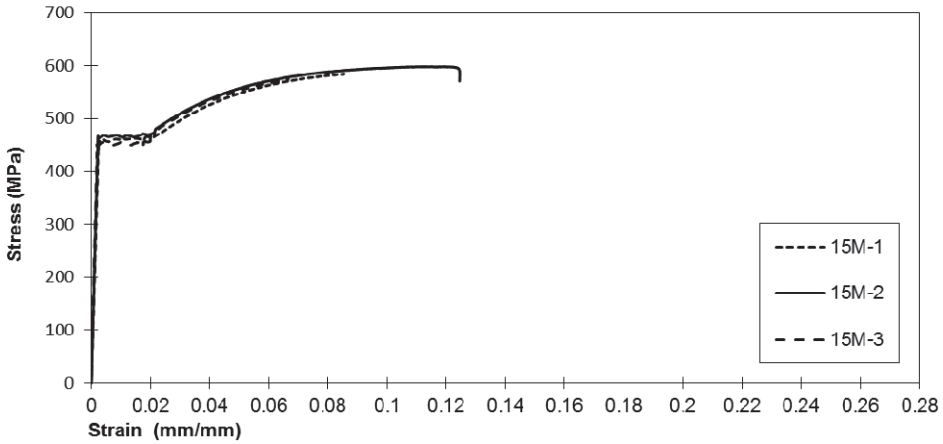

Figure A-3: Stress vs. Strain Relationship for 15M Reinforcement Tensions Coupons.

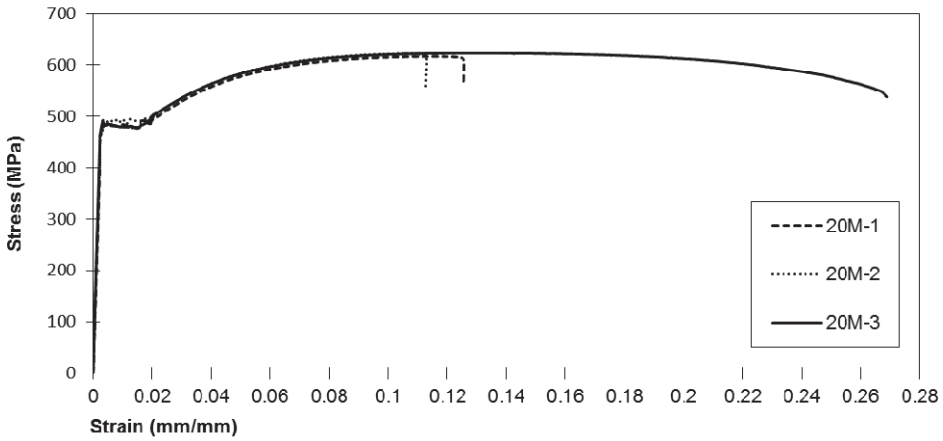

Figure A-4: Stress vs. Strain Relationship for 20M Reinforcement Tensions Coupons.

Figure A-5: Steel Tension Coupons Prior to Testing.

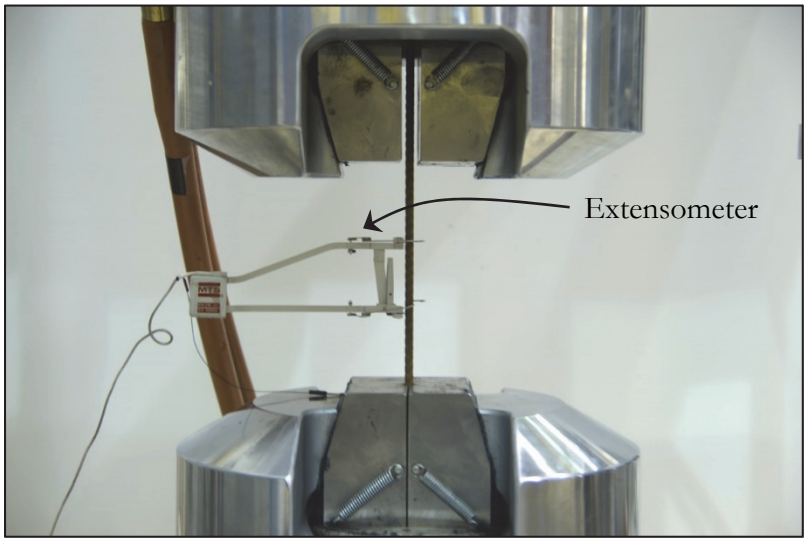

Figure A-6: Typical Tensions Coupon Test Setup.

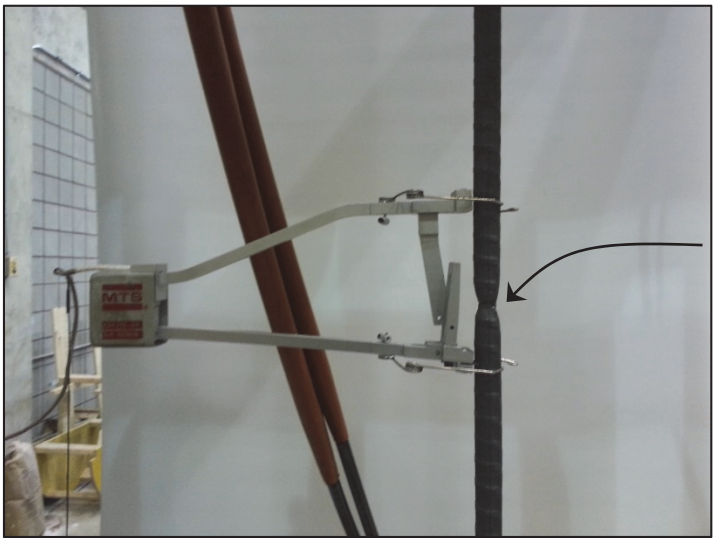

Figure A-7: Typical 10M Steel Reinforcement Rupture.

Figure A-8: Typical 20M Steel Reinforcement Rupture.

CONCRETE

The concrete used in the fabrication of the shear wall specimens has a specified nominal 28 day compressive strength of 20 MPa, 100 mm slump, no air entrainment, and a 10 mm maximum aggregate size with the addition of a super plasticizing agent to ensure continued workability and avoid air entrapment during concrete casting. Continuous slump tests were completed throughout casting to verify the material properties throughout the wall fabrications stage. Standard concrete cylinders measuring 100 x 1500 mm are cast throughout the construction of the shear wall specimens. All concrete cylinders were cured in the same environment as the wall specimens. 28-day compressive strength values for the walls foundations, cap beams and wall panels are shown in Table A-2. The concrete compressive strength on the test-day for each of the wall specimens is also shown in Table A-3.

Table A-2: 28-day Concrete Compressive Strengths.

Concrete Element	28 Day Compressive Strength (MPa)
Foundation Block	80.6
Cap Beams	67.1
Wall Panels	23.0

Table A-3: Test Day Compressive Strengths.

Wall Specimen	Compressive Strength (MPa)
SLCW	21.9
SLRW	20.6
SLSW	19.7

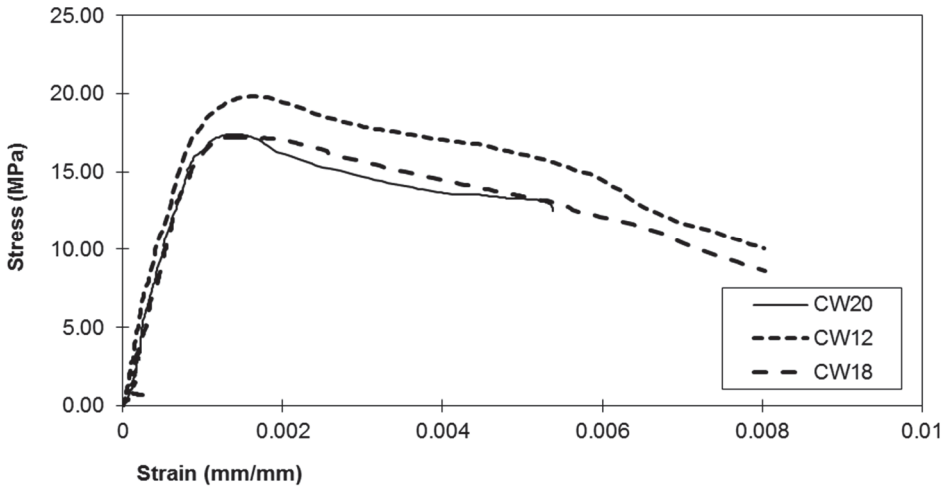

Figure A-9: Typical Stress vs. Strain Response of Concrete Cylinders.

High Strength Capping Compound

Figure A-10: Capping of Concrete Cylinders Prior to Testing.

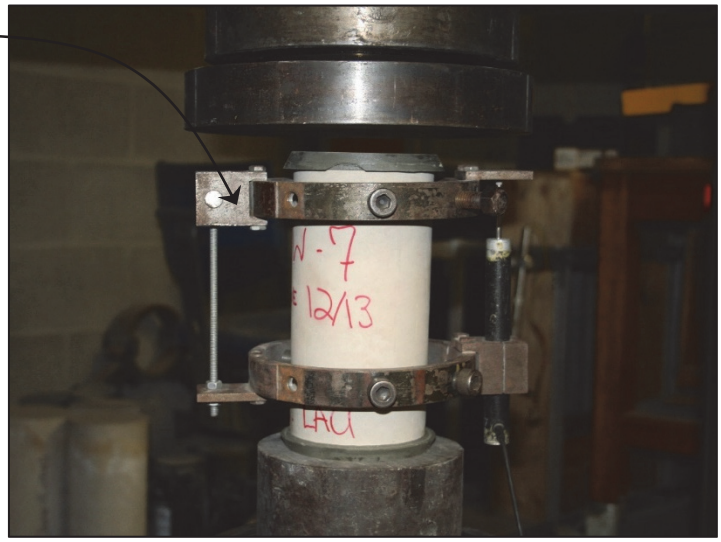

Figure A-11: Typical Cylinder Compression Test Setup.

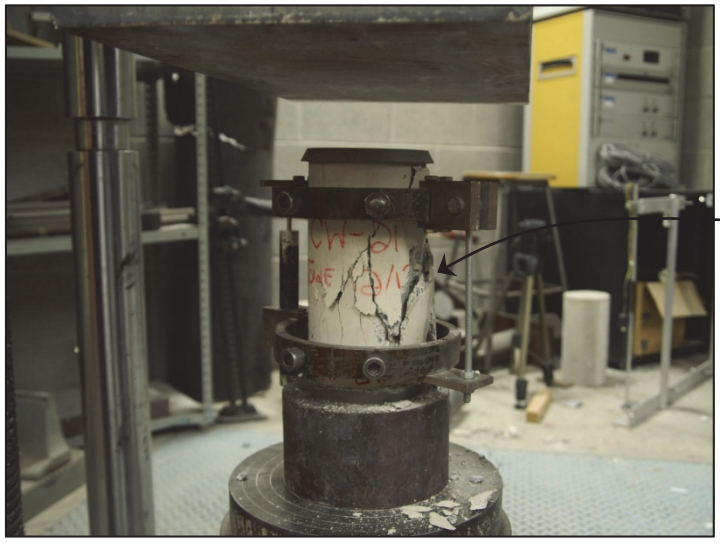

Figure A-12: Typical Failure of Concrete Cylinder.

FIBRE REINFORCED POLYMER (TYFO® SCH-41)

The fibre reinforced polymer selected for this particular project is Tyfo SCH-41 carbon fibre-reinforced polymer composite, manufactured by Fyfe Co. The material is shipped in individual rolls measuring 500.8mm in width and a thickness of 0.11mm. Each roll of FRP composite measures 200m in length prior to being cut into appropriately sized strips. Mechanical properties of the dry FRP material are shown in Table A-4.

Table A-4: Mechanical Properties of Dry CFRP Sheets.

	Tensile Modulus (MPa)	Tensile Strength (MPa)	Ultimate Elongation (me)	Density (g/cm^2)	Weight (g/m^2)	Thickness of Sheet (mm)
Tyfo SCH-41 (Fyfe Co.)	230,000	4000	1.7%	1.74	200.0	0.11

Note that values in this table are obtained from the manufacturer of the FRP.

EPOXY SATURANT (TYFO® S)

The bonding agent between the FRP composite and the concrete substrate is a two part epoxy resin. The two components of the epoxy are identified as Tyfo S epoxy parts A and B. The pot life of the mixed epoxy resin is 3-6 hours at a temperature of 20°C. The density of the mixed epoxy is 1.11 kg/L and each batch of epoxy has approximately 2 years of shelf life prior to expiry. Mechanical properties for the Tyfo S epoxy are shown in Table A-5.

Table A-5: Mechanical Properties of Tyfo S Saturant Epoxy.

	Tensile Modulus (MPa)	Tensile Strength (MPa)	Ultimate Elongation (me)	Compressive Strength (MPa)	Compressive Modulus (MPa)	Flexural Strength (MPa)
Tyfo S (Fyfe Co.)	318,000	72.4	5.0%	86.2	320,000†	123.4

Note that values in this table were not tested experimentally, data obtained from manufacturer.

GROSS COMPOSITE LAMINATE (TYFO® SCH-41 FRP + TYFO® S)

Once applied to the wall specimen in strengthening and repair applications, the previously described Tyfo SCH-41 CFRP acts together with the Tyfo S epoxy to resist the imposed loads in what is referred to as the gross composite laminate. To accurately predict the response of the gross laminate, several FRP coupons are cast during the application of the FRP material. The coupons were then tested 72 hours after casting (recommended FRP curing time, are provided by the manufacturer). Results of the FRP coupon tests are shown in Table A-6.

Table A-6: Gross Laminate Properties of the FRP Material.

	Tensile Modulus (MPa)	Tensile Strength (MPa)	Ultimate Elongation (me)	Compressive Strength (MPa)	Flexural Strength (MPa)
Tyfo S (Fyfe Co.)	91943.5	930.6	0.995%	86.2†	123.4†

†Values provided from the manufacturer and were not tested in lab.

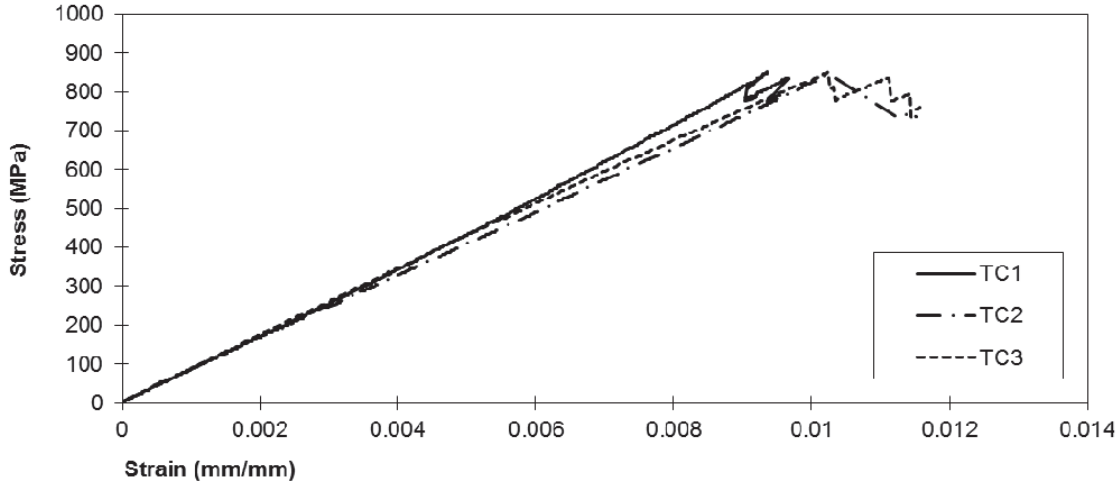

Figure A-13: Typical Stress vs. Strain Response of the FRP Tensions Coupons.

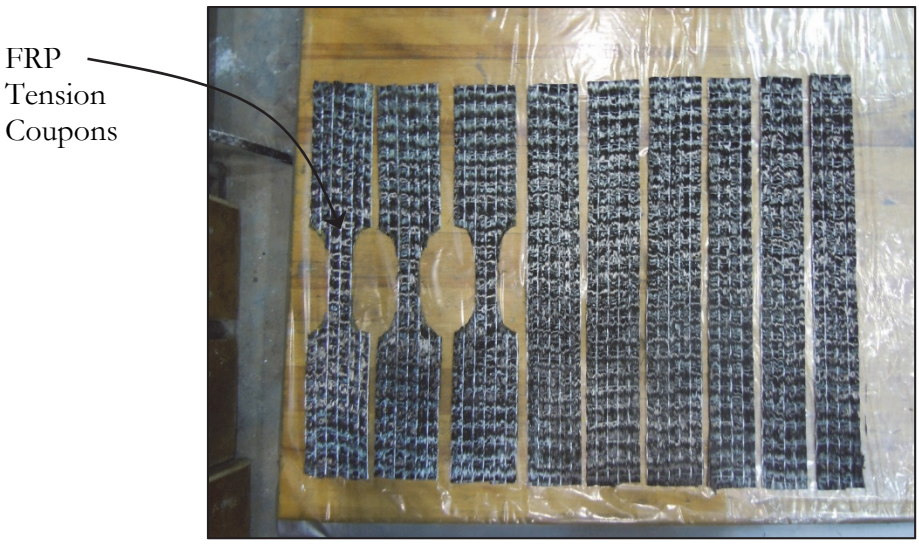

Figure A-14: FRP Tensile Coupons Prior to Testing.

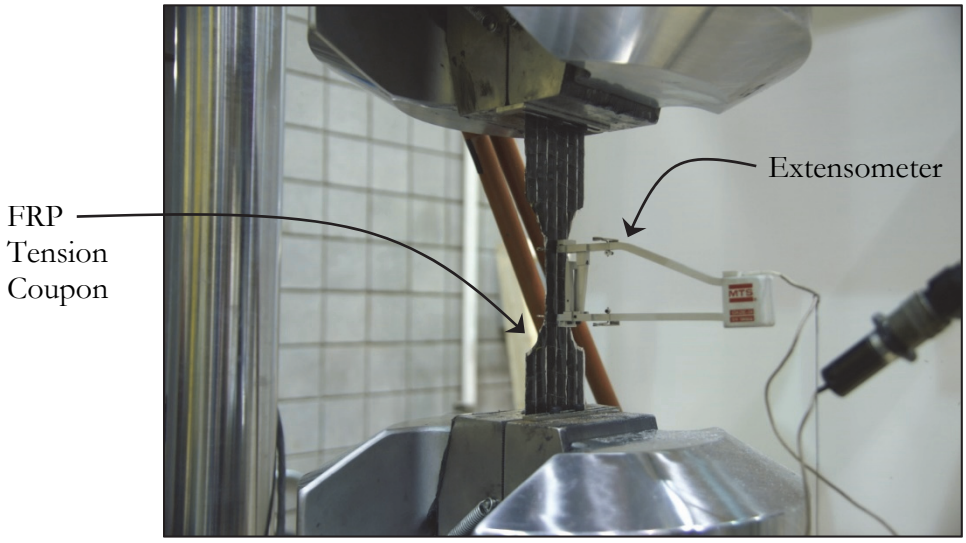

Figure A-15. Typical FRP Coupon Test Setup.

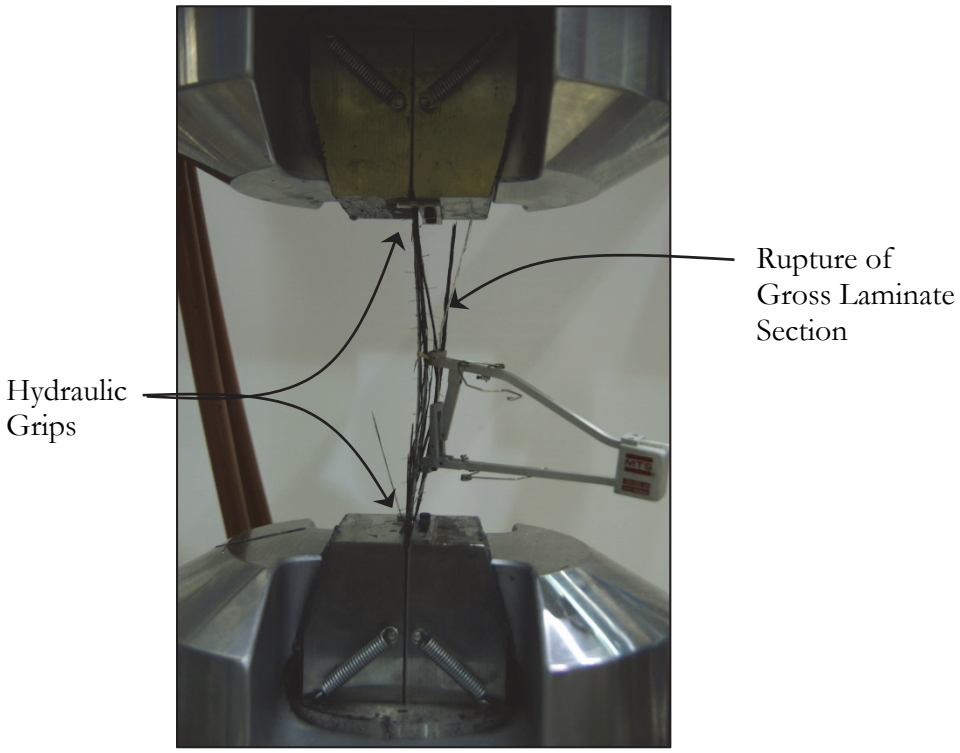

Figure A-16: Typical Tensile Failure of the FRP Coupon.

ANCHOR MATERIAL PROPERTIES

The anchor system tube is fabricated of rolled over mandrel (ROM) steel section measuring 2.25" (57.15 mm) in diameter with a 0.375" (9.525 mm) wall thickness. The ROM steel pipe is ordered in 24 ft. (7.3152 m) sections and cut to the appropriate length for the wall specimens. Mechanical properties for the steel pipe are shown in Table A-7. The pipe meets the specification requirements for ASTM A513 Type 508A steel. The steel pipe is bolted to the walls foundation through the use of several steel anchor rods. Hilti HAS 5.8 steel threaded anchor rods (TARs) measuring 1" (25.4mm) in diameter and 16" (406.4mm) in length are embedded 12" (304.8mm) into the concrete foundation at the base of the wall specimen. Mechanical properties for the high strength steel anchor rods are shown in Table A-7. The material specifications for the high strength rod materials meet the requirements of ASTM A 193, Grade B7.

Table A-7**:** Mechanical Properties of Steel Pipe and Anchor Rods for Tube Anchor System.

	Yield Stress (MPa)	Ultimate Tensile Strength (MPa)	Percent Elongation (me)
ROM Pipe 2.25" (57.15mm) x 0.375" (9.525 mm)	589.96	667.03	32.15%
Hilti HAS 5.8 TARs	724.0	862.0	32.15%

APPENDIX B: ADDITIONAL PLOTS

CONTROL WALL SPECIMEN (SLCW)

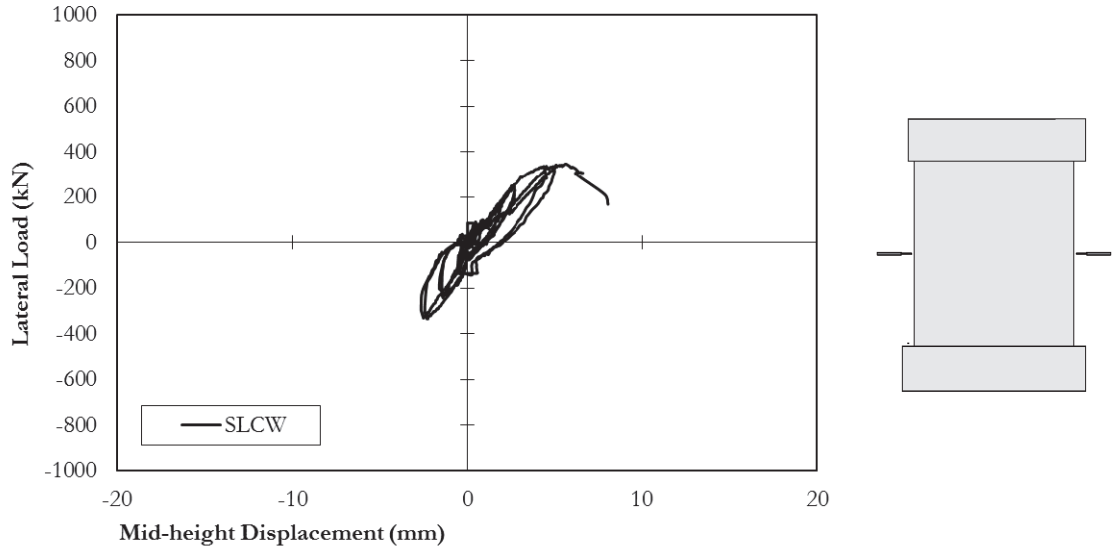

Figure B-1: Mid-Height Displacement of Control Wall Specimen.

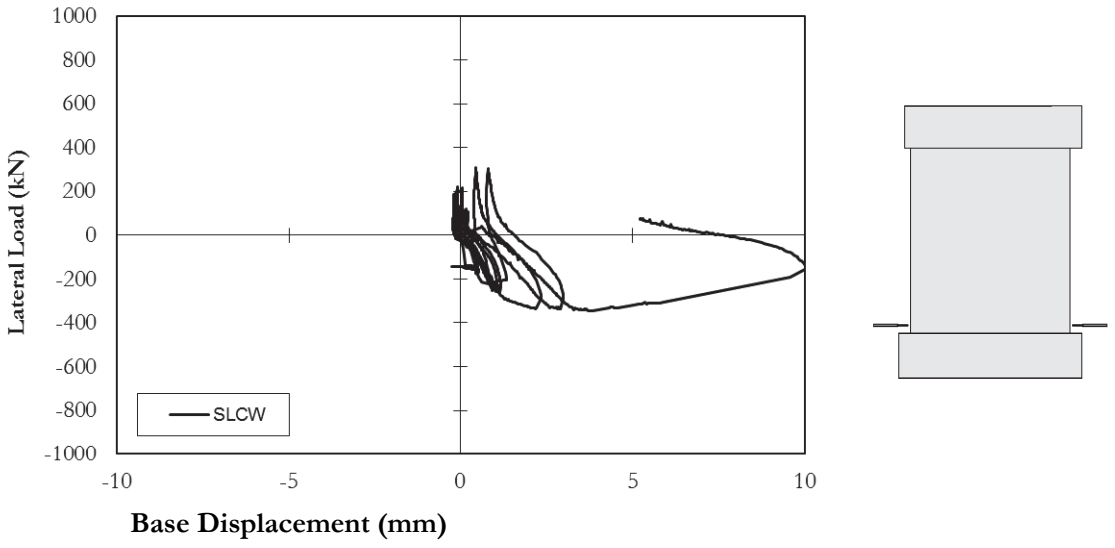

Figure B-2: Base displacement of Control Wall Specimen.

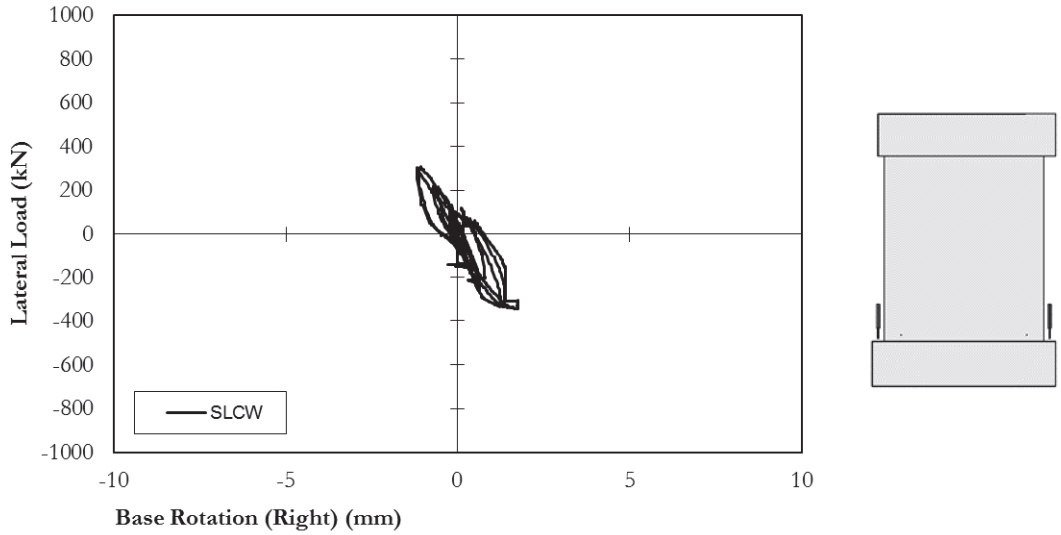

Figure B-3: Base Rotation of Control Wall Specimen.

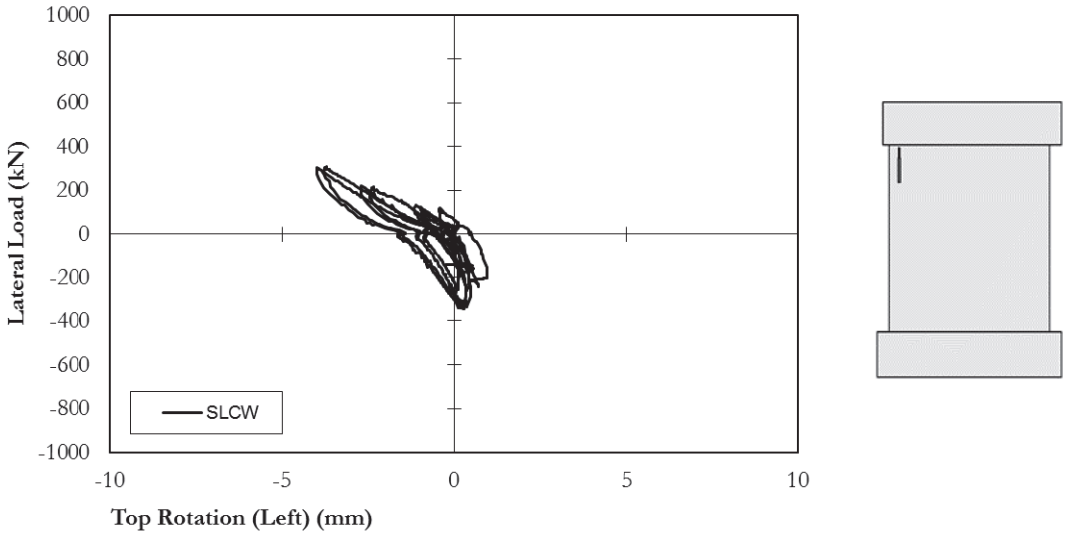

Figure B-4: Top Rotation (left) of Control Wall Specimen.

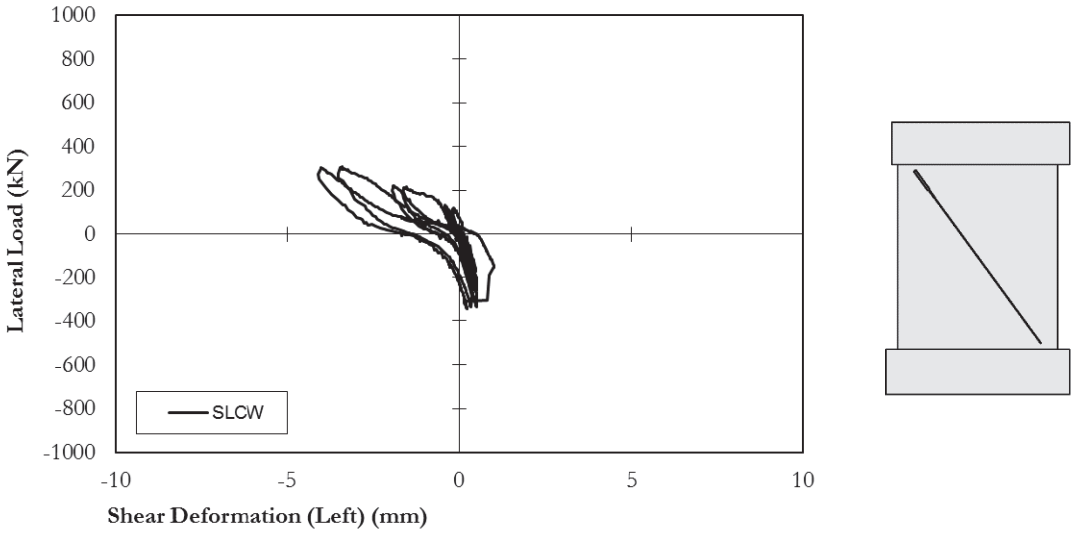

Figure B-5: Shear Deformation (left) of Control Wall Specimen.

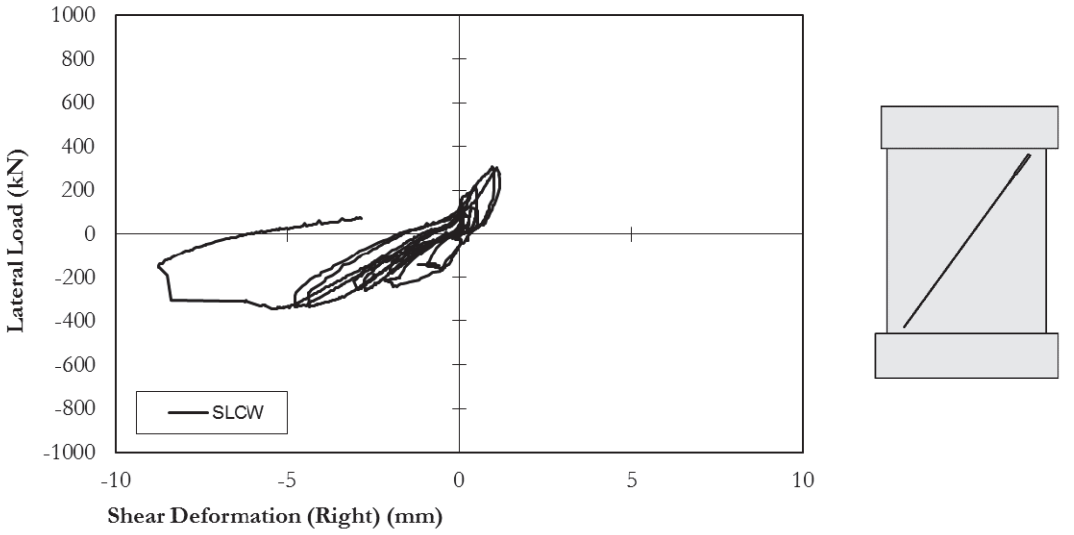

Figure B-6: Shear Deformation (right) of Control Wall Specimen.

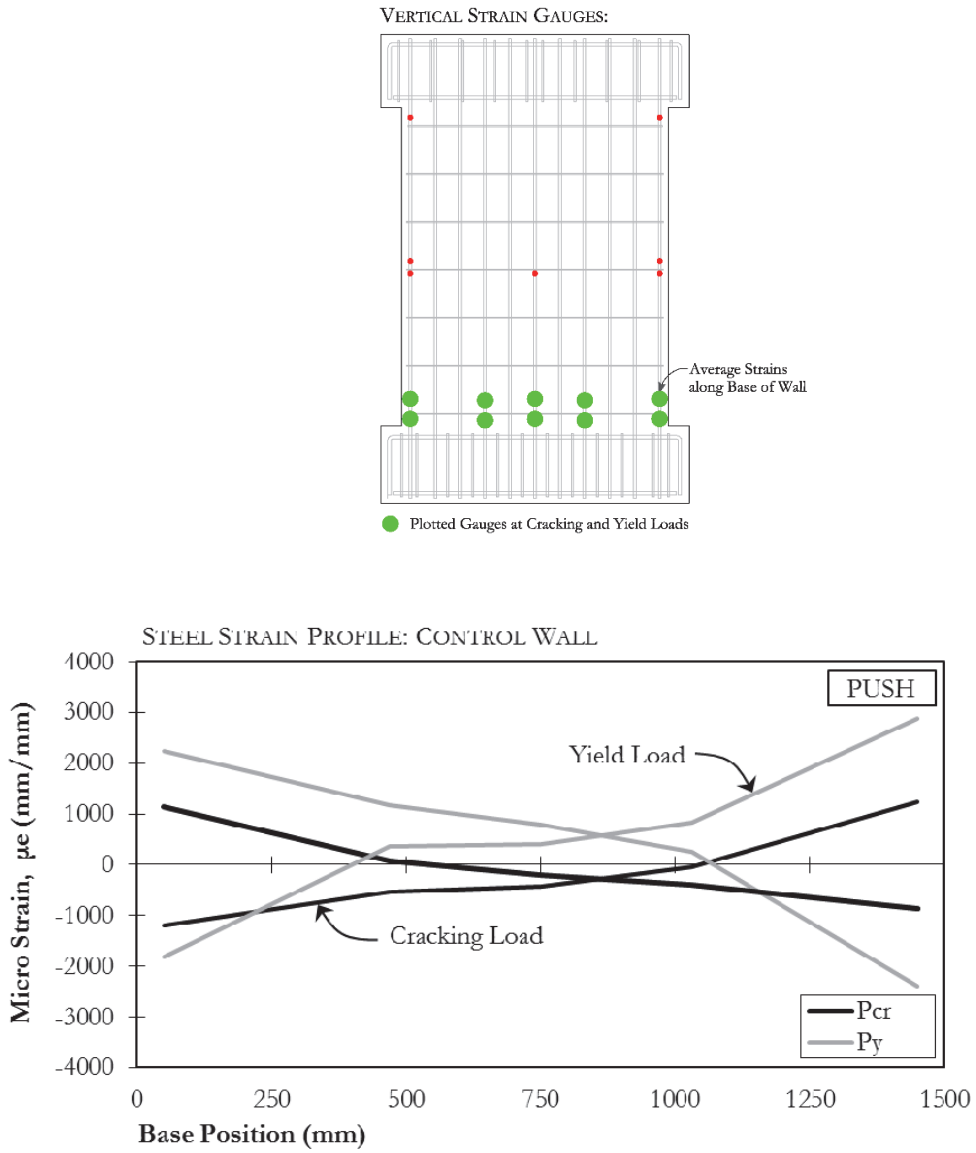

Figure B-7: Longitudinal Steel Strain Profile in Control Wall.

REPAIRED WALL SPECIMEN (SLRW)

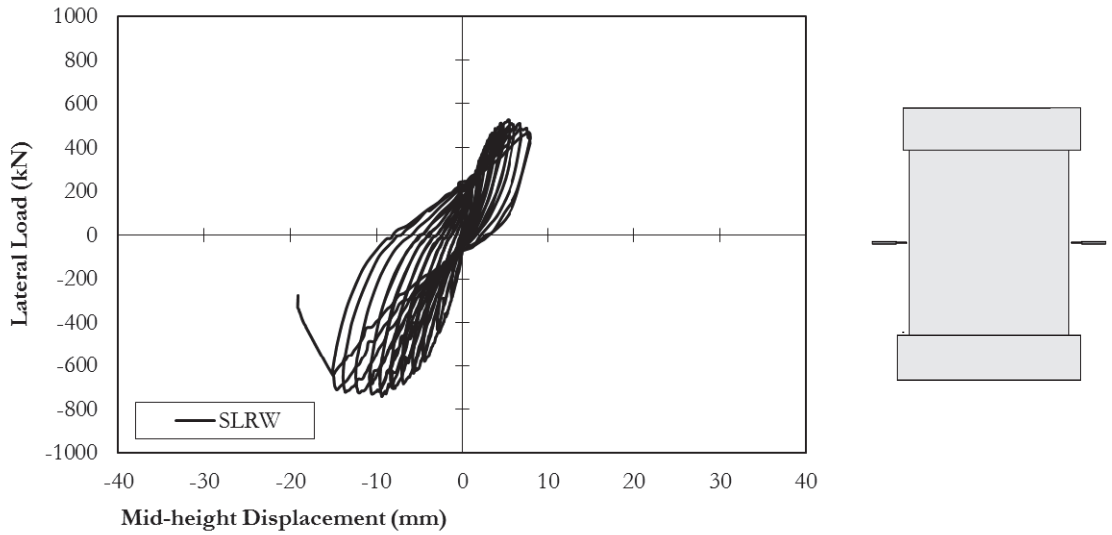

Figure B-8: Mid-height Displacement of Repaired Wall Specimen.

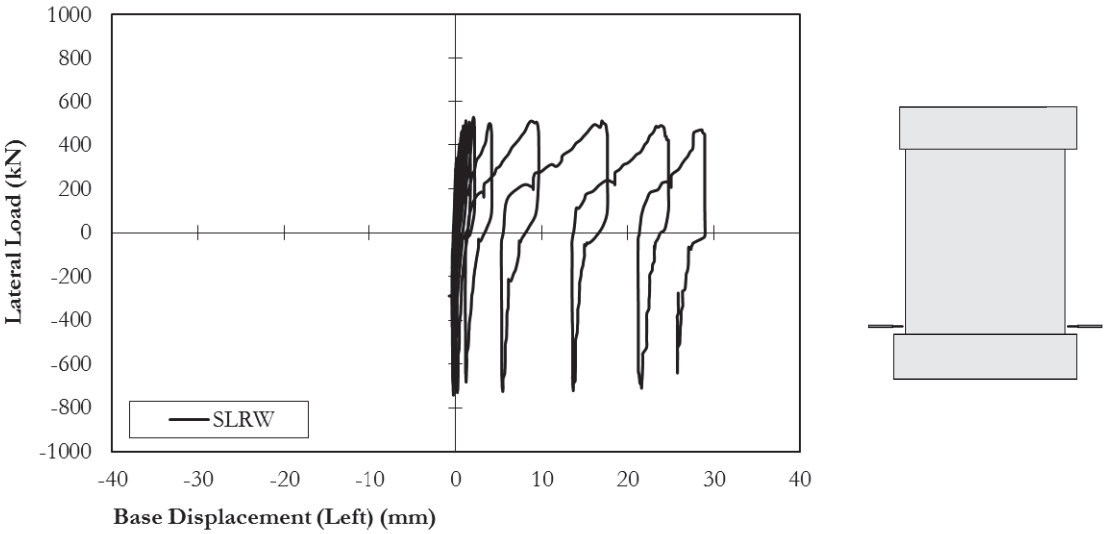

Figure B-9: Base Displacement of Repaired Wall Specimen.

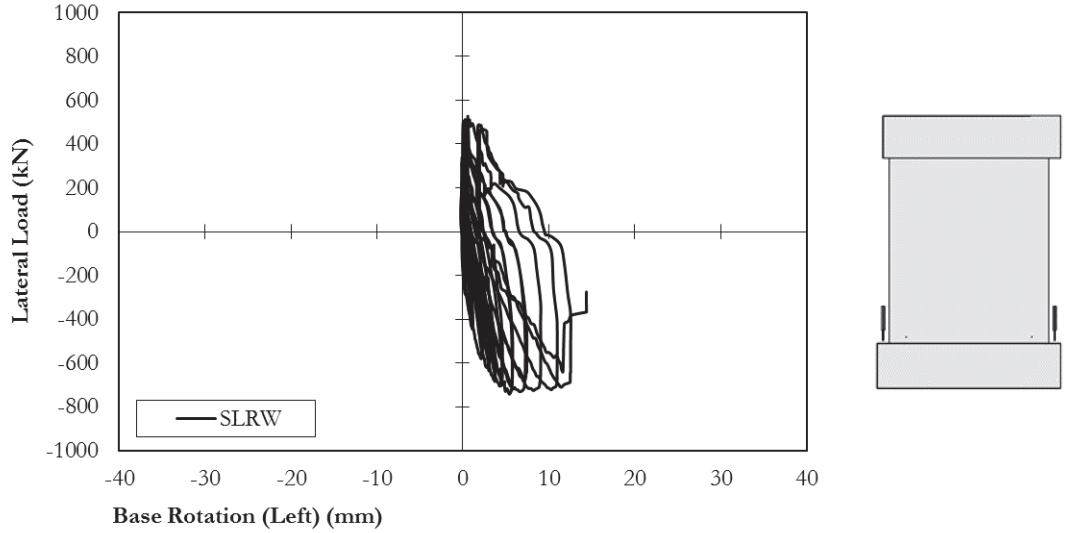

Figure B-10: Base Rotation Displacement of Repaired Wall Specimen.

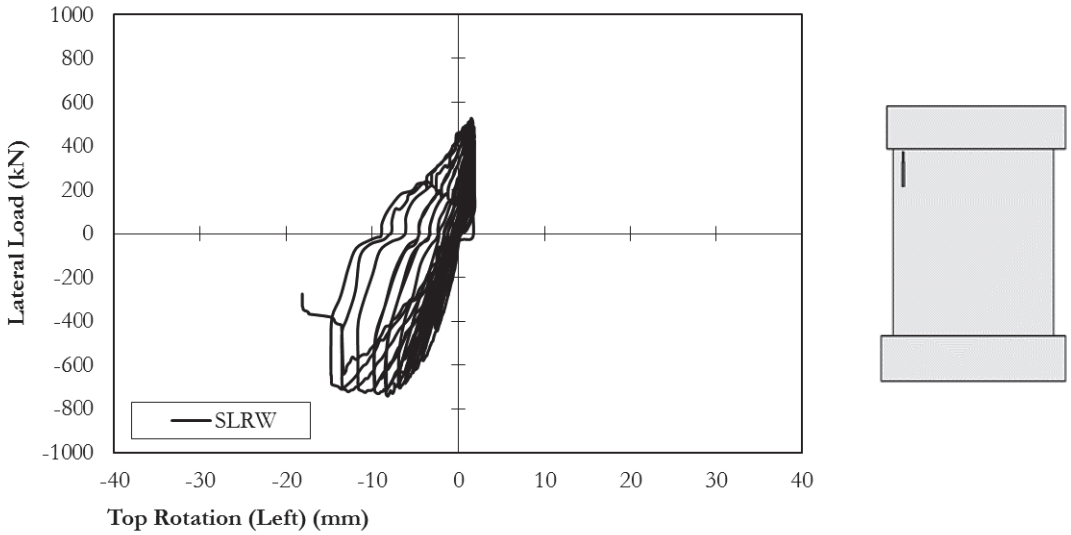

Figure B-11: Top Rotation (left) of Repaired Wall Specimen.

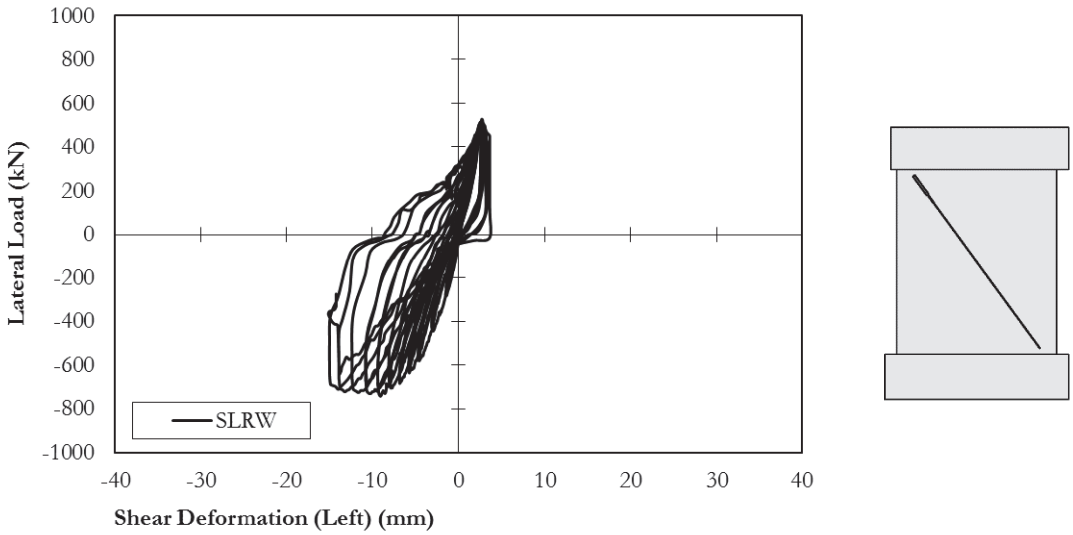

Figure B-12: Shear Deformation (left) of Repaired Wall Specimen.

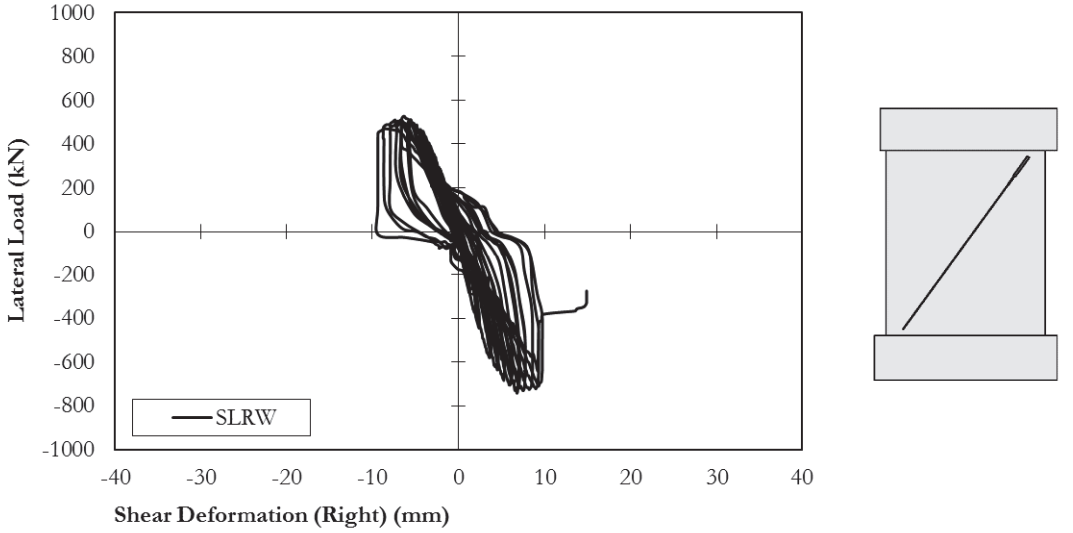

Figure B-13: Shear Deformation (right) of Repaired Wall Specimen.

STRENGTHENED WALL SPECIMEN (SLSW)

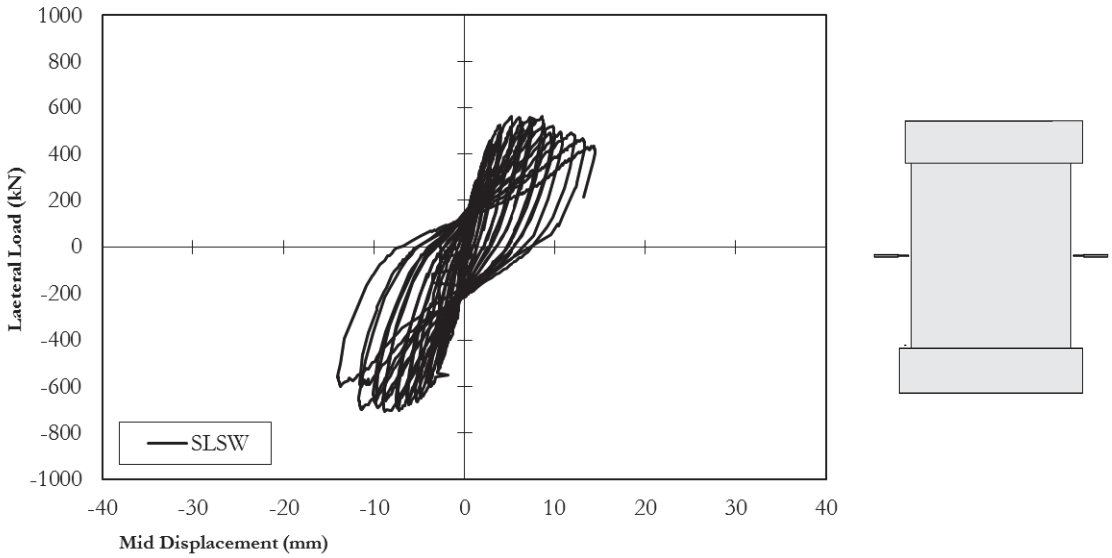

Figure B-14: Mid-height Displacement of Strengthened Wall Specimen.

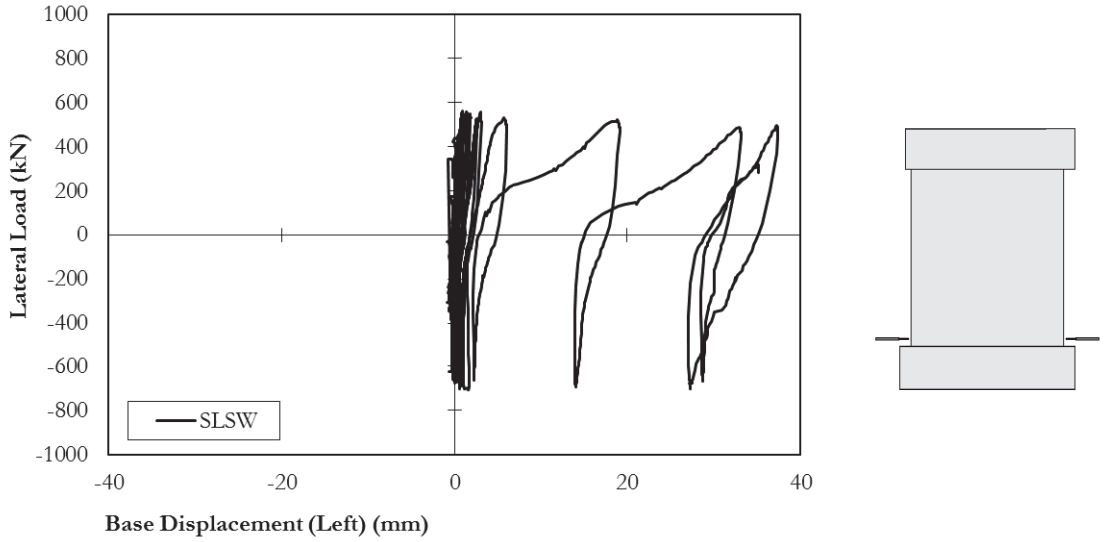

Figure B-15: Base Displacement of Strengthened Wall Specimen.

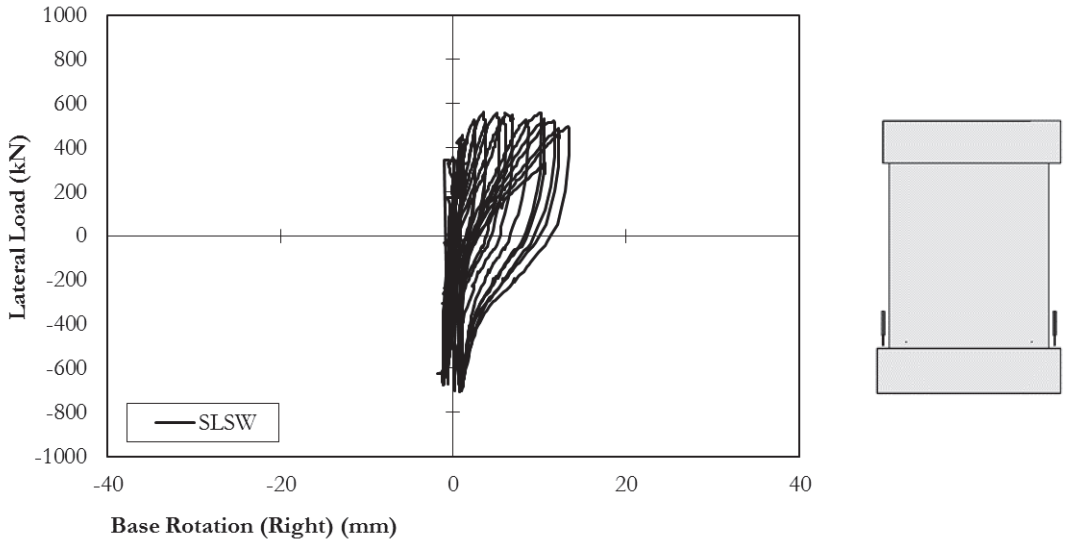

Figure B-16: Base Rotation of Strengthened Wall Specimen.

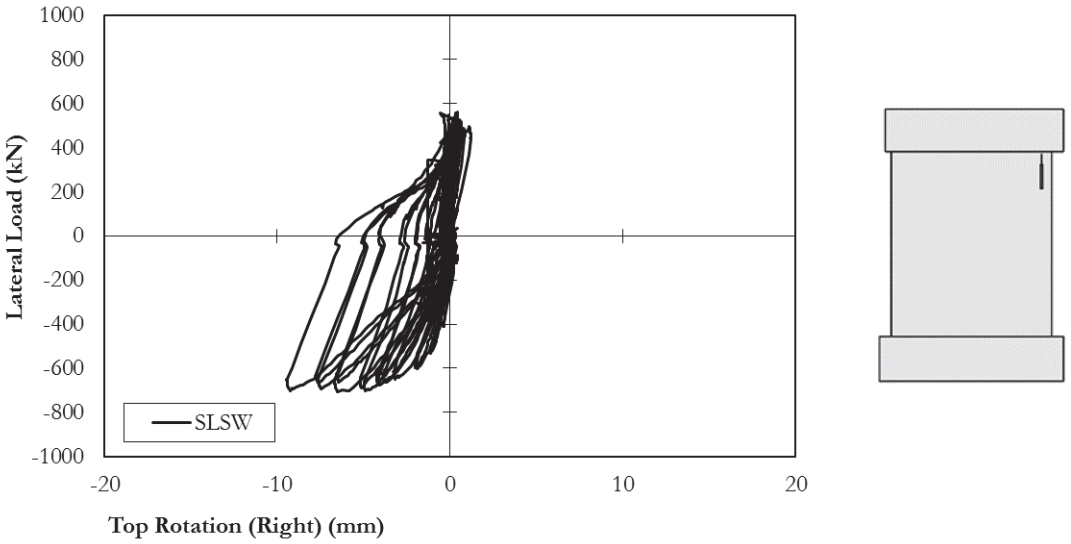

Figure B-17: Top Rotation (right) of Strengthened Wall Specimen.

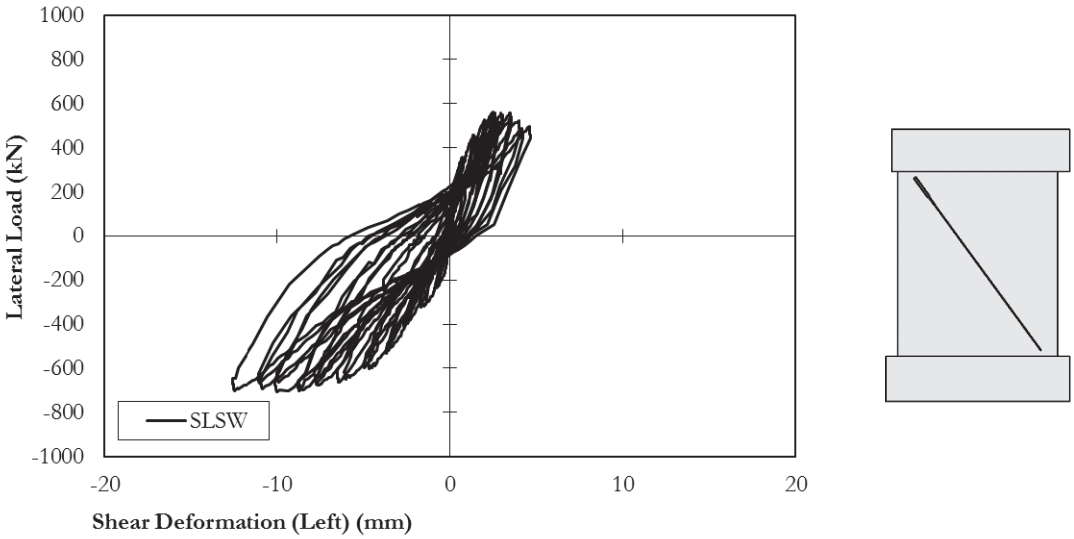

Figure B-18: Shear Deformation (left) of Strengthened Wall Specimen.

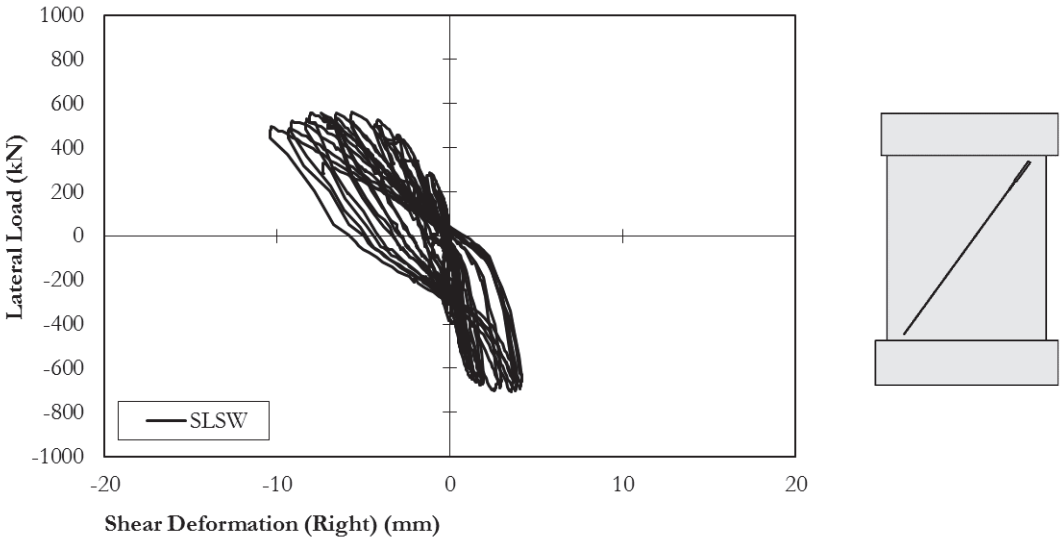

Figure B-19: Shear Deformation (right) of Strengthened Wall Specimen.

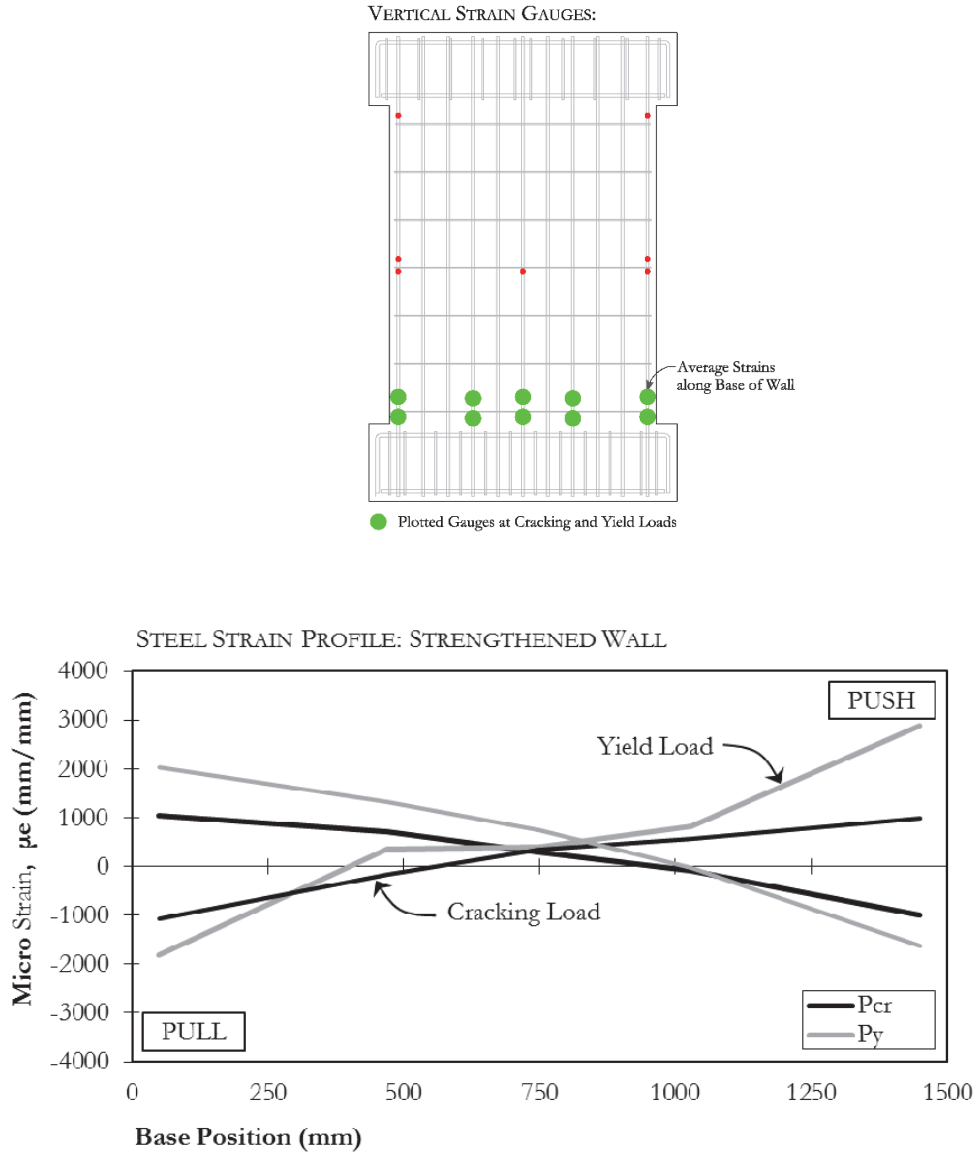

Figure B-20: Longitudinal Steel Strain Profile in Strengthened Wall Specimen.